Suncor Exploration Drilling Project: Environmental Impact Statement

Chapter 5 – Physical Environment

Prepared for:
Suncor Energy

Prepared by:
Stantec Consulting Ltd.
141 Kelsey Drive
St. John's, NL A1B 0L2
Tel: (709) 576-1458
Fax: (709) 576-2126

File No: 121417383

April 2023

Stantec

Table of Contents

LIST OF TABLES

LIST OF FIGURES

5.0 MARINE PHYSICAL ENVIRONMENT

5.1 Marine Geology

The Project Area, EL 1161, is located on the eastern edge of the Grand Banks of Newfoundland (Grand Banks) within the Jeanne d'Arc Basin. The Grand Banks is comprised of a series of several shallow banks encompassing 140,000 km² and is the largest in a series along the Eastern Canadian continental shelf (Grant and McAlpine 1990; Keen and Piper 1990; King 2014). The Grand Banks extend 400 km off Newfoundland, are up to 720 km long by 480 km wide and lie in waters less than 100 m deep (Keen and Piper 1990). The Grand Banks are bordered by the Laurentian Channel to the south, the Jeanne d'Arc Basin and Flemish Pass to the east, and the Northeast Newfoundland Shelf to the north (Keen and Piper 1990).

The Grand Banks formed during the opening of the Atlantic Ocean in the Early Cretaceous period (Louden et al. 2004). Most of the underlying bedrock geology of the Grand Banks consists of rifted Paleozoic or Carboniferous sediments with the southwestern margin formed by transform faulting (Keen and Piper 1990). The mid-shelf is covered with coastal plain sediments deposited in the Cretaceous and Tertiary (King 2014). These deposits are overlain by Cenozoic sediments which have been strongly influenced by Quaternary glaciation (Piper 1991).

The surficial geology of the Grand Banks has been influenced and mechanically altered by successive glacial periods, sea-level fluctuations, and storm-driven currents. (King and MacLean 1970, Sonnichsen and King 2005; Shaw 2006; Shaw et al. 2006; King 2010). Glacial deposits on the Banks include till sheets overlain by proglacial silts (Piper 1991) and prominent till ridges have been documented at the shelf margin in the Sackville Moraine complex (Huppertz and Piper 2009). Less than 20% of the Banks are deeper than 200 m and portions are shallow enough to have been emergent at glacial low stands in the Late Wisconsin (Sonnichsen and King 2005; Piper 2005; Shaw 2006). Iceberg grounding and scouring have mechanically reworked the seafloor and sub-seafloor shelf and upper slope sediments throughout the Quaternary (Banke 1989). Regional estimates of the minimum scouring frequency are on the order of 2×10^{-4} scour events/km²/year (Banke 1989). Sonnichsen et al. (2005) estimate the scour frequency on the Grand Banks to be 2.7×10^{-4} scour events/km²/year. Additionally, in shallow areas, storm-driven currents have formed sandy bedforms on the Grand Banks (King and MacLean 1970).

Sand ridges and waves, shell beds, iceberg scouring, pockmarks, and seabed depressions are widespread throughout the eastern Grand Banks (IAAC 2021). The surficial geology of the Grand Banks consists predominantly of a sand matrix (>90%) with more than 50% gravel content (Figure 5-1).

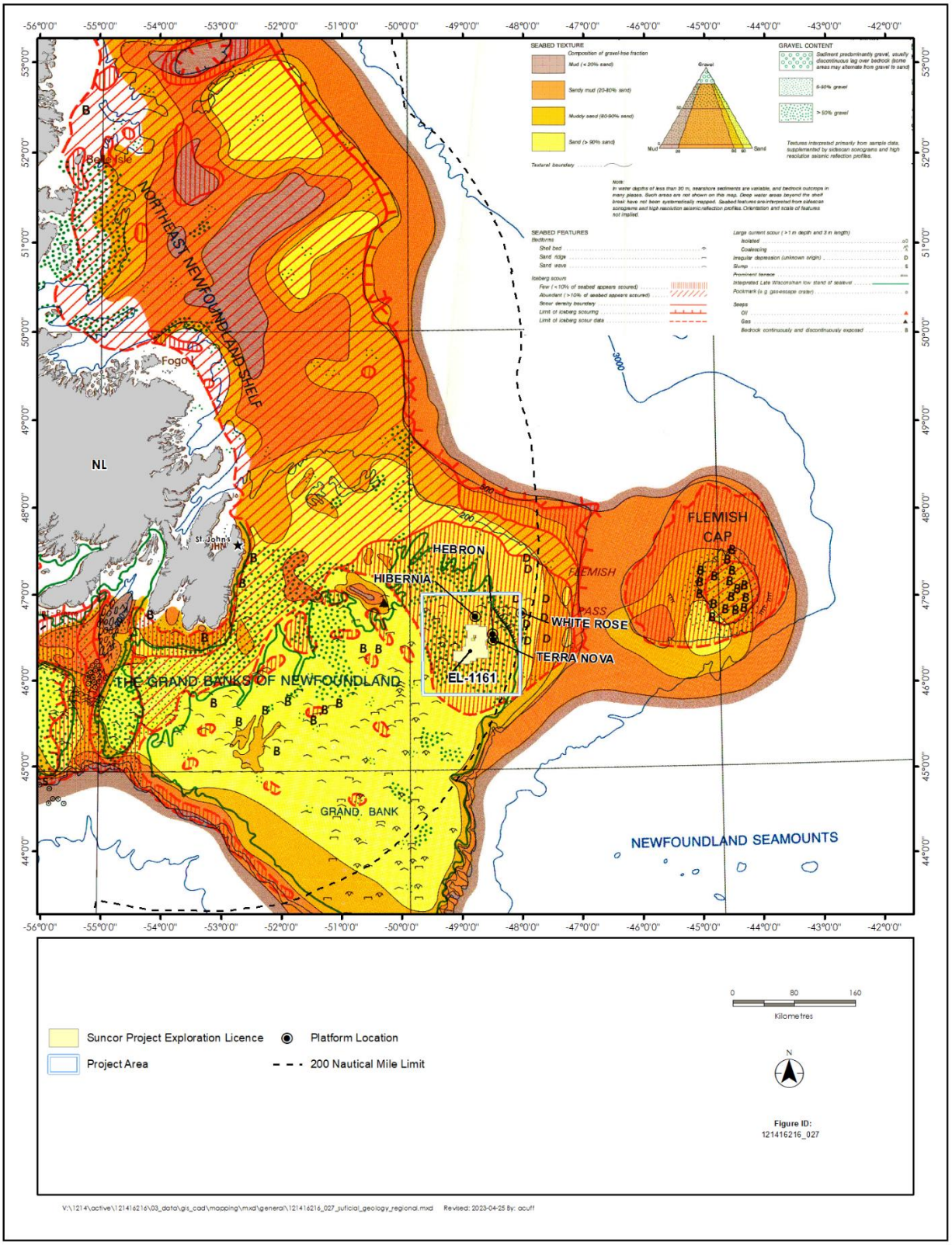

Source: Cameron and Best 1985

Figure 5-1 Geology of the Grand Banks and the Northeast Newfoundland Shelf

During periods of widespread shelf-crossing glaciation, sedimentation on the Grand Banks substantially increased (Piper 2005). The large volumes of suspended sediments were transported to the slope edge and reworked by storm-driven and shallow ocean currents. When sea level rose at the end of the last glacial episode, the surficial sediments were reworked, and the result was a relatively thin (average 1 to 3 m) veneer of sand and gravel (Fader and King 1981; Stoffyn-Egli et al. 1992). The reworked coarse-grained sediments comprise the Grand Banks Sand and Gravel seabed formation. The Grand Banks Sand and Gravel is interpreted as a basal transgressive deposit formed by winnowing of fines and is usually exposed between 90 and 110 m water depth or covered with a thin veneer of sand (Sonnichsen et al. 1994).

Within EL 1161, the surficial geology is comprised predominantly of Grand Banks Sand and Gravel: gravel with sand, gravel with minor sand, and continuous sand (Figure 5-2). The Grand Banks Sand and Gravel consists of pro-glacial Quaternary sediments (Piper and Campbell 2005) and is related to the Wisconsinan-Holocene transgression but continues to undergo present-day reworking (Sonnichsen et al. 1994).

The Grand Banks Drift seabed formation is highly irregular and underlies the Grand Banks Sand and Gravel as it extends into the EL. The Adolphus Sand Formation, which blankets the surrounding ELs, consists of fine-grained sand matrix with minor gravel and shells (Sonnichsen et al. 1994).

5.2 Atmospheric Environment

The Grand Banks of Newfoundland are among the harshest and most variable environmental operating areas in the world. This is an area that is affected by numerous climatic factors that vary from year to year, seasonally, and, at times, from storm to storm. The Grand Banks are located near the boundary of the maritime and continental air masses, and hence can be affected from storms that originate from the ocean or from the North American continent. Continental and maritime storms have different characteristics and each vary in their predictability. There are also situations in the winter when the cold Arctic air mass spills over the Grand Banks in “cold outbreaks,” causing gales and a rapid build-up of high sea state conditions. In the late summer and fall, the Maritime Tropical air mass to the south of the region can cause the formation of tropical storms that eventually track across the region, bringing high winds and seas. Warm air masses moving from the Gulf Stream over the colder Labrador Current waters produce heavy fog, especially in spring and summer, when the air-sea temperature differences are greatest. The confluence of the Labrador Current and the Gulf Stream produce temperature contrasts that frequently cause migrating low pressure systems to develop as they cross the Grand Banks, sometimes explosively. Severe storms occur most frequently in the fall, due to hurricanes or other tropical systems, and in the months of January through March as large winter storms transit the area from the southwest to the northeast.

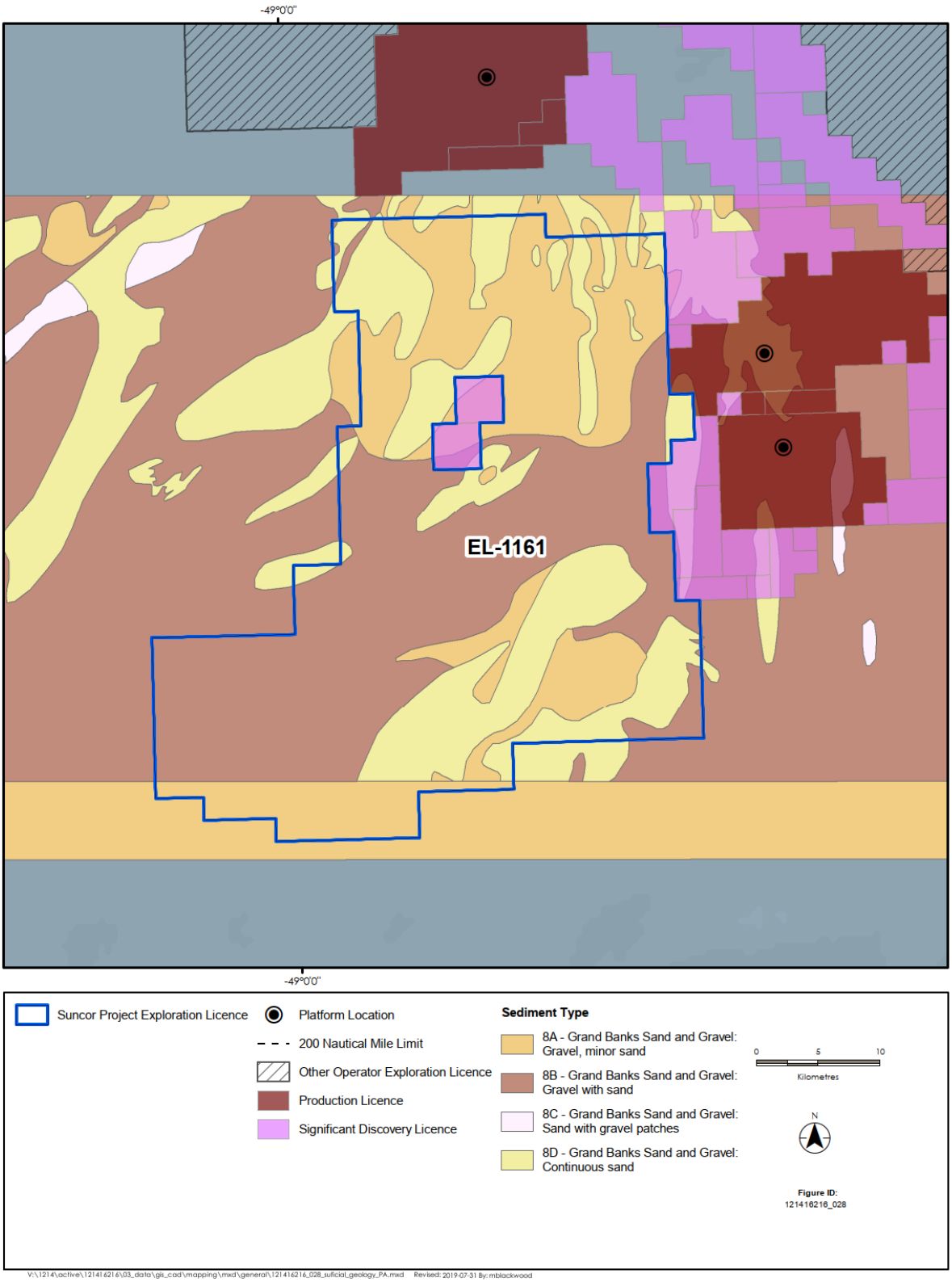

Figure 5-2 Distribution of Surficial Sediments for the Project Area Eastern Grand Banks

5.2.1 Wind Climatology

The primary characterization of the wind climatology of the Project Area is derived from the most recent release of the MSC50 wind and wave hindcast statistics for the North Atlantic Ocean and which span 1954 to 2018. The MSC50 dataset includes hourly wind and wave parameters of the North Atlantic Ocean (Swail et al. 2006, DFO 2022). The hindcast data were produced through the kinematic reanalysis of substantial tropical and extra-tropical storms in the North Atlantic. The dataset covers hourly wind and wave parameters and includes consideration of periods with sea ice coverage. Ice concentration data considered are mean monthly values through 1961 inclusive and Canadian Ice Service (CIS) mean weekly ice concentrations for 1962 onwards. Given the poorer resolution of ice information data from 1954 to 1961, this period of the MSC50 dataset was excluded from the present analysis. The 1962 to 2018 periods are considered for winds and waves (refer to Section 5.3.3).

The overall resolution of MSC50 hindcast data grid points (nodes) is high, with one point every 0.1° latitude by 0.1° longitude (approximately 7.4 km east-west and 11.2 km north-south near 47°N). To provide a characterization of wind (and wave – see Section 5.3.3) conditions, one node M6010432 at 46.4°N, 48.8°W in a water depth of 67.4 m in the centre of the Project Area was selected; the node location is shown in Figure 5-3. In addition to the MSC50 wind and wave hindcast data node, Figure 5-3 also shows the locations of Ocean Data Inventory (ODI) current (Section 5.3.2) measurements and previously drilled oil and gas exploration wells (C-NLOPB 2019).

The MSC50 wind speeds are 1-hour average wind speeds for a height of 10 m above sea level. Wind speed measurements are frequently averaged over shorter durations (e.g., 10 minutes for marine reports and two minutes for aviation, and a one- minute average is used for the categorization of tropical cyclones). Wind gusts are typically for one and three second durations. Several formulas (e.g., International Standards Organization 2015) can be used to scale winds to averaging times less than one hour and for different reference elevations, (e.g., between 10 m and drilling installation anemometer height or vice versa). These are routinely applied in design criteria studies applying measured and hindcast wind data sets.

Wind conditions are summarized with monthly and annual statistics for MSC50 node M6010432 are presented in Table 5.1. Monthly mean hourly wind speeds range from 6.1 m/s in July to 11.0 m/s in January with winds most frequently from the west in fall and winter and from the southwest in spring and summer. Monthly maximum wind speeds range from 19.2 m/s in July (from the west) to 32.4 m/s in February (from the northwest).

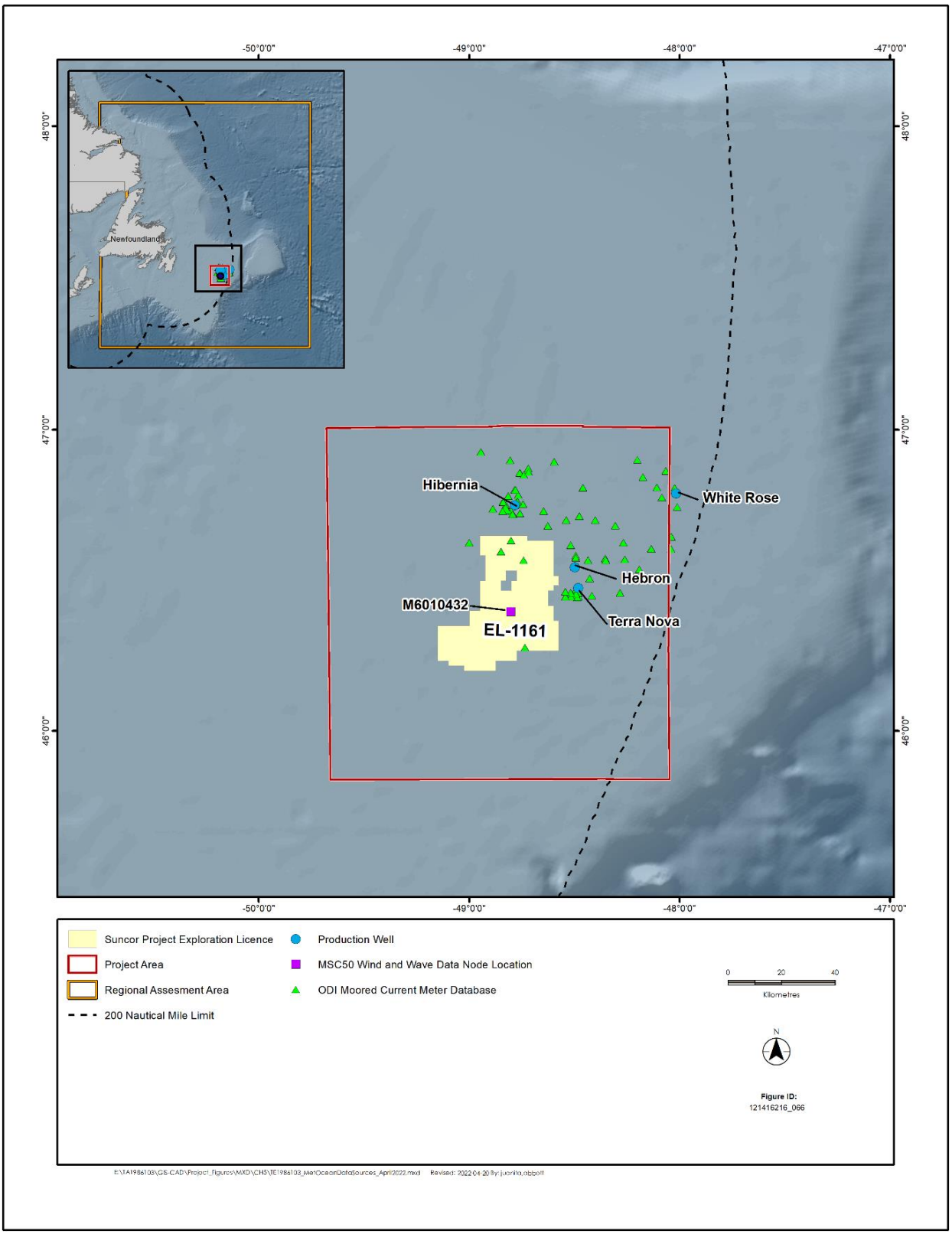

Figure 5-3 Met-Ocean Data Sources

Table 5.1 Monthly and Annual Wind Statistics, MSC50 Node M6010432 (1962-2018),

Location	Jan	Feb	Mar	Apr	May	Jun	Jul	Aug	Sep	Oct	Nov	Dec	Year
Mean Wind Speed (m/s)													
M6010432	11.0	10.8	9.8	8.3	7.0	6.6	6.1	6.4	7.5	8.8	9.5	10.6	8.5
Most Frequent Direction (from)													
M6010432	W	W	W	SW	SW	SW	SW	SW	SW	W	W	W	SW
Maximum Wind Speed (m/s)													
M6010432	28.8	32.4	27.6	25.5	21.2	22.7	19.2	26.3	25.1	27.4	27.3	27.1	32.4
Direction of Maximum Wind Speed (from)													
M6010432	W	NW	NW	N	NW	NW	W	S	S	S	W	W	NW
Source: M6010432 based on DFO (2022)													

Monthly and annual directional wind distributions for node M6010432 are shown in the wind roses of Figures 5-4 and 5-5. A wind rose illustrates the percent frequency of distribution of wind direction and wind speed, for a given time period (e.g., annually, or a given month), as well as the distribution of wind speed within each directional sector or bar. Bars represent the total percentage frequency of winds observed from each direction. Each circle equals 10% (e.g., 10% of winds are from the south). The total bar length represents the total percent occurrence of winds from that direction (e.g., a bar of length of 29% for January in Figure 5-4 pointing to the left shows 29% of winds are from the west. Each section of a wind rose bar corresponds to winds of a given speed range or bin, with bins being the noted 6, 12, …, 36 m/s in size. The section length (radial distance out from the middle of the rose) is the percentage of all observations that are in a given wind speed range, for the given direction. The section widths increase in size as wind speed increases, after the first and third sections, and as the bar extends out from the origin. The length of the first bar section represents the percentage of observations in the wind speed range 0 to 6 m/s, the length of the second bar section represents the percentage of observations in the range 6 to 12 m/s and so on. A bar with six sections will therefore report a percentage of observations up to the largest wind speed range of 30 to 36 m/s.

The seasonal picture of predominantly southwest winds in the summer with a shift to stronger, more westerly and northwesterly winds in fall and winter is evident. In July winds are from the southwest for 38% of the time and from the southwest quadrant 76% of the time. In January winds are from the west 29% of the time and from the southwest through northwest quadrant for 66% of the time. Wind directions are more uniformly distributed during spring (e.g., April) ranging from 8% of winds being from the northeast to 17% and 18% from the west and southwest, respectively.

The predominance of westerly winds is evident in Figure 5-5 with winds from the southwest through northwest 57% of the time compared for example with winds from northeast through southeast for just 20% of the time.

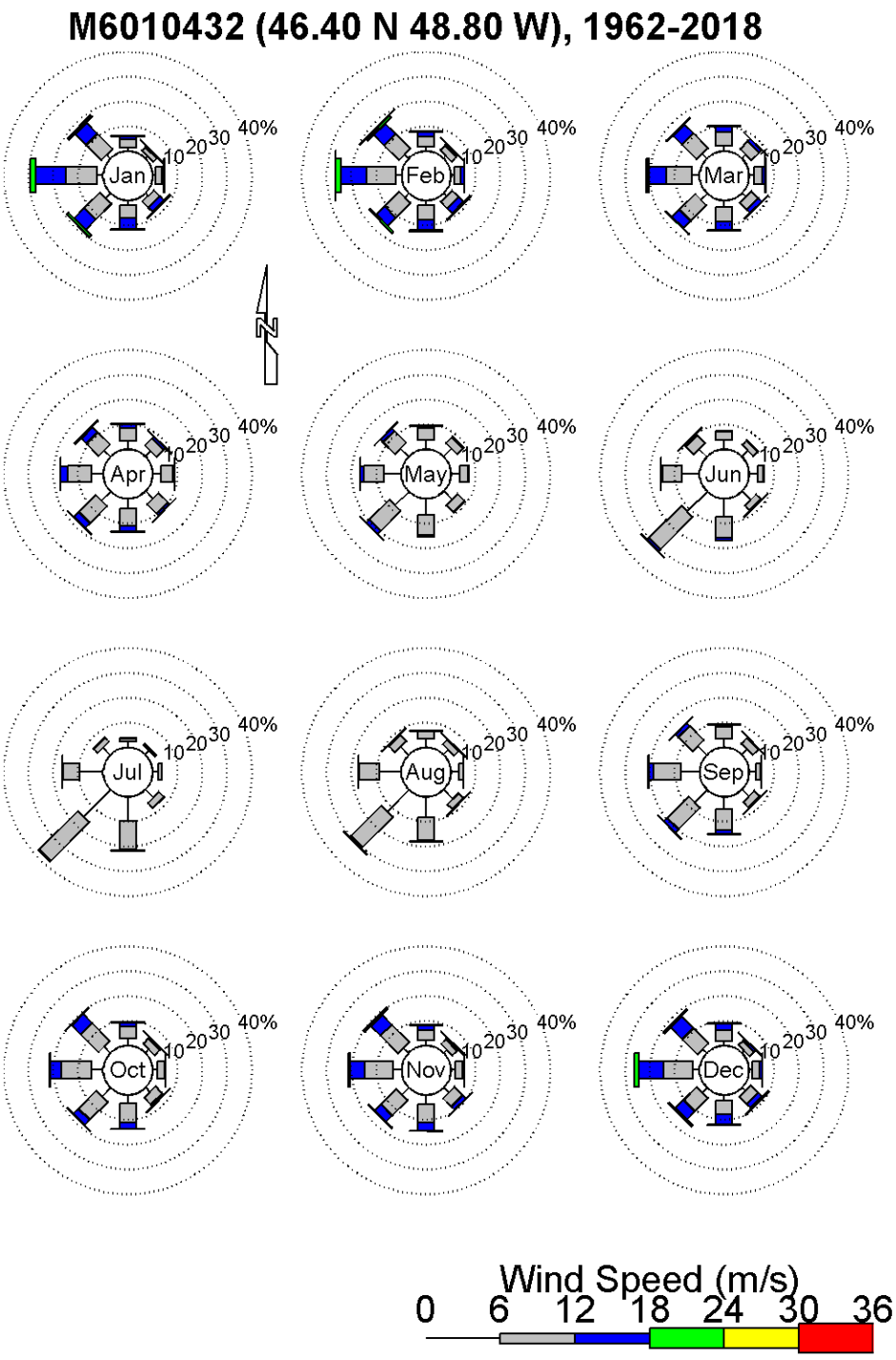

Source: Based on DFO (2022)

Figure 5-4 Monthly Wind Roses, MSC50 Node M6010432, 1962-2018

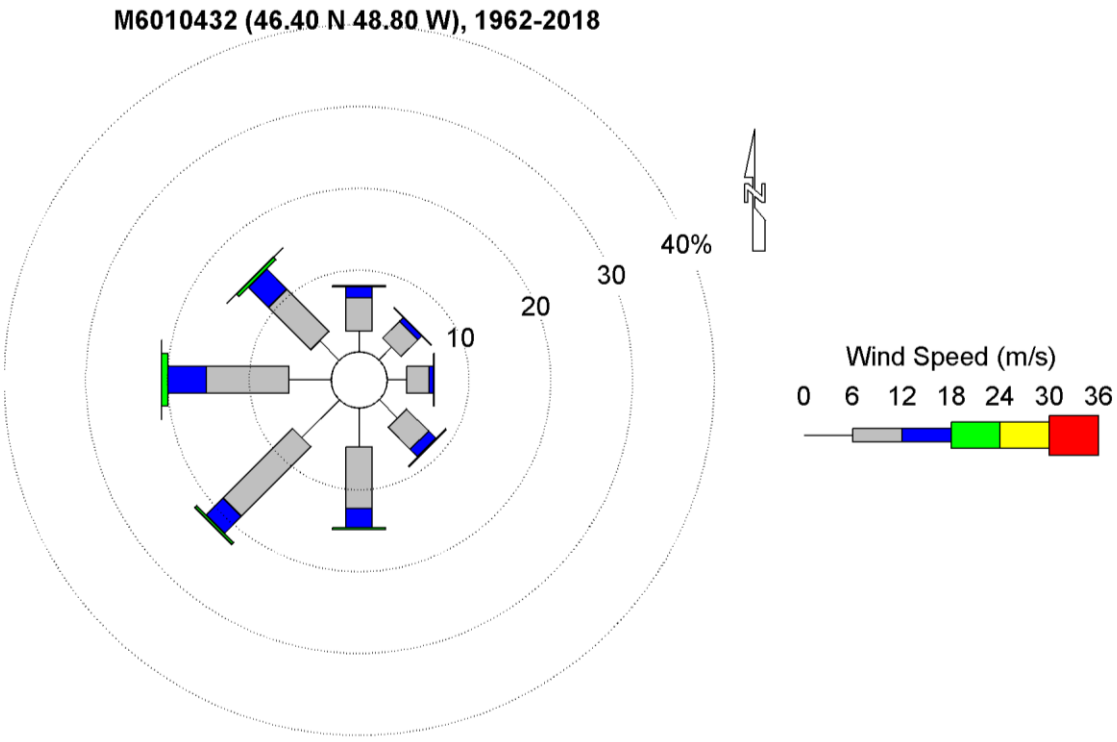

Source: Based on DFO (2022)

Figure 5-5 Annual Wind Rose, MSC50 Node M6010432, 1962-2018

5.2.2 Air and Sea Surface Temperature

Atmospheric properties over the ocean surface, including air and sea surface temperature, precipitation, and visibility have been characterized using the International Comprehensive Ocean-Atmosphere Data Set (ICOADS). ICOADS represents the most extensive available database of observations of atmospheric and sea conditions. The dataset consists of global marine observations recorded from 1962 to the present, compiled by the United States National Centre for Atmospheric Research (Freeman et al. 2017).

To characterize conditions within the Project Area, air temperature, sea surface temperature, precipitation and lightning, visibility and marine icing conditions, have been characterized by selecting all ICOADS observations within the Project Area for the period 1 January 1980 to 30 June 2019 (Research Data Archive et al. 2019). The resultant data points shown in Figure 5-6 illustrate good spatial coverage of the Project Area. The monthly number of observations for the various climatology and marine icing parameters are listed in the respective monthly statistics tables. Temporal coverage is also good, with several thousand observations present for each year from 1980 to 2019 and typically several hundred each year-month, the exception being several years from 1989 to 1996 with frequently less than 1,000 observations. Overall, this data set provides a good climatology characterization.

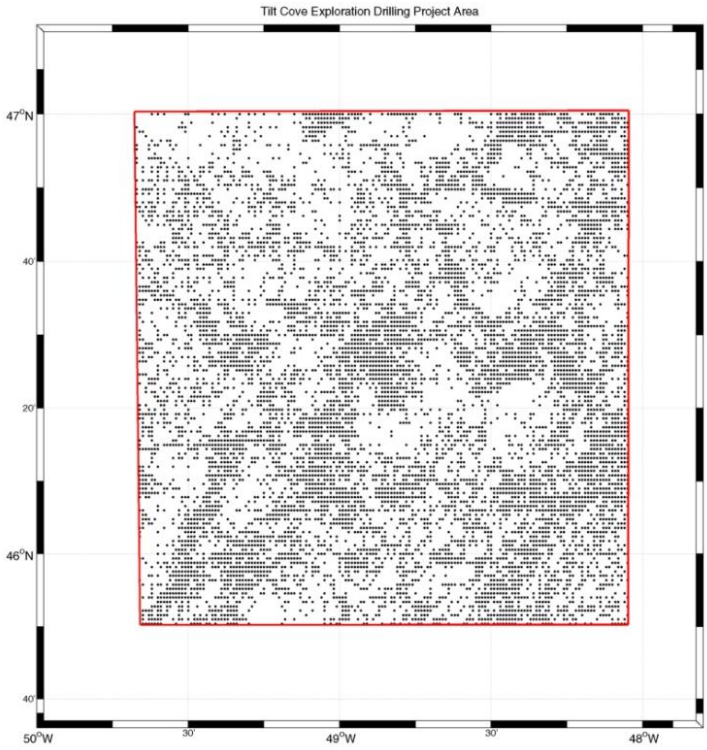

Source: based on Research Data Archive et al. (2019)

Figure 5-6 Location of ICOADS Observations, Project Area, 1980-2019

Monthly air temperature statistics for the Project Area are presented in Table 5.2 and Figure 5-7. Air temperature exhibits strong seasonal variations, with mean temperatures ranging from -0.4°C in January to 14.5°C in August. The coldest observed air temperature on record (-13.6°C) was in February with minimum temperatures in June of -1.0°C. The highest observed temperature is 23.0°C in July with maximum temperatures of 15.5°C in January.

Monthly sea surface temperature statistics for the Project Area are presented in Table 5.3 and Figure 5-8. Sea surface temperature exhibits a strong seasonal variation, with mean temperatures fairly constant between 0.4 to 1.2°C from January through April, then warming to 6.1°C by June and 14.1°C by August. Cooling from the atmosphere reduces mean temperatures to 10.1°C by October and 3.2°C by December. The coldest observed sea surface temperature is -2.8°C in February with the warmest being 22.4°C in September.

Table 5.2 Monthly Air Temperature (°C) Statistics (ICOADS), Project Area, 1980-2019

Month	Mean	Max	Min	Std Dev	Number of Values
Jan	0.3	15.5	-12.8	3.2	14,206
Feb	-0.4	14.6	-13.6	3.2	13,000
Mar	0.3	13.1	-11.0	2.9	14,038
Apr	1.9	13.0	-6.5	2.5	13,993
May	4.2	15.0	-5.0	2.4	15,588
Jun	7.3	20.5	-1.0	2.5	15,286
Jul	12.2	23.0	1.2	2.6	14,885
Aug	14.5	22.5	7.0	2.2	14,719
Sep	12.9	22.5	1.4	2.5	14,025
Oct	9.3	21.2	-0.7	3.0	14,587
Nov	5.5	16.1	-4.6	3.1	14,371
Dec	2.3	16.5	-10.2	3.3	13,597
Source: based on Research Data Archive et al. (2019)					

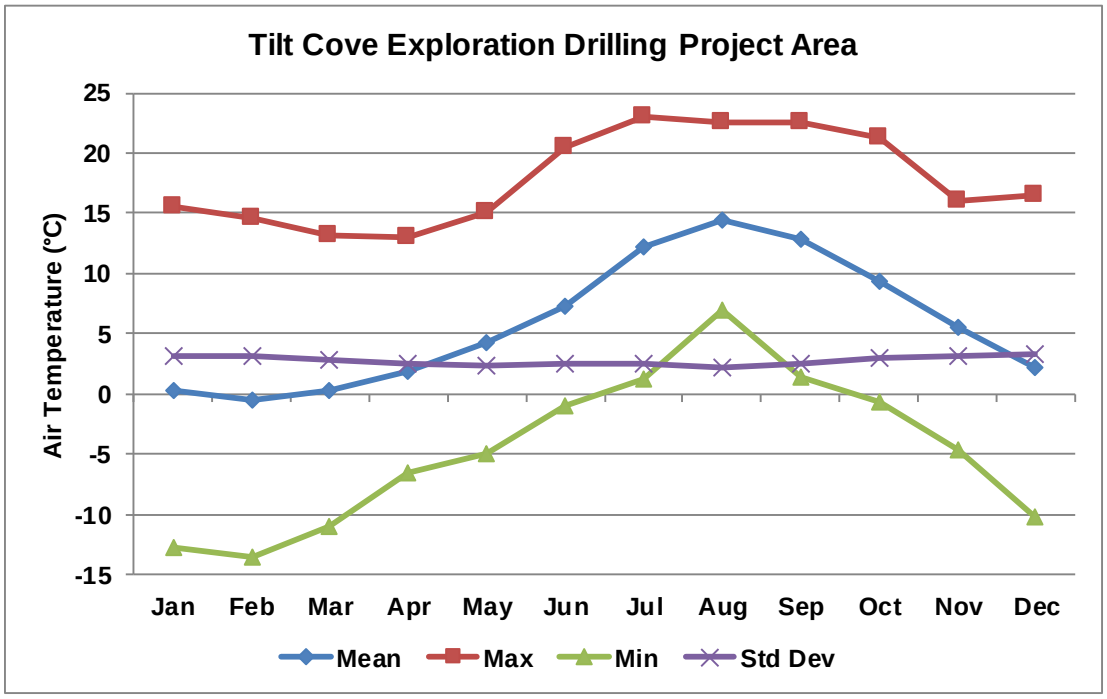

Source: based on Research Data Archive et al. (2019)

Figure 5-7 Monthly Air Temperature Statistics (ICOADS), Project Area, 1980-2019

Table 5.3 Monthly Sea Surface Temperature (°C) Statistics (ICOADS), Project Area, 1980-2019

Month	Mean	Max	Min	Std Dev	Number of Values
Jan	1.2	12.3	-2.4	1.2	13,782
Feb	0.5	11.6	-2.8	1.0	11,966
Mar	0.4	13.8	-2.7	1.0	13,603
Apr	1.0	10.8	-1.9	1.1	13,060
May	3.1	12.7	-2.0	1.7	15,542
Jun	6.1	17.0	0.1	1.8	18,110
Jul	10.7	20.2	0.9	2.2	18,391
Aug	14.1	22.0	6.6	2.0	15,546
Sep	13.6	22.4	1.6	2.1	14,383
Oct	10.1	19.3	0.5	2.4	14,393
Nov	6.1	17.0	-1.8	2.2	13,654
Dec	3.2	14.0	-2.0	1.9	12,856
Source: based on Research Data Archive et al. (2019)					

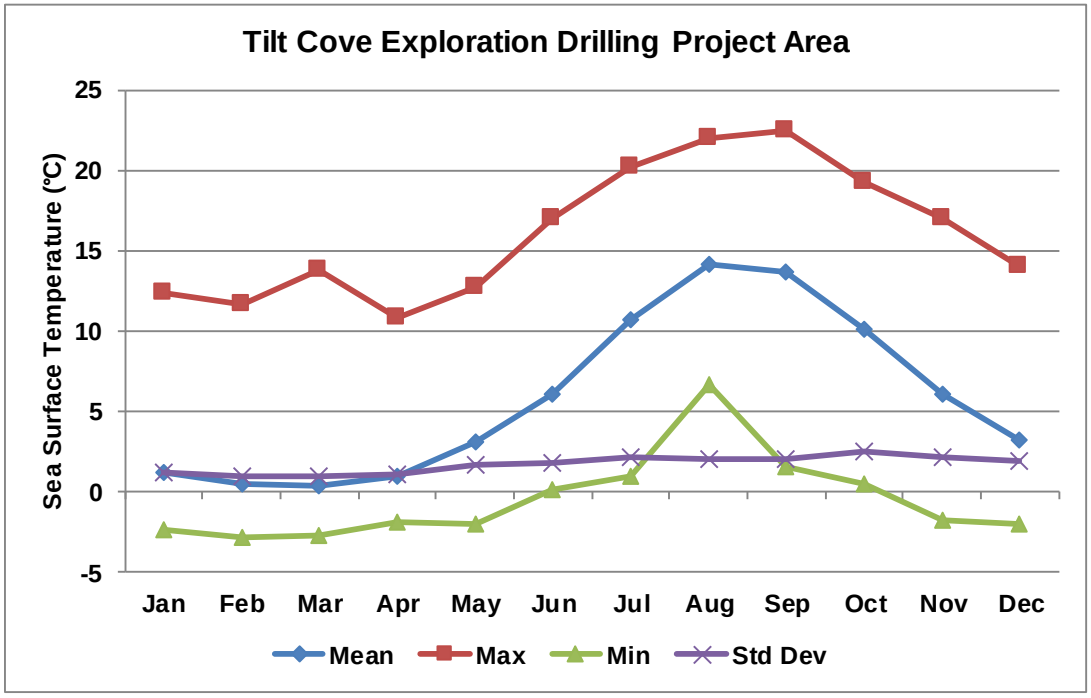

Source: based on Research Data Archive et al. (2019)

Figure 5-8 Monthly Sea Surface Temperature Statistics (ICOADS), Project Area, 1980-2019

5.2.3 Precipitation

The ICOADS database contains observations of several precipitation types and thunderstorm occurrence. The weather state is recorded and categorized as an event based on the type (but not the amount) of precipitation during that event. The frequency of occurrence of the different precipitation types and thunderstorms have been calculated as a percentage of the total monthly and annual weather observations for the same data set described in Section 5.2.2 for air and sea surface temperature, with observations spanning 1 January 1980 to 30 June 2019.

A degree of variability of precipitation patterns within localized regions of the overall Project Area is expected. The statistics shown below in Table 5.4 are the percentage of a certain distinct weather states (e.g., rain, thunderstorms, hail) for weather reports available on record for that month. The weather states have been consolidated from 50 different ICOADS classifications, separating (without overlap) rain from freezing rain and snow (although some overlap may exist between these states and mixed rain/snow, hail, and thunderstorm, which represent a small percentage of the data). The frequency of occurrence (i.e., the percent of time the given condition(s) occurs), in a given month (or annually) can most closely be characterized as representing unspecified periods of time, for a percentage of all days.

For the Project Area, the ICOADS data indicate that most of the observed precipitation events are in the form of rain, snow, and drizzle, while other precipitation types, such as mixed rain, freezing rain, and hail, occur less frequently. Rain occurs approximately 9 to 15.3% of the time for all months of the year and occurs annually 11.7% of the time. Snow is most likely to occur in February at 16.3% of the time but may reach 2.9% as early as November and 3.7% as late as April, and is an annual occurrence 4.9% of the time (Table 5.4, Figure 5-9). Hail is infrequent for the Project Area occurring greater than 0.1% of the time from October through April with the greatest occurrence at 0.5% in January. Thunderstorms can occur any time of the year, albeit infrequently. The occurrence of thunderstorms is greatest at about 0.1% in August (Table 5.4, Figure 5-10).

Table 5.4 Frequency of Occurrence (%) of Precipitation and Thunderstorms (ICOADS), Project Area, 1980-2019

Month	Rain / Drizzle	Freezing Rain / Drizzle	Rain / Snow Mixed	Snow	Hail	Thunderstorm	Number of Values
Jan	10.9	0.5	0.3	15.3	0.5	0.02	13,264
Feb	9.0	0.9	0.2	16.3	0.2	0.0	12,382
Mar	9.6	1.2	0.2	10.3	0.2	0.02	13,003
Apr	11.7	0.4	0.1	3.7	0.1	0.01	13,001
May	11.4	0.08	0.03	0.7	0.03	0.0	14,272
Jun	11.8	0.0	0.02	0.03	0.01	0.03	13,880
Jul	10.3	0.0	0.07	0.07	0.03	0.07	13,780
Aug	11.0	0.01	0.1	0.1	0.02	0.1	12,895
Sep	11.4	0.01	0.02	0.03	0.0	0.02	12,122
Oct	15.3	0.02	0.05	0.3	0.1	0.0	12,450
Nov	15.2	0.06	0.2	2.9	0.4	0.03	12,504
Dec	12.5	0.2	0.3	9.3	0.4	0.01	12,830
Annual	11.7	0.3	0.1	4.9	0.2	0.03	156,383
Source: based on Research Data Archive et al. (2019)							

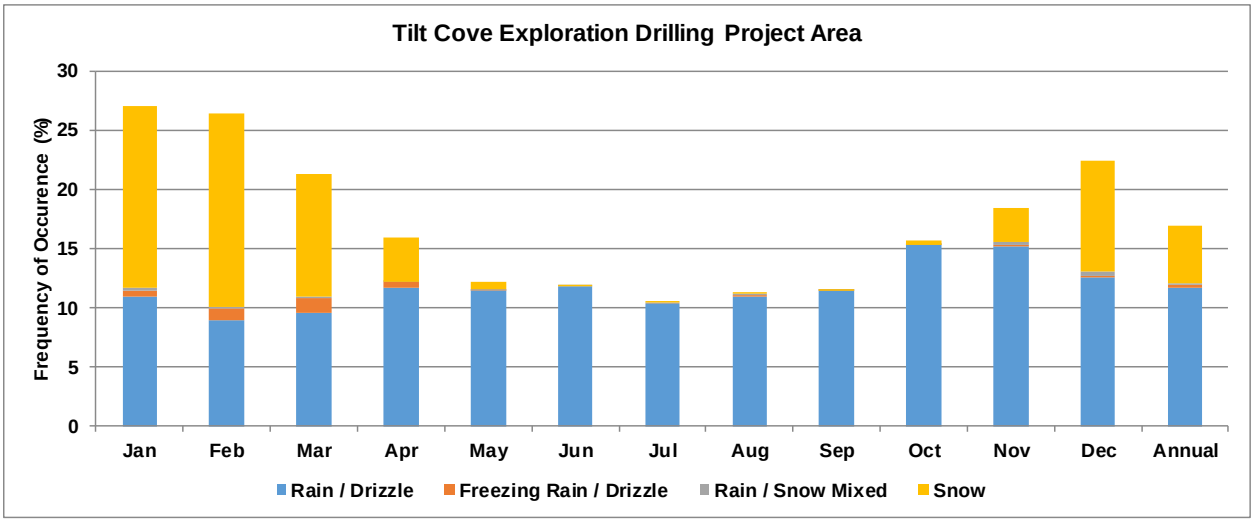

Source: based on Research Data Archive et al. (2019)

Figure 5-9 Frequency of Occurrence (%) of Precipitation by Type (ICOADS), Project Area, 1980-2019

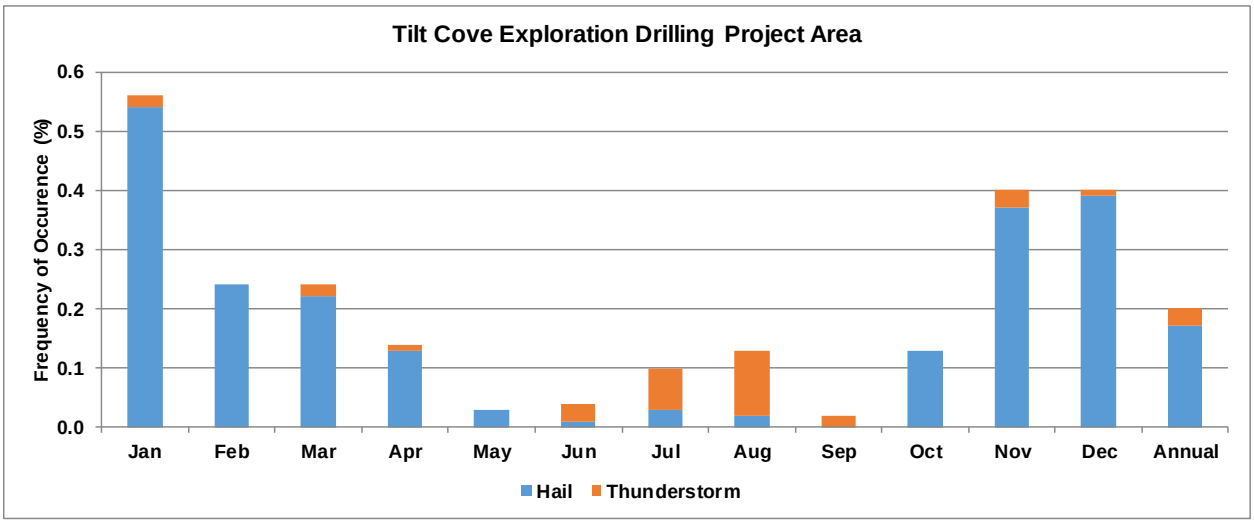

Source: based on Research Data Archive et al. (2019)

Figure 5-10 Frequency of Occurrence (%) of Thunderstorm and Hail (ICOADS), Project Area, 1980-2019

5.2.4 Icing

Marine rime icing, most frequently from freezing spray, is a marine condition that can hinder and limit shipboard or production installation activities and increase a vessel's weight and alter its centre of gravity. Freezing spray is most likely to occur from November through April. Air temperatures must be lower than -2°C to produce freezing spray in salt water. Icing conditions worsen with colder temperatures, high winds, and large waves (Bowyer 1995).

A standardized way to determine the potential ice build-up rate has been developed by Overland (1990), which bases an algorithm on empirical observations and the heat balance equation of an icing surface. This algorithm has been used to derive estimates of icing potential by using concurrent air and sea temperature and wind speed data from ICOADS. The results have been sorted into four different categories based on the severity (light, moderate, heavy, and extreme) and are summarized below.

The icing potential for vessels in the Project Area (Figure 5-11) is greatest in February approaching 32%, with a 24% likelihood in January, 21% in March, 11% in December and 5% in April. The frequency of occurrence for moderate, heavy, or extreme icing potential is greatest in February at 11%. Extreme icing potential is greatest in February at 1.8%. No icing potential is reported for June through October. Annually, the frequency of occurrence of icing is 7.2% with 5.0% of that being light icing.

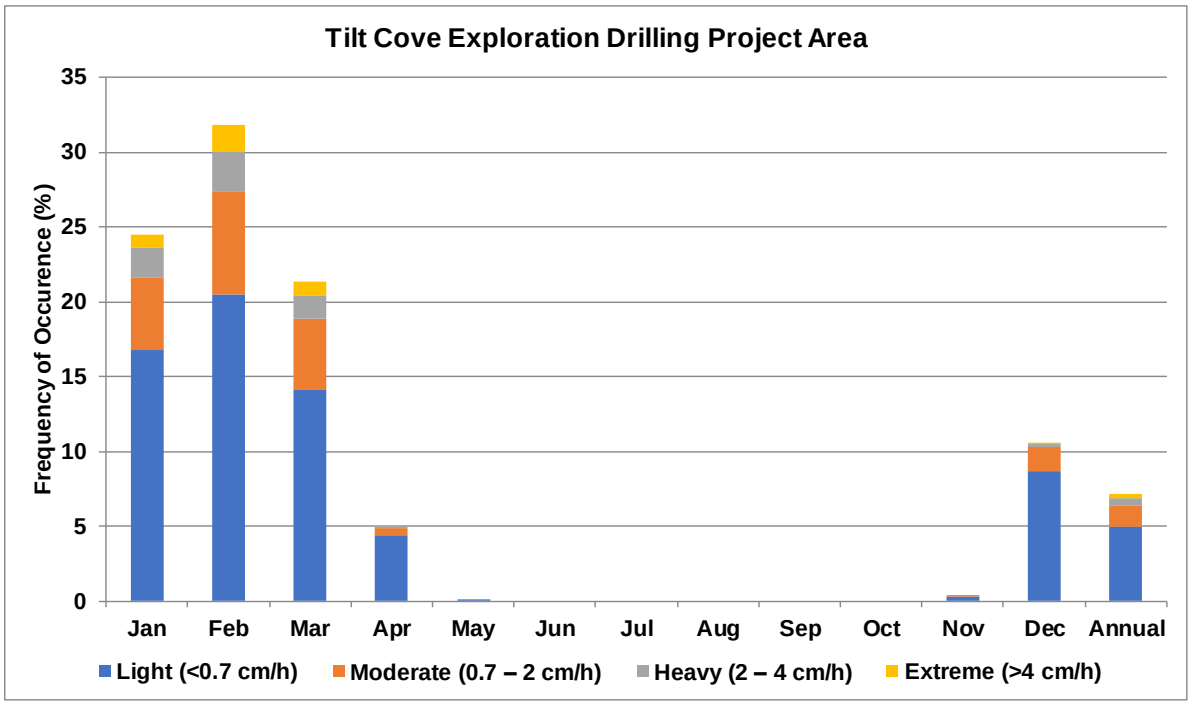

Source: based on Research Data Archive et al. (2019)

Figure 5-11 Icing Potential (ICOADS), Project Area, 1980-2019

5.2.5 Visibility

The Project Area and surrounding areas have some of the highest occurrence rates of marine fog in North America, which in these regions is commonly advection fog. Advection fog is formed when warm moist air flows over a cold surface, such as the cold northwest Atlantic Ocean, and persists for days or weeks. This type of fog is most prevalent in spring and summer. Visibility is affected by the presence of fog, the number of daylight hours, as well as frequency and type of precipitation.

Visibility from the ICOADS dataset (observations span 1 January 1980 to 30 June 2019) has been classified as very poor (<0.5 km), poor (0.5 to 1 km), fair (1 to 10 km) or good (greater than 10 km). For offshore flying, helicopters need visual confirmation at 0.25 NM (approximately 0.5 km) out and need a visibility of 1 km, or greater, to land. Fog and visibility conditions and seasonal variability are expected to vary across the Project Area.

As shown in Table 5-5 and Figure 5-12, visibility within the Project Area varies considerably throughout the year. Annually, visibility is very poor 18% of time, poor 3% of the time, fair 17% of the time, and good 62% of the time. The best visibility occurs from September through March when fair or good visibility (greater than 1 km) occurs approximately 87 to 91% of the time each month. From April through August poor visibility (less than 1 km) occurs from 24% (in April) to 49% (in July) of the time monthly, averaging 34% of the time during these months. Visibility is poorest in July with very poor visibility (<0.5 km) occurring 45% of the time.

Table 5.5 Monthly and Annual Frequencies (%) of Occurrence of Visibility (ICOADS), Project Area, 1980-2019

Month	Very Poor (<0.5 km)	Poor (0.5 – 1 km)	Fair (1 – 10 km)	Good (>10 km)	Number of Values
Jan	7.3	2.3	18.9	71.5	16,465
Feb	8.9	2.6	20.3	68.3	14,708
Mar	10.5	2.7	19.3	67.6	16,397
Apr	20.3	3.4	18.6	57.7	15,660
May	26.3	4.7	17.2	51.8	17,339
Jun	33.2	4.9	17.7	44.3	19,731
Jul	44.6	4.7	14.9	35.9	20,182
Aug	22.6	3.2	15.5	58.7	17,282
Sep	11.5	1.8	13.3	73.4	16,007
Oct	8.6	1.4	13.7	76.3	15,955
Nov	9.7	2.0	15.6	72.7	15,341
Dec	7.8	1.7	17.6	72.9	14,714
Annual	17.9	3.0	16.9	62.3	199,781
Source: based on Research Data Archive et al. (2019)					

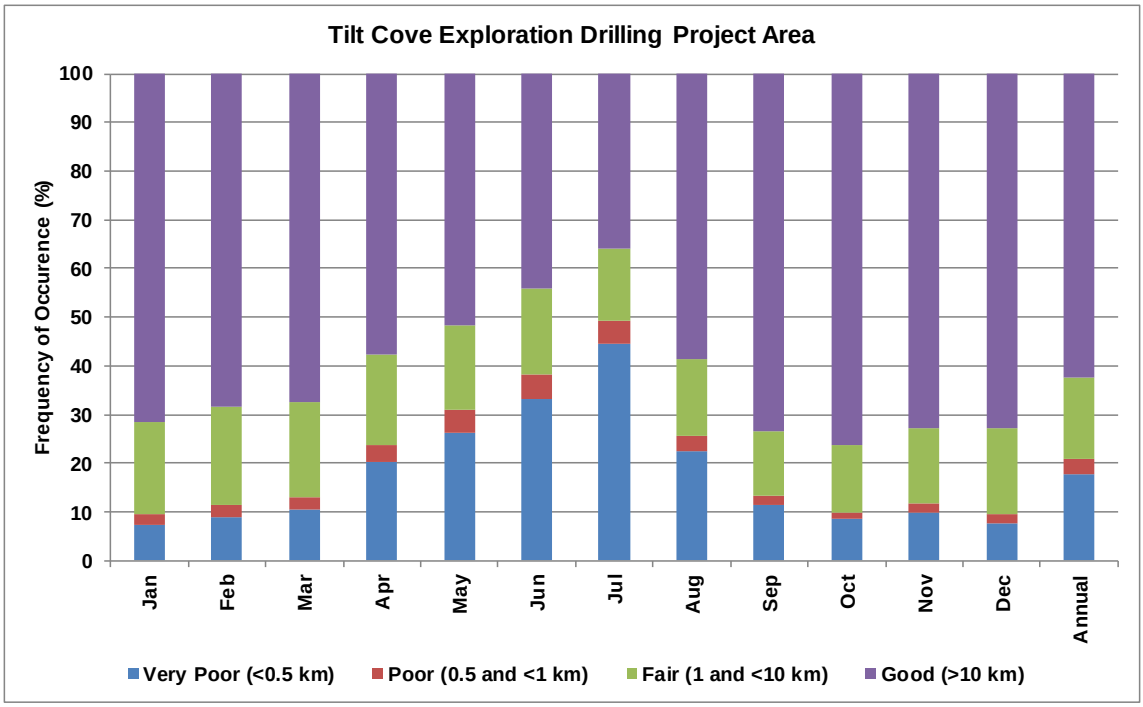

Figure 5-12 Frequency of Occurrence of Visibility (ICOADS), Project Area, 1980-2019

5.2.6 Lightning

Lightning is an electrical discharge most commonly produced in thunderstorms, usually accompanied by thunder. It occurs in clouds with vigorous convection where enough electrical charge is separated through the movement of cloud droplets and precipitation particles. By its nature, lightning is a localized phenomenon and, as a result, it is one which is difficult to accurately represent in numerical models. Measurements are available from the Canadian Lightning Detection Network; however, this is a land-based network, with coverage extending only to eastern NL (i.e., the Grand Banks is on the far eastern edge of the network).

The available lightning statistics from ECCC for eastern Canada provide some indication of conditions over the western portion of a vessel traffic route (ECCC 2016). This includes average dates for the beginning and ending of lightning season for eastern Canada as shown in Figure 5-13. Lightning occurs virtually year-round offshore Newfoundland (south of Newfoundland the lightning season starts in January, blue, and ends in December, red [Figure 5-13]). During winter, stronger strikes are possible.

5.2.7 Tropical Systems

While hurricanes making landfall in Newfoundland and Labrador are relatively rare occurrences, tropical systems, whether they are weakened hurricanes, tropical storms or post-tropical storms, do affect portions of the province and the marine offshore once or twice each year on average. These storms are tropical cyclones, “the generic term for non-frontal synoptic scale low-pressure systems over tropical or sub-tropical waters with organized convection (i.e., thunderstorm activity) and definite cyclonic surface wind circulation” (Holland 1993). Tropical depressions are tropical cyclones with maximum sustained surface wind speeds of less than 34 knots (17 m/s, 39 mph). Once wind speeds reach at least 34 knots these tropical cyclones are typically called tropical systems, and at 64 knots (33 m/s, 74 mph) are called hurricanes.

Hurricanes and tropical systems feed off warm ocean waters south of the Gulf Stream. Tropical systems tend to weaken considerably once they approach Newfoundland and Labrador due to the colder water temperatures. On occasion, tropical storms and hurricanes maintain their strength or weaken slowly as they approach the province for various reasons. Two important possibilities for stronger tropical systems affecting this area are the forward speed of the system and sea surface temperature anomalies. If the tropical storm/hurricane is travelling at a higher than average speed, the system does not have time to weaken, despite the cooler waters entering its core. Also, if sea surface temperatures south of Newfoundland are warmer than average (especially late in the summer and in early fall), the storm may be able to survive slightly longer as it approaches Atlantic Canada.

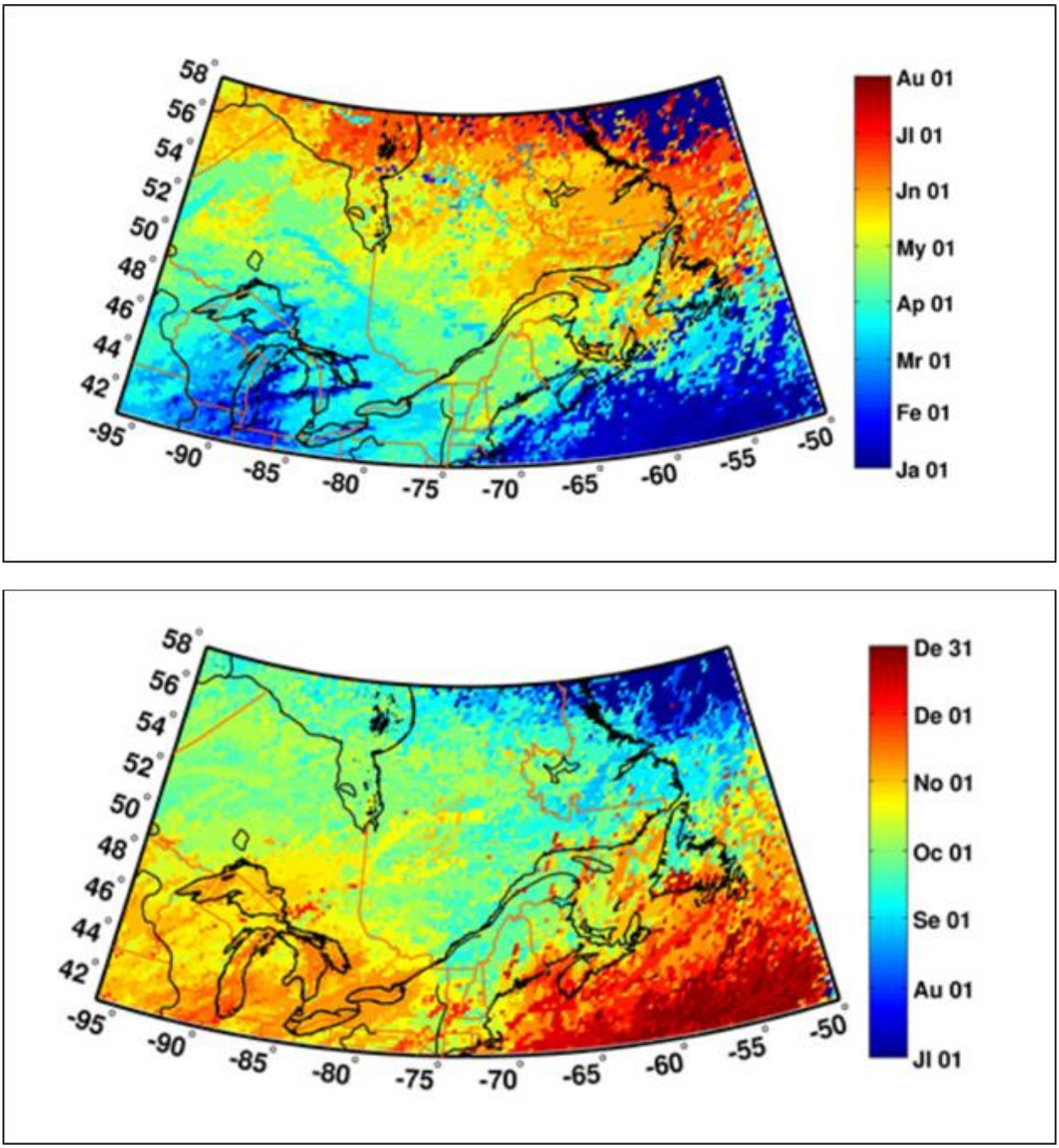

Source: ECCC (2016)

Figure 5-13 Average Start (top) and End (bottom) Dates of the Lightning Season for Eastern Canada, 1999-2013

Post-tropical storms are former tropical cyclones that no longer possess sufficient tropical characteristics to be considered a tropical cyclone yet can continue carrying heavy rains and high winds. One such class of post-tropical cyclone is an extra-tropical cyclone, a storm system that primarily gets its energy from the horizontal temperature contrasts that exist in the atmosphere. The storm obtains characteristics of extra-tropical (northern latitude) storms, developing frontal systems or merging with existing low pressure systems that have frontal systems. That is, the energy of the storm changes from being mainly due to the heat and moisture of the warm waters of the South Atlantic to energy due to cold versus warm air temperature contrasts. Extra-tropical cyclones often retain energy due to high moisture content and deep convection; this energy can be released into kinetic energy (winds) when a significant pool of cold air moves into the west side of the storm. For this reason, extra-tropical cyclones are often more volatile than 'typical' extra-tropical storms and can regenerate in intensity, often very rapidly.

Tropical systems can affect the Newfoundland offshore anytime during the Atlantic hurricane season (June 1 to November 30), but most activity generally occurs in the late summer to early fall. One of the main reasons for the increased activity during this time of year is the shift of the Bermuda High to the east, allowing systems over the Caribbean to track northward towards Atlantic Canada. The Bermuda High is a dominant ridge of high pressure over the Atlantic typically centered near Bermuda, which guides weather systems over the southern Atlantic Ocean towards the southeastern United States, and provides the dominant southwesterly flow to Eastern Canada during the summer. The sea surface temperatures south of Newfoundland typically reach their peak in late September, allowing systems that approach from the south to maintain their strength as they track towards Newfoundland.

The tropical storm history near the Project Area is provided from inspection of the tropical cyclone re-analysis database HURDAT2 which includes best-track estimates at 6-hourly intervals for tropical cyclone activity in the North Atlantic for the period 1851 to 2021 (National Hurricane Center [NHC] 2022a, 2022b).

Figure 5-14 shows the historical tracks of all tropical cyclones passing within 150 NM (278 km) of 46.4°N, 48.8°W near the Project Area centre, for the past 30 years of record, 1992 to 2021. Acknowledging the size of hurricanes can vary considerably, typical hurricanes may be on the order of 300 miles wide. Based on analysis of 1999-2009 storms in the North Atlantic, Chavas et al. (2016) calculated a mean storm radius size of approximately 274 km (148 NM).

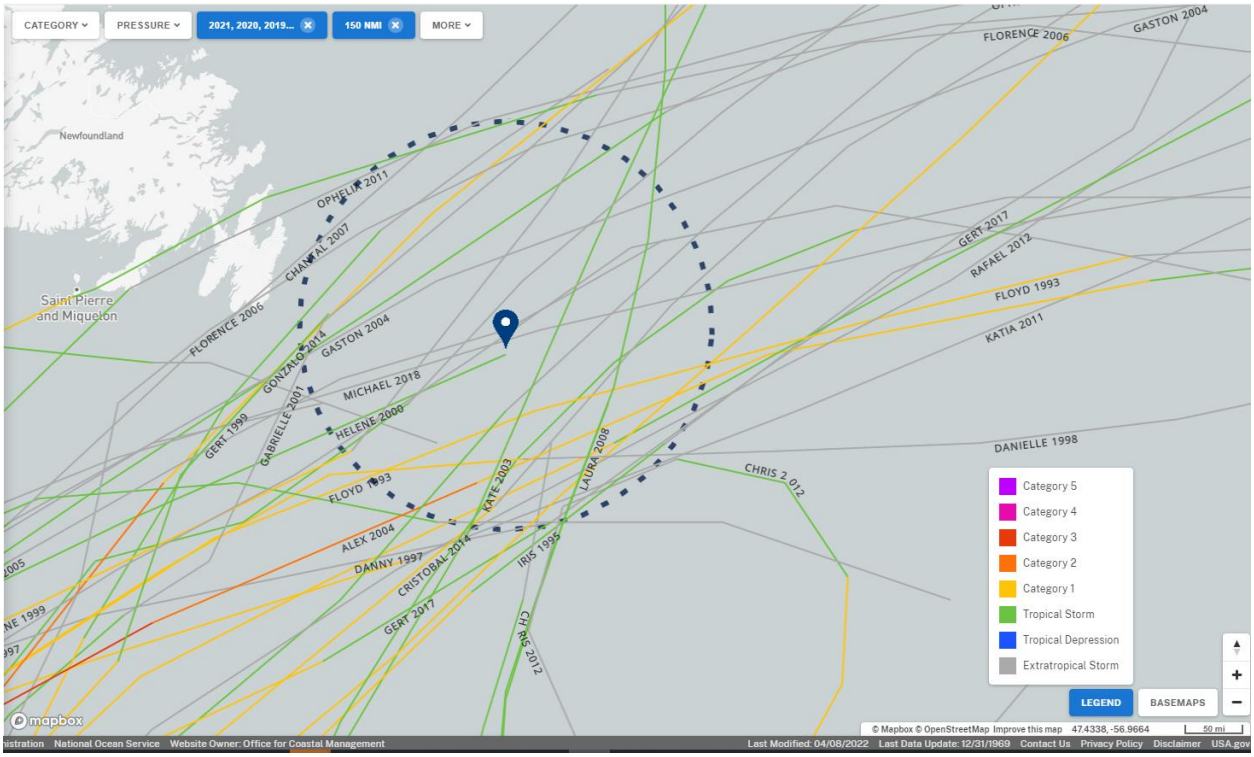

Source: based on NHC 2022b

Figure 5-14 Tropical Cyclones Passing within 150 n.mi. of 46.4°N, 48.8°W, 1992-2021

During the period 1992 to 2021, 37 storms passed through the selected region near the Project Area, 24 of them as extra-tropical cyclones. A storm summary is presented in Table 5.6 showing the dates of nearest approach and largest maximum sustained surface winds associated with any storm track position within the 150 NM of 46.4°N, 48.8°W (approximated by 44.0° to 49.0°N, 45.0° to 52.5°W). The 37 storms include 4 in July, 6 in August, 11 in September, 11 in October, and 2 in November. Five of the 37 storms were of hurricane strength when they passed near the Project Area, Gonzalo in 2014 being the most recent, which passed 50 NM to the northwest of the Project Area midday on 19 October 2014 (Figure 5-15). Also in 2014, Cristobal passed farther southeast of the Project Area on 29 August as an extratropical cyclone (after transitioning from a category 1 hurricane over the southern Grand Banks) with wind speeds of 65 knots. Bertha passed through the region as an extratropical (or post-tropical) storm with speeds of 40 knots on 7 August 2014. Prior to Gonzalo in 2014 the last hurricane tracking near the Project Area was Alex on the morning of 6 August 2004 with maximum sustained surface winds of 75 knots. The most recent tropical cyclone to pass near the Project Area was tropical cyclone Epsilon on 25 Oct 2020 with maximum sustained winds of 60 knots.

Table 5.6 Maximum Sustained Surface Wind (knots) of Tropical Cyclones Passing within 150 NM of 46.4°N, 48.8°W, 1992-2021

Storm (status)	Jul	Aug	Sep	Oct	Nov
FRANCES 1992 (TS)				60	
FLOYD 1993 (HU)			65		
FELIX 1995 (TS)		50			
CHANTAL 1995 (EX)	50				
IRIS 1995 (EX)			60		
HORTENSE 1996 (EX)			35		
DANNY 1997 (EX)	30				
BONNIE 1998 (EX)		45			
DANIELLE 1998 (HU)			65		
GERT 1999 (EX)			60		
IRENE 1999 (EX)				80	
HELENE 2000 (TS)			45		
DEAN 2001 (EX)		45			
GABRIELLE 2001 (EX)			60		
NOEL 2001 (EX)					50
FABIAN 2003 (HU)			70		
KATE 2003 (TS)				60	
GASTON 2004 (EX)			45		
ALEX 2004 (HU)		75			
FRANKLIN 2005 (EX)	40				
WILMA 2005 (EX)				40	
FLORENCE 2006 (EX)			65		
ISAAC 2006 (EX)				55	
CHANTAL 2007 (EX)		55			
LAURA 2008 (LO)				40	
BILL 2009 (TS)		60			
KATIA 2011 (EX)			75		
OPHELIA 2011 (EX)				45	
CHRIS 2012 (EX)	40 (June)				
RAPHAEL 2012 (EX)				55	
BERTHA 2014 (EX)		40			
GONZALO 2014 (HU)				70	
CRISTOBAL 2014 (EX)		65			
GERT 2017 (EX)		50			
RINA 2017 (LO)					40

Table 5.6 Maximum Sustained Surface Wind (knots) of Tropical Cyclones Passing within 150 NM of 46.4°N, 48.8°W, 1992-2021

Storm (status)	Jul	Aug	Sep	Oct	Nov
MICHAEL 2018 (EX)				65	
EPSILON 2020 (TS)				60	
Total	4	9	11	11	2

Source: based on NHC 202219a

Status legend:

EX - Extratropical cyclone (of any intensity)

HU - Tropical cyclone of hurricane intensity (> 64 knots)

LO - A low that is neither a tropical cyclone, a subtropical cyclone, nor an extratropical cyclone (of any intensity)

SS - Subtropical cyclone of subtropical storm intensity (> 34 knots)

TD – Tropical cyclone of tropical depression intensity (< 34 knots)

TS - Tropical cyclone of tropical storm intensity (34-63 knots)

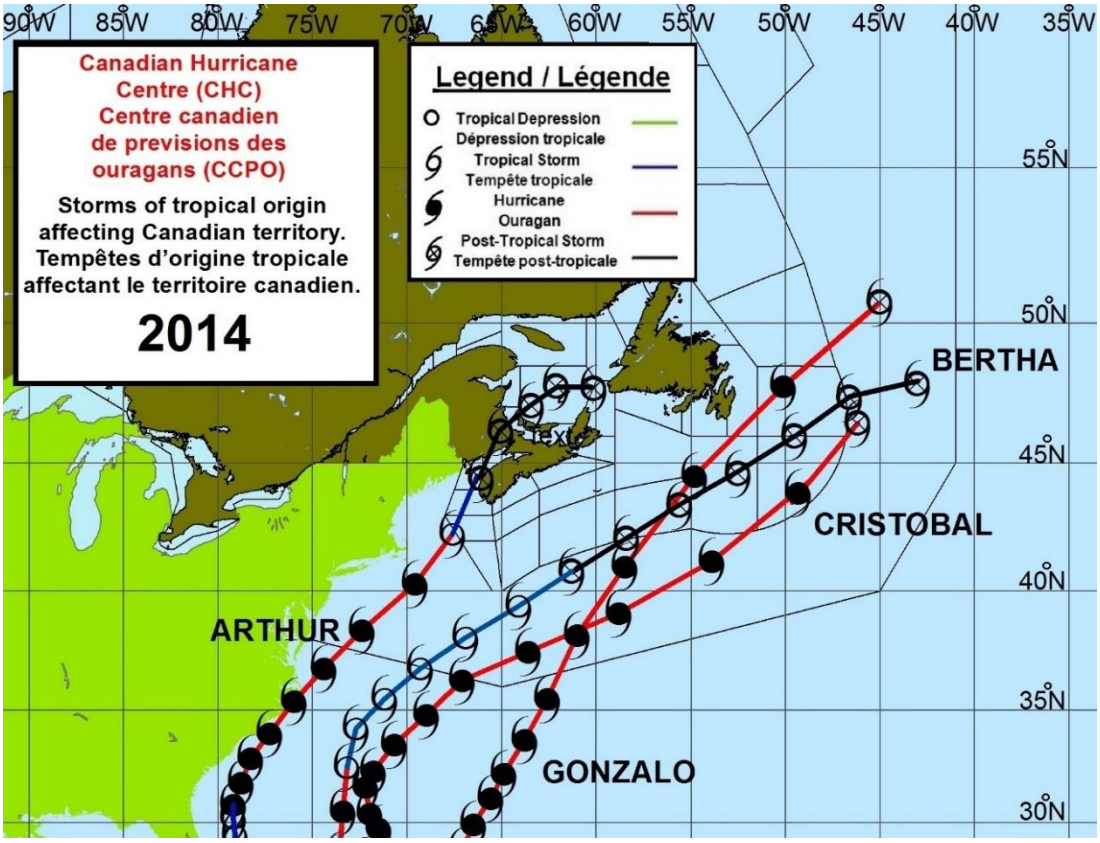

Source: Government of Canada 2019

Figure 5-15 2014 Storm Tracks

5.3 Physical Oceanography

The physical oceanography setting for the Project Area is described in terms of bathymetry, ocean currents, waves, extreme winds and waves, tides, storm surge and water properties.

Additional details for the larger Eastern Newfoundland Offshore Area and regions between St. John's and the Project Area are provided in the Eastern Newfoundland SEA, Section 4.1 (IAAC 2021).

5.3.1 Bathymetry

The bathymetry of the Project Area and surrounding region is generally well known (Figure 5-16). The Project Area is located on the Grand Banks of Newfoundland and extends from 240 km from St. John's in the northwest to 400 km from St. John's in the southeast. The Project Area is shallowest to the southwest with depths ranging from approximately 60 to 80 m and deepens to approximately 120 m to the east. The 200 m depth contour lies at the southeast corner of the Project Area and is approximately 40 to 50 km east of the Project Area to the north.

Approximately 150 km to the northeast of the Project Area lies the Sackville Spur which extends the nose of the Grand Banks at depths of up to 1,000 m. To the east of the Grand Banks lies the Flemish Pass, with depths of almost 1,300 m. On the eastern side of the Flemish Pass, water depths rise again to the Flemish Cap, a large bathymetric feature of approximately 50,000 km² with depths rising back up to approximately 130 m. The Flemish Pass extends to the northeast, remaining at depths of approximately 1,000 to 1,100 m, and separates the Orphan Basin to the northwest and the Flemish Cap to the east. Water depths in the Orphan Basin range from approximately 1,200 m at the edge of the continental shelf to as deep as 3,300 m south of the Orphan Knoll. The Orphan Knoll lies about 100 km to the northeast, in water depths of around 2,000 m, and is a bathymetric high in the centre of the Orphan Basin. The Labrador Basin and deep ocean lie farther offshore to the north and east of the Orphan Basin and Flemish Cap, with depths from approximately 3,000 m to greater than 4,000 m.

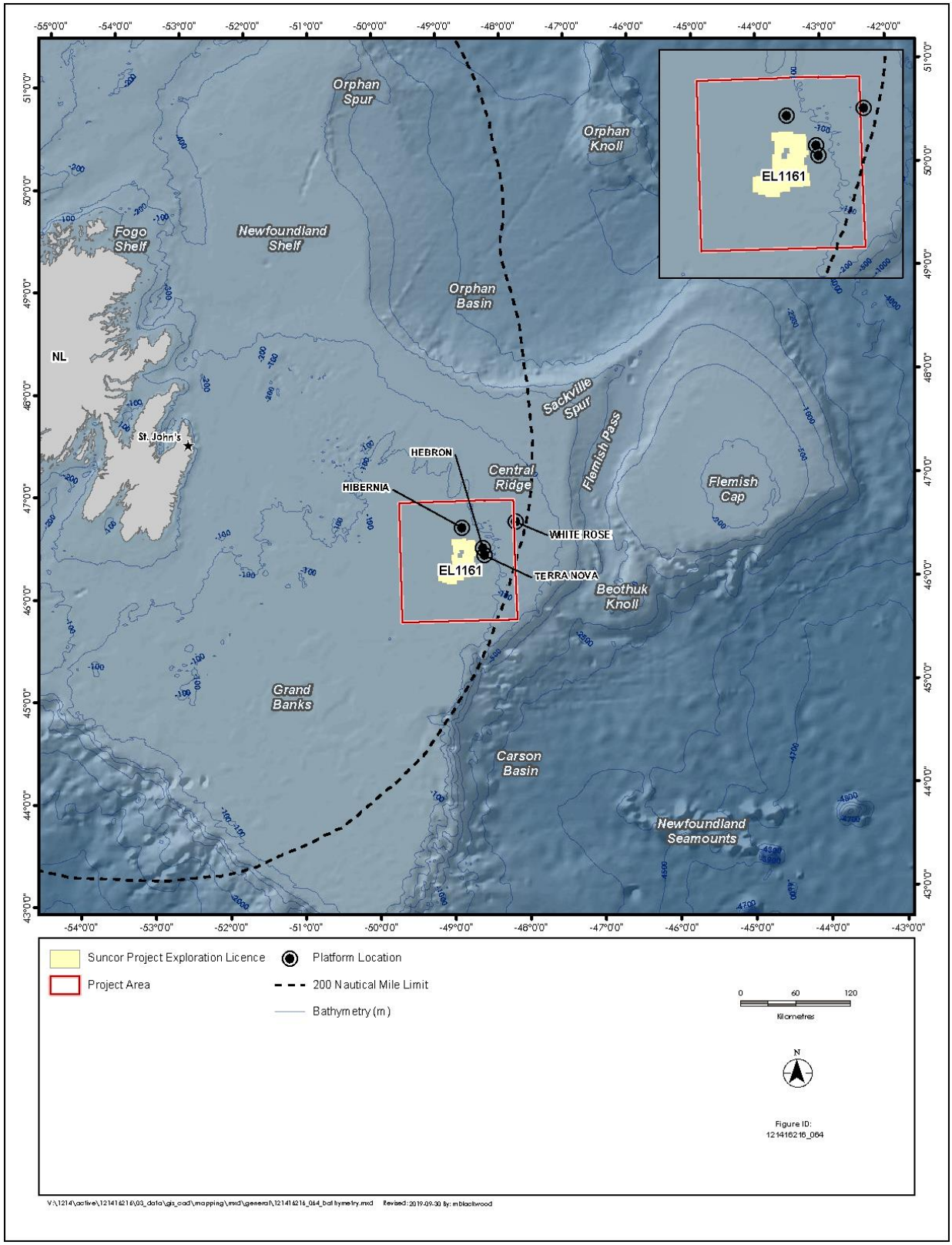

Figure 5-16 General Bathymetry

5.3.2 Ocean Currents

The cold Labrador Current dominates the general circulation over the Eastern Newfoundland Offshore Area. The Labrador Current is divided into two streams: an inshore branch that flows along the coast on the continental shelf; and an offshore branch that flows along the outer edge of the Grand Banks (Figure 5-17). The Labrador Current's inshore branch tends to flow mainly in the Avalon Channel closely along the coast of the Avalon Peninsula but may sometimes also spread farther out on the Grand Banks. The offshore branch flows over the upper Continental Slope at depth, and through the Flemish Pass with depths almost to 1,300 m.

The offshore Labrador Current (which remains bathymetrically trapped over the upper Continental Slope) has average speeds of approximately 40 cm/s carrying approximately 85% of the total transport, mainly between the 400 and 1,200 m isobaths (Lazier and Wright 1993). Over areas of the Grand Banks with water depths less than 100 m, such as the southwest region of the Project Area, the mean currents are generally weak (less than 10 cm/s) and flow southward, dominated by wind-induced and tidal current variability (Seaconsult Ltd. 1988). Warm Gulf Stream waters are generally located south of the Grand Banks, but do on occasion move north onto the southern edge of the banks.

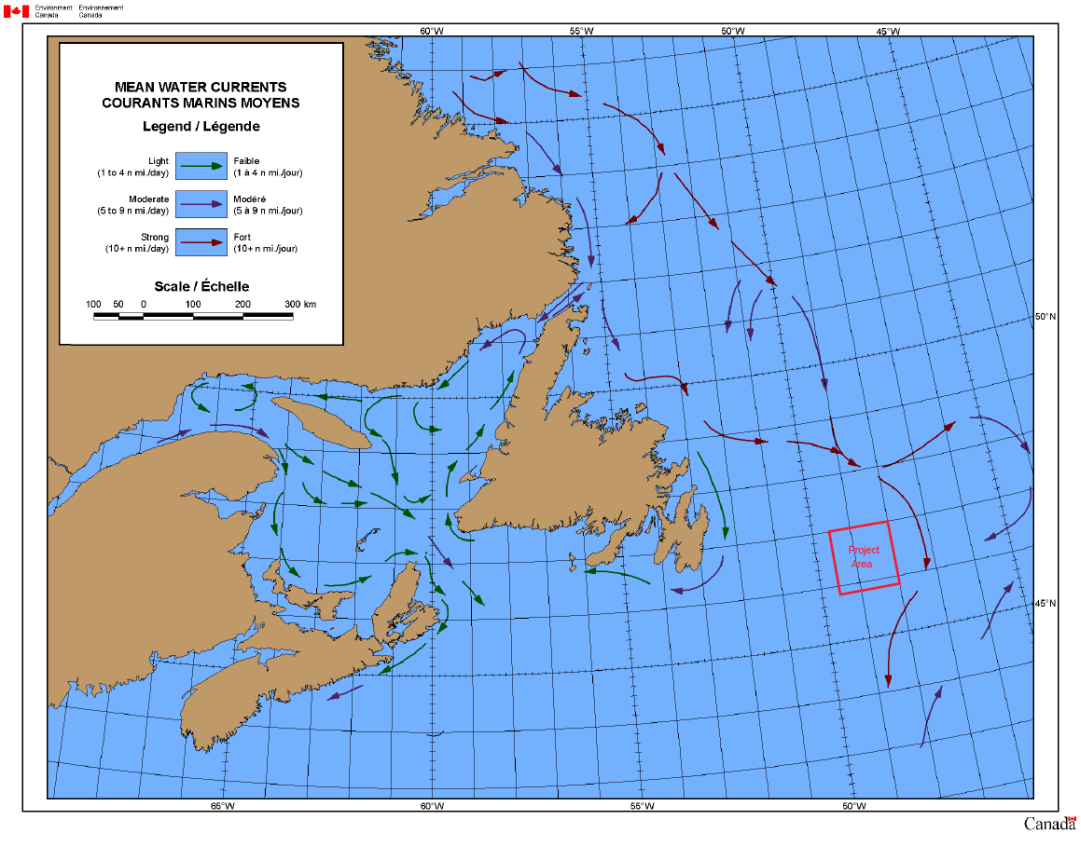

Source: Based on CIS (2011)

Figure 5-17 Mean Water Currents

For a characterization of currents over the Project Area, current meter measurement statistics from the Bedford Institute of Oceanography (BIO) ODI (Gregory 2004) database are reported. The database consists of all current meter records that have a record length of at least five days within a given month. The database was queried for the area extending from 45°N to 48°N, 47°W to 50°W (DFO 2019a) and values were further subset to include those just within the Project Area.

A total of 674 monthly current statistic records were returned for the Project Area, from 223 mooring stations at instrument depths ranging from 1 to 126 m. These measurements are limited to the northeastern quadrant of the Project Area as shown in Figure 5-3. The 674 monthly mean and maximum currents speeds are shown in Figure 5-18.

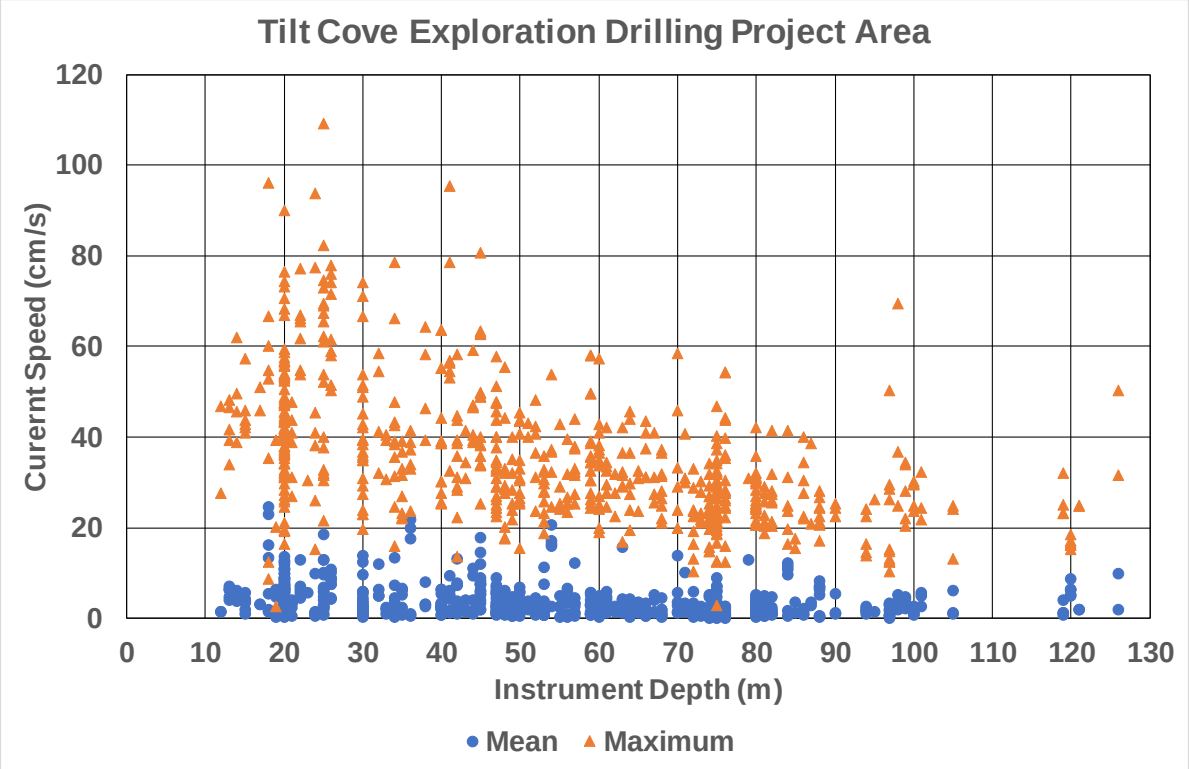

Source: Based on DFO (2019b)

Figure 5-18 Mean and Maximum Ocean Currents, Project Area

Statistics based on the monthly mean and monthly maximum current speeds are summarized in Table 5.7 based on depth, and in Table 5.8 based on month. The average of all monthly mean current speeds is on the order of 4 cm/s for all depths with maximum monthly mean speeds ranging from 9.9 cm/s for depths greater than 100 m to 24.6 cm/s for a near-surface depth bin of 0 to 30 m. The average of all monthly maximum current speeds is on the order of 36 cm/s for all depths with monthly maximum speeds of 96 to 109 cm/s for instrument depths above 60 m (Table 5.7). Current speeds are generally greatest in the late summer through early winter with average monthly mean speeds up to 5.3 cm/s in October and maximum monthly mean speeds of 24.6 cm/s in September; corresponding spring values are approximately one half. The average monthly maximum current speeds range from 25.7 cm/s in April to 43.6 cm/s in November, with monthly maximum speeds of 109.3 cm/s in August (Table 5.8).

Table 5.7 Mean and Maximum Ocean Currents, by Depth, Project Area

Instrument Depth	Mean Current Speed (cm/s)			Maximum Current Speed (cm/s)			Number of Monthly Values
	Minimum	Average	Maximum	Minimum	Average	Maximum	
0 to 30 m	0.20	5.0	24.60	2.60	46.8	109.3	167
30 to 60 m	0.20	4.0	21.70	13.50	37.7	95.5	234
60 to 100 m	0.10	2.4	15.80	2.90	27.6	69.5	249
100 to 200 m	0.70	3.5	9.90	13.00	24.8	50.3	24
Total	0.10	3.7	24.60	2.60	35.8	109.3	674
Source: Based on DFO (2019b)							

Table 5.8 Mean and Maximum Ocean Currents, by Month, Project Area

Month	Mean Current Speed (cm/s)			Maximum Current Speed (cm/s)			Number of Monthly Values
	Minimum	Average	Maximum	Minimum	Average	Maximum	
Jan	0.20	4.5	20.60	2.60	37.4	78.6	53
Feb	0.40	4.7	18.40	10.20	36.6	63.7	45
Mar	0.30	3.4	15.90	8.70	34.5	55.3	30
Apr	0.10	3.0	17.00	10.20	25.7	52.2	40
May	0.10	2.5	11.00	14.50	27.4	67.3	69
Jun	0.20	2.9	11.50	2.90	33.3	82.4	66
Jul	0.30	2.7	13.40	13.00	32.6	65.6	79
Aug	0.20	2.8	16.10	16.10	34.3	109.3	68
Sep	0.20	3.4	24.60	16.60	41.5	96.2	63
Oct	0.10	5.3	23.00	16.40	40.6	77.4	64
Nov	0.60	5.0	21.70	18.40	43.6	77.9	52
Dec	0.80	4.9	12.80	23.20	43.1	95.5	45
Source: Based on DFO (2019b)							

A further illustration of currents in the Project Area is provided by the WebDrogue CECOM (Canadian East Coast Ocean Model) model (DFO 2015a), and tidal predictions for a full year derived from the WebTide model (DFO 2015b).

Wu et al. (2012) conducted an extensive comparison of the CECOM model results and 11 years of observational data, including both qualitative visual comparisons, and quantitative methods based on statistical analysis. Their comparisons indicated that the main circulation features from the observations were successfully reproduced by the model. Furthermore, the comparison indicated particularly good levels of agreement between model predictions and observations in the regions of the Labrador Shelf, Newfoundland Shelf, and the Flemish Pass, with a mean correlation coefficient of 0.91 (ideal value is 1) across all seasons and depths within the Flemish Pass, and an average ratio of kinetic energy difference to the observations of 0.12 (where a lower value is better, and the value of 0.5 indicates "a fair agreement").

SUNCOR

The models yield currents at five depth levels: surface, 100 m, 500 m, 1,000 m and bottom. To provide an illustration of the range of current speeds for the Grand Banks and Flemish Pass region, spring and fall conditions (when speeds are generally least and greatest) are shown for surface and bottom depths (the two of the five depth levels most relevant for the Project Area) in Figures 5-19 to 5-22; closer views of fall currents focusing on the Project Area are shown in Figures 5-23 and 5-24.

Modelled surface current speeds are less than 10 cm/s over most of the Project Area, only reaching as high as 20 to 25 cm/s in the southeast corner of the Project Area. Bottom currents are about half the magnitude of the surface current speeds. Mean currents, light as they are, are predominantly to the south or south-southwest. Much greater speeds of the Labrador Current of 30 to 50 cm/s and above are evident in the Flemish Pass to the east.

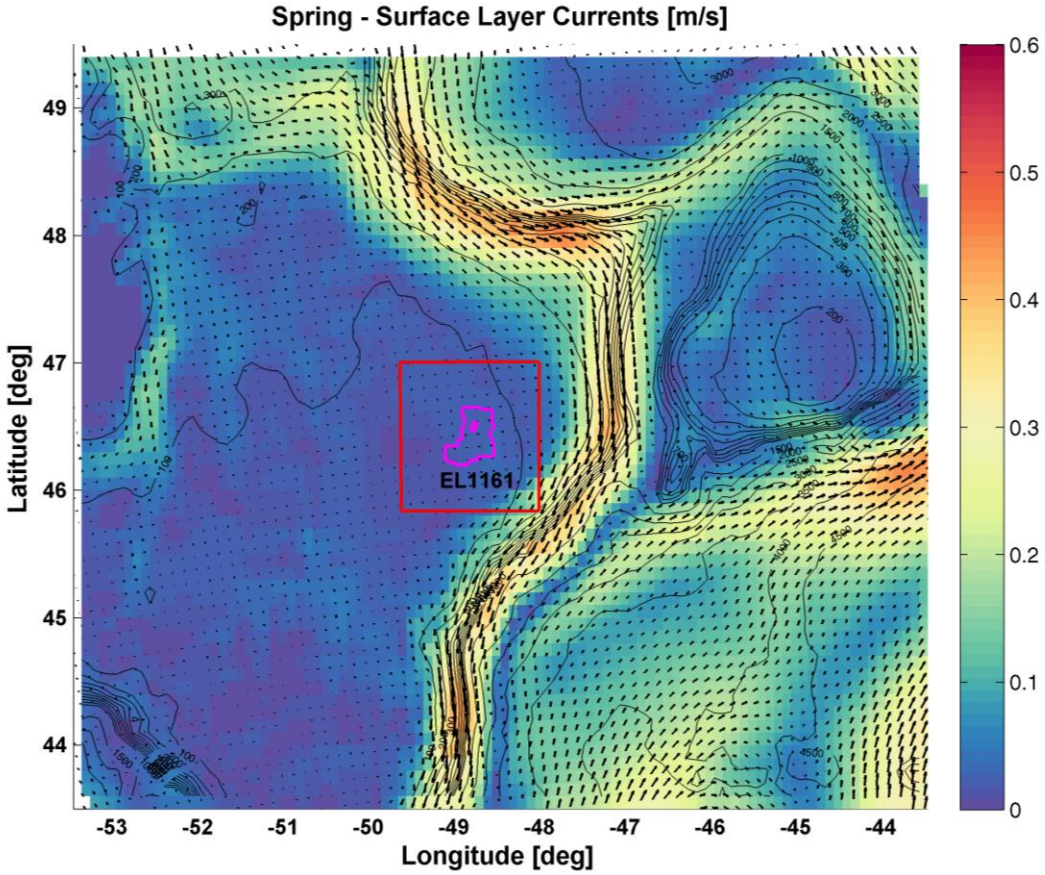

Source: based on WebDrogue CECOM (DFO 2015a), WebTide (DFO 2015b)

Figure 5-19 Spring, Surface Currents

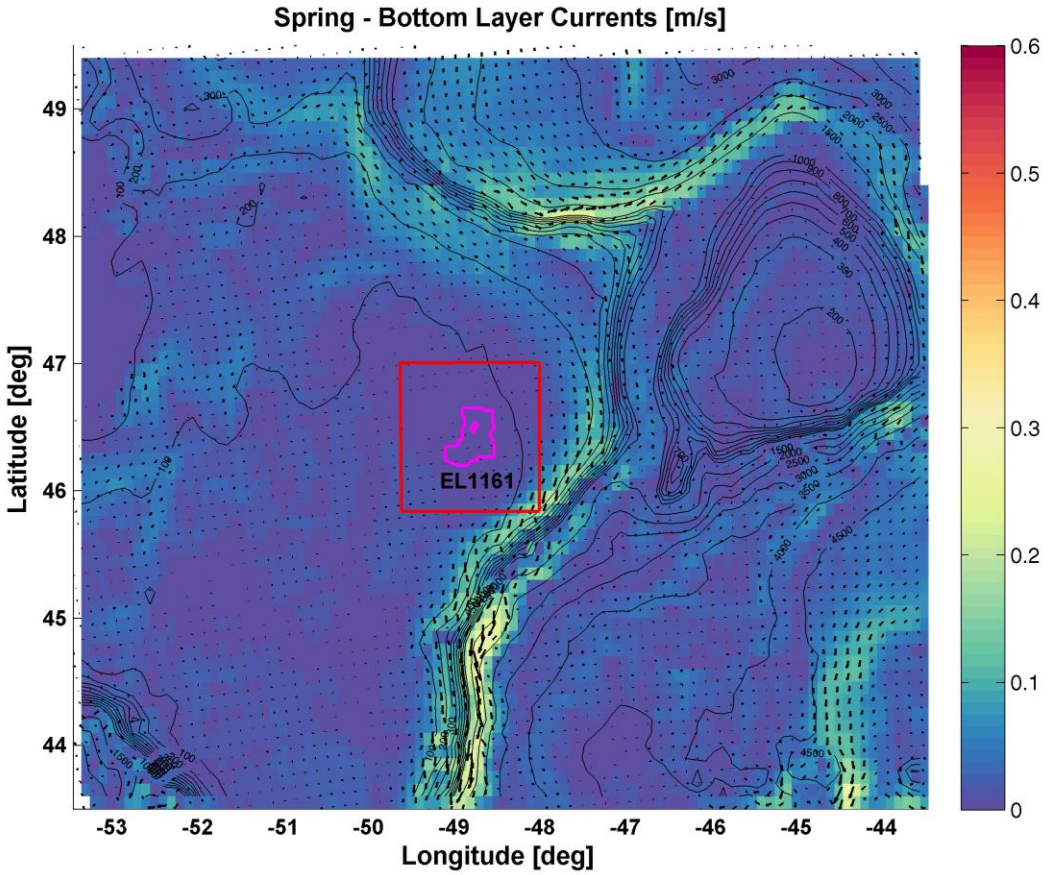

Source: based on WebDrogue CECOM (DFO 2015a), WebTide (DFO 2015b)

Figure 5-20 Spring, Bottom Currents

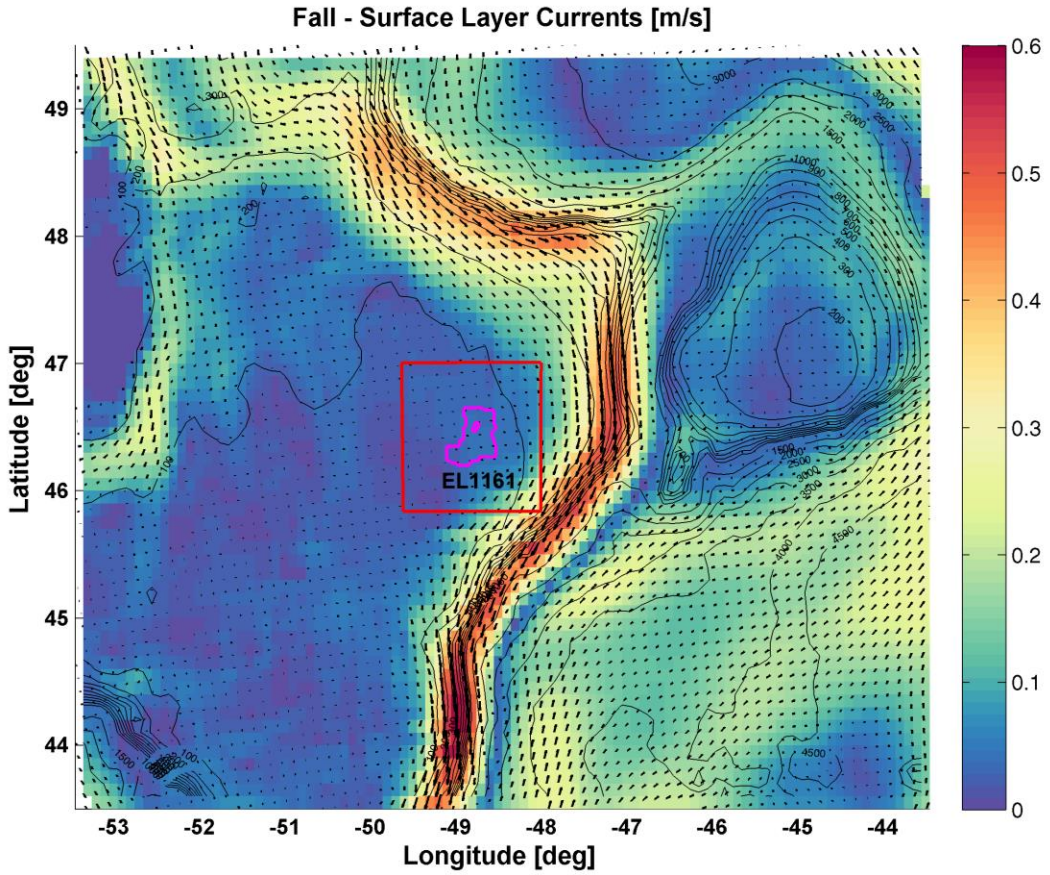

Source: based on WebDrogue CECOM (DFO 2015a), WebTide (DFO 2015b)

Figure 5-21 Fall, Surface Currents

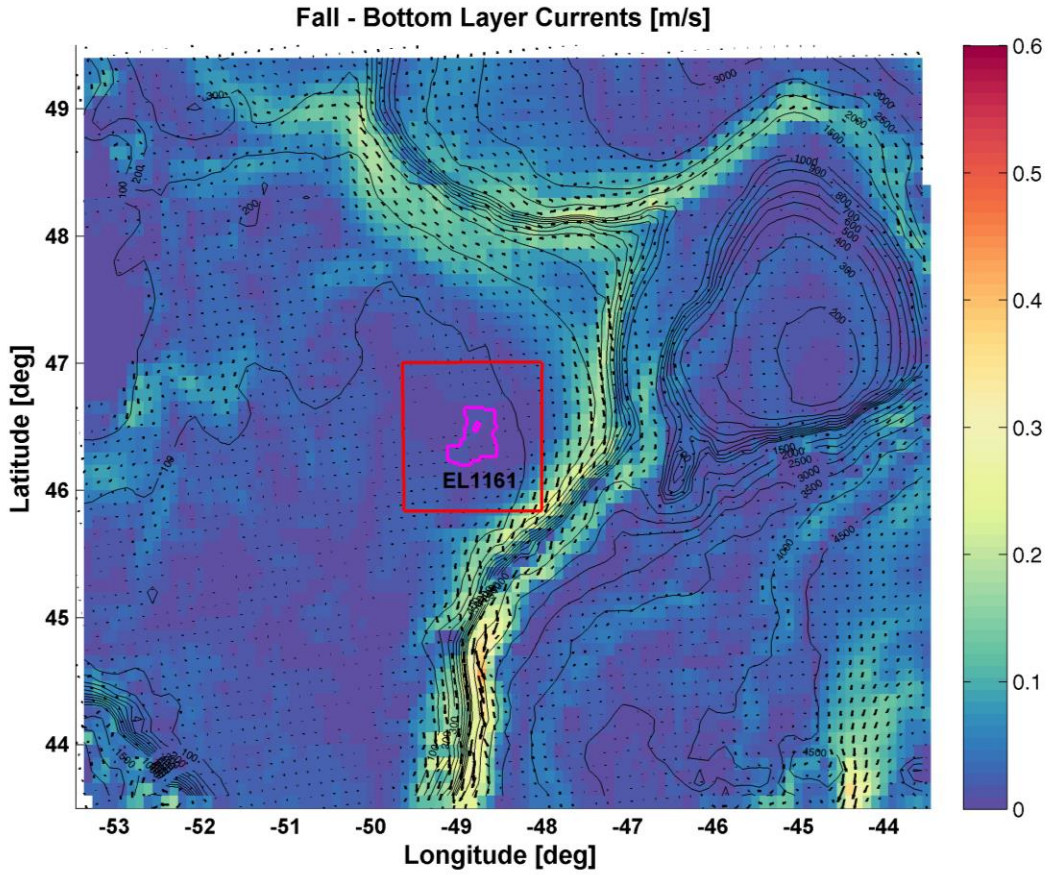

Source: based on WebDrogue CECOM (DFO 2015a), WebTide (DFO 2015b)

Figure 5-22 Fall, Bottom Currents

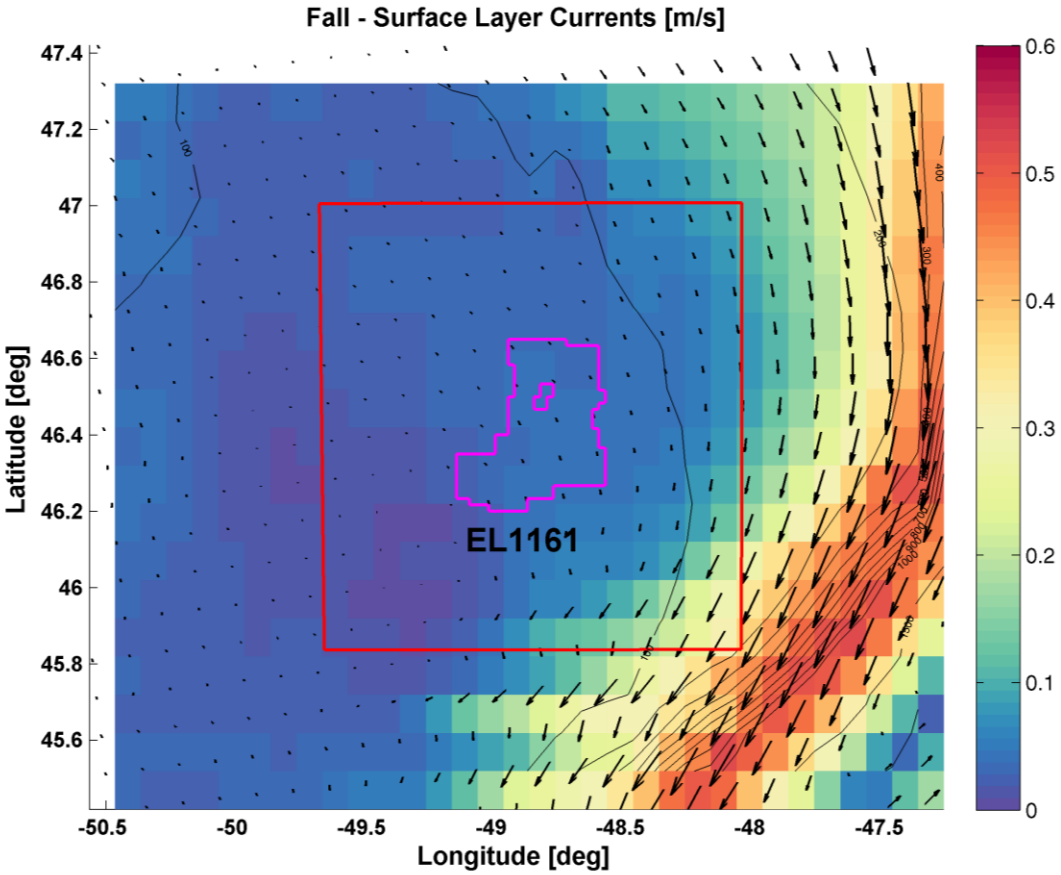

Source: based on WebDrogue CECOM (DFO 2015a), WebTide (DFO 2015b)

Figure 5-23 Fall, Surface Currents, Magnified to View EL 1161

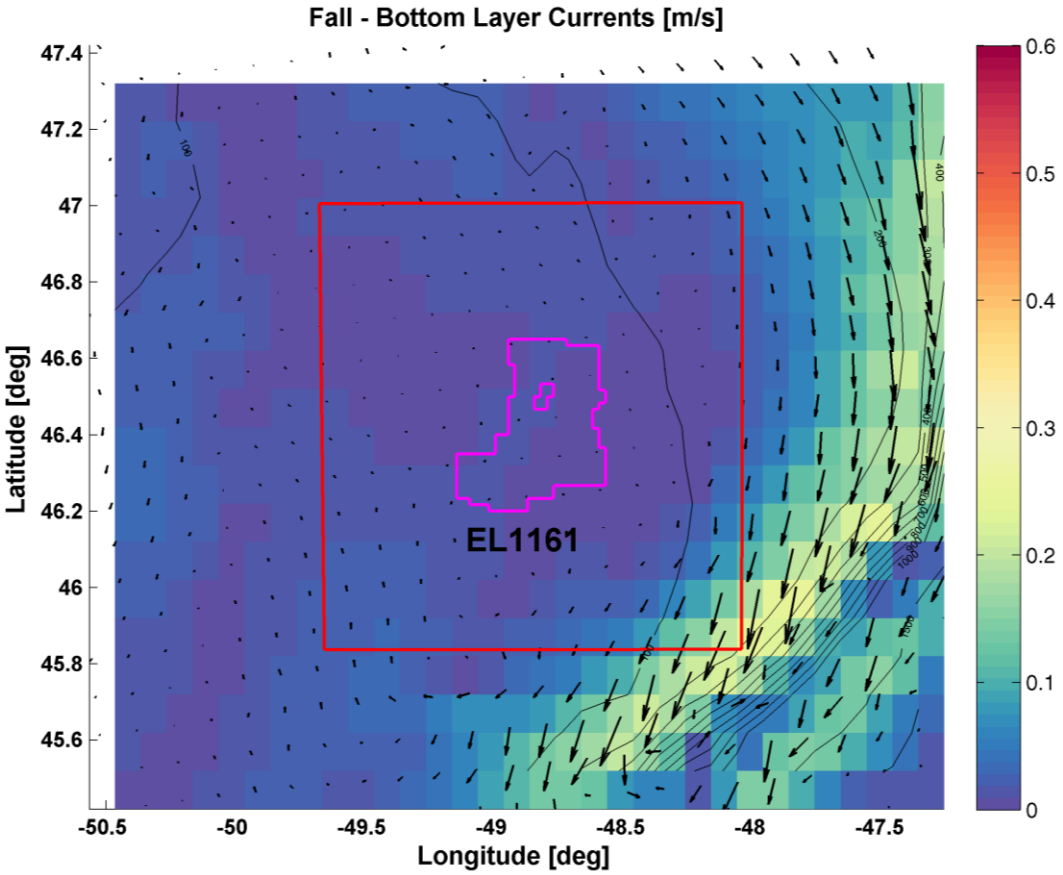

Source: based on WebDrogue CECOM (DFO 2015a), WebTide (DFO 2015b)

Figure 5-24 Fall, Bottom Currents, Magnified to View EL 1161

5.3.3 Wave Climatology

The wave climate within the Project Area has been characterized by descriptive statistics derived from the MSC50 wind and wave hindcast dataset (DFO 2022). The wave hindcast was conducted by using the wind field reanalysis to force a third-generation wave model (Swail et al. 2006) over the north Atlantic Ocean. The model used was Oceanweather's OWI-3G, adopted onto a 0.5 degree grid on a basin-wide scale. Inscribed in the 0.5 degree model was a further refined 0.1 degree shallow water implementation of the OWI-3G model, which allowed for shallow water effects to be accounted for in the maritime region. The MSC50 methodology and results have been extensively documented and validated (Swail and Cox 2000; Woolf et al. 2002; Caires et al. 2004).

As presented earlier for wind conditions, the MSC50 grid point M6010432 located in the centre of the Project Area is taken as representative of the Project Area (see Figure 5-3). This provides a general indication of wave conditions, however, is not intended as a substitute for detailed oceanographic information for design or operational purposes.

The wave climate is described in terms of the significant wave height (Hs, defined as four times the square root of the total variance of the wave energy spectrum), and the peak wave spectral period (Tp, defined as the period of waves with the highest contribution to the energy spectrum). Ocean waves are created by wind at the air / water interface. Winds are caused by dominant local and regional weather systems and exhibit a pronounced seasonal variability. Wind waves (or sea) will be generated in the immediate area of wind, developing quickly within an hour. Swells are remnants of the wind waves after they propagate away from where they were generated. Swells are long waves that contain a lot of wave energy and can take days to subside. The range of wave periods for wind waves and swells overlap considerably with wind waves having periods up to 15 seconds (s) for large wind speeds, while swells of 5 seconds are possible.

Table 5.9 presents monthly wave height and wave period statistics for MSC50 node M6010432. Mean wave heights range from approximately 1.7 m in July to 4.0 m in January. The most severe sea states, above 12 m, occur during December through February with maximum significant wave heights of up to 14.0 m in February. These maximum wave heights are reported for directions from southwest. Associated wave peak periods are 15 to 16 s. In contrast, maximum significant wave heights are less than half of this (6.1 m) in July, with associated peak periods of 11 s.

Monthly and annual wave roses for node M6010432 are shown in Figures 5-25 and 5-26. A general description of roses is provided in Section 5.2.1 for the directional distribution of winds. Wave roses for the directional distribution of significant wave height can be similarly interpreted.

Waves are predominantly from the southwest from spring through summer and shifting to the southwest through northwest for fall and winter. In July, waves are from the southwest 51% of the time and from the south through west 83% of the time. July waves are 3 m or less 97% of the time and above 5 m just 0.2% of the time. In January, waves are predominantly from the west, 25% of the time, and from the southwest through northwest 63% of the time. January waves are 3 m or less 26% of the time and above 5 m for 20% of the time. Significant wave height values are in the 1 to 5 m range, annually, 90% of the time; peak wave period values are in the 5 to 16 s range 95% of the time.

Table 5.9 Monthly and Annual Wave Statistics, MSC50 Node M6010432, 1962-2018

Location	Jan	Feb	Mar	Apr	May	Jun	Jul	Aug	Sep	Oct	Nov	Dec	Year
Mean Hs (m)													
M6010432	4.0	3.8	3.2	2.7	2.2	1.9	1.7	1.8	2.3	2.9	3.3	3.9	2.8
Mean Tp (s)													
M6010432	10.3	10.0	9.4	9.0	8.5	7.9	7.7	7.7	8.7	9.3	9.7	10.2	9.0
Most Frequent Direction (from)													
M6010432	W	W	SW	SW	SW	SW	SW	SW	SW	W	NW	W	SW
Maximum Hs (m)													
M6010432	12.3	14.0	11.0	10.8	9.7	9.4	6.1	8.8	11.0	11.4	12.0	12.9	14.0
Tp of Maximum Hs (s)													
M6010432	14.9	15.9	14.4	14.3	13.8	13.0	10.8	13.3	14.2	14.4	14.4	15.5	15.9
Maximum Tp (s)													
M6010432	17.3	17.1	17.7	17.1	17.3	14.1	17.2	17.4	17.3	17.6	15.9	17.3	17.7
Direction of Maximum Hs (from)													
M6010432	SW	SW	SW	SW	NW	NW	NW	SW	SW	SW	W	SW	SW
Source: M6010432 based on DFO (2019b2022), M6011422 (Husky Energy 2018)													

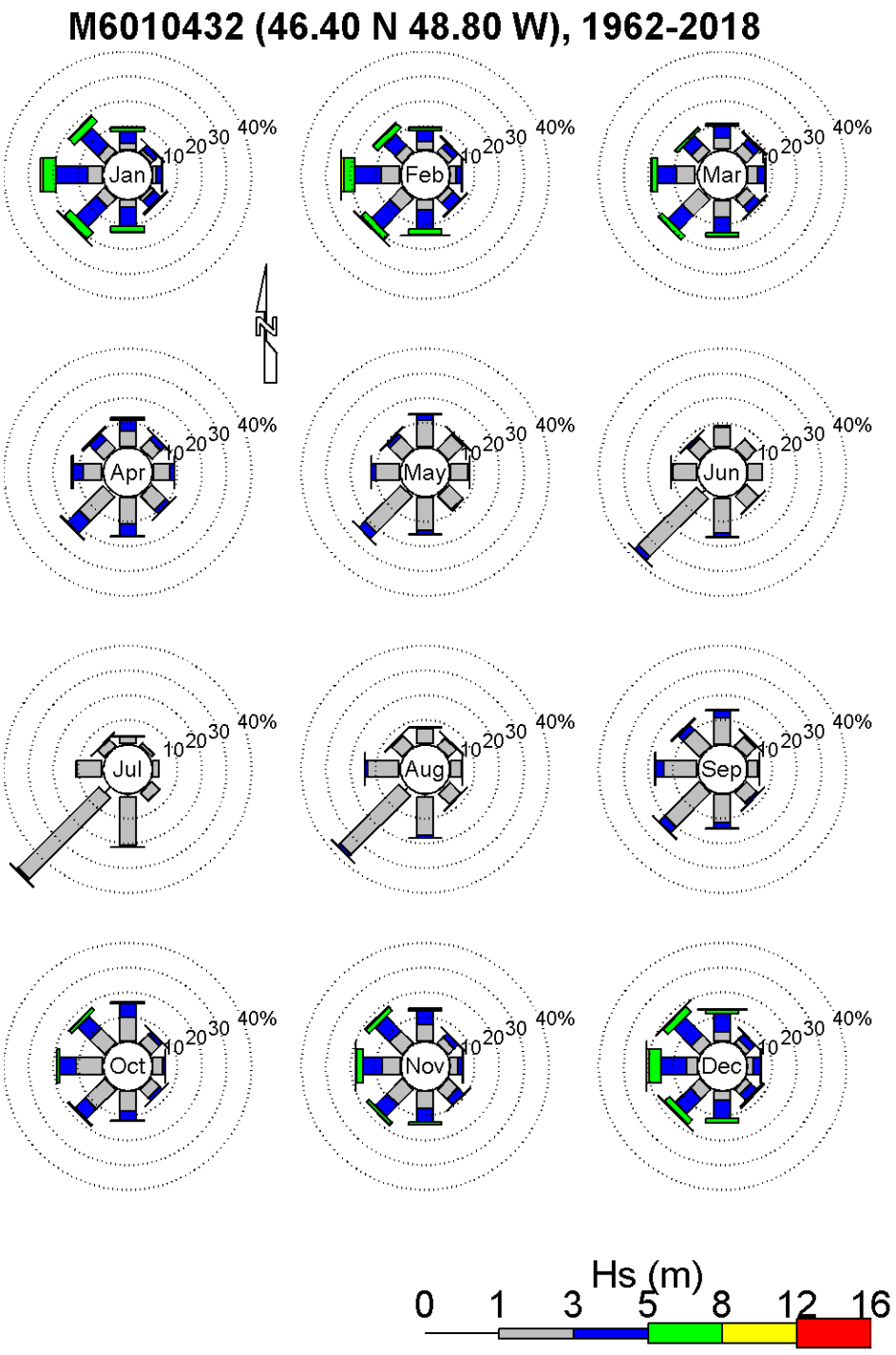

Source: Based on DFO (2022)

Figure 5-25 Monthly Wave Roses, MSC50 Node M6010432, 1962-2018

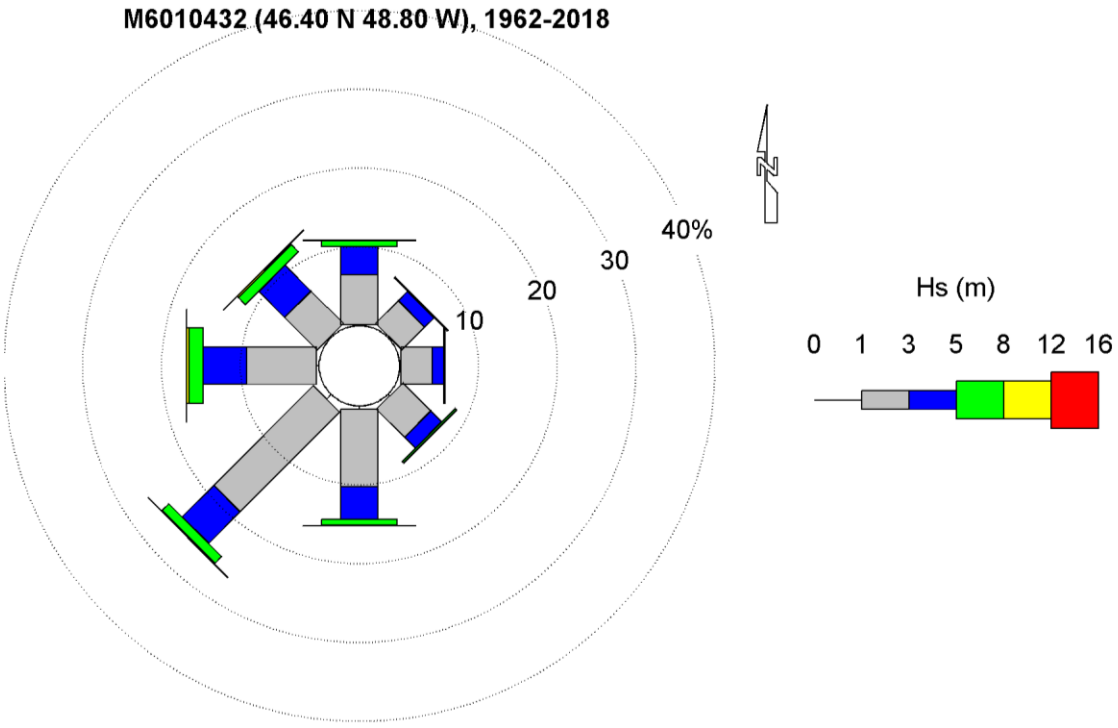

Source: Based on DFO (2022)

Figure 5-26 Annual Wave Rose, MSC50 Node M6010432, 1962-2018

5.3.4 Extreme Winds and Waves

To estimate extreme wind and wave conditions, extremal analysis was performed with the MSC50 node M6010432 (see also Section 5,2,1 and 5.3.3) to determine the highest expected values for wind speed, and significant wave height. The analysis was based on the Gumbel distribution to which the data were fitted using the maximum likelihood method. The analysis includes both tropical and extra-tropical storms over the entire period. The Gumbel fit is done using the maximum likelihood method. Lower and upper 95% confidence intervals are calculated.

Extreme values were estimated for four different return periods: 1, 10, 50 and 100 years (Table 5.10). In the Project Area, extreme wind speeds range from 23.8 m/s to 34.2 m/s for the 1-year and 100-year return periods, respectively, while extreme significant wave heights range from 9.5 m to 15.3 m for the 1-year and 100-year return periods, respectively.

Table 5.10 Extreme Wind and Wave Estimates, MSC50 Node M6010432, 1962-2018

Return Period (years)	1	10	50	100
Wind Speed (m/s)	23.8 +/- 0.44	29.2 +/- 1.2	32.7 +/- 1.8	34.2 +/- 2.1
Significant Wave Height (m)	9.5 +/- 0.3	12.6 +/- 0.6	14.5 +/- 0.9	15.3 +/- 1.0
Source: based on DFO (2022)				

5.3.5 Tides

Water level variations due to tides in the Project Area are generally quite predictable. Several models are available for the prediction of water levels at specific locations where the tidal constituents are known or can be extrapolated from other locations.

Using the WebTide model (DFO 2015b, Dupont et al. 2002), based on tidal modelling studies conducted by DFO, tidal water levels are computed for the Project Area at the same location of the referenced MSC50 node (used for wind and wave analysis). These results are presented in Table 5.11.

Table 5.11 Tidal Predictions

Project Area Location	Tidal Constituent	Constituent Amplitude (cm)	Phase (deg GMT)
46.4°N, 48.8°W	M_2	21.4	333.9
	K_1	7.3	160.2
	N_2	4.2	313.0
	S_2	9.8	13.5
	O_1	5.5	142.0

Source: based on WebTide (DFO 2015b)
Notes:
K1 = Diurnal, luni-solar diurnal, tide-producing force constituent
M2 = Semi-diurnal, principal lunar, tide-producing force constituent
N2 = Semi-diurnal, larger lunar elliptic, tide-producing force constituent
O1 = Diurnal, principal lunar diurnal, tide-producing force constituent
S2 = Semi-diurnal, principal solar, tide-producing force constituent

5.3.6 Storm Surge

Storm surge is the abnormal rise in seawater level during a storm, measured as the height of the water above the normal predicted astronomical tide. Storm surge amplitudes can be high in coastal areas, but surges with comparatively smaller amplitudes can also occur offshore, away from the coastline. A hazard from storm surges is elevated mean water levels, specifically when they occur at high tide. Extreme storm surge calculations based on a study by Bernier and Thompson (2006), which used a hindcast of water levels over 40 years, and calculated a potential 100-yr storm surge of 90 cm in the northwest Atlantic at the location of the MSC50 M6010432 data point, 46.4°N, 48.8°W with a 10,000-yr storm surge of 1.17 m.

5.3.7 Temperature, Salinity, pH and Turbidity

Statistical summaries of sea temperature and salinity are presented using the hydrographic database of the BIO ODI (DFO 2019c) which was queried for the Project Area for depths down to 200 m, and with 10 m bin size averaging. The query returned 16,060 results for temperature that span the years 1960 to 2009 and for depths down to 150 m. As shown in Figure 5-27 the observations are generally well-distributed over the Project Area with concentrations near Hibernia, Terra Nova and Hebron, and east towards White Rose. All months and depths are sampled in the data set. Winter months have the fewest observations, 75 to 120 for January through March, while April through July each provide from 1913 to 4393 observations. Each depth from 0 to 80 m has from 1249 to 1683 observations (89% of the total observations).

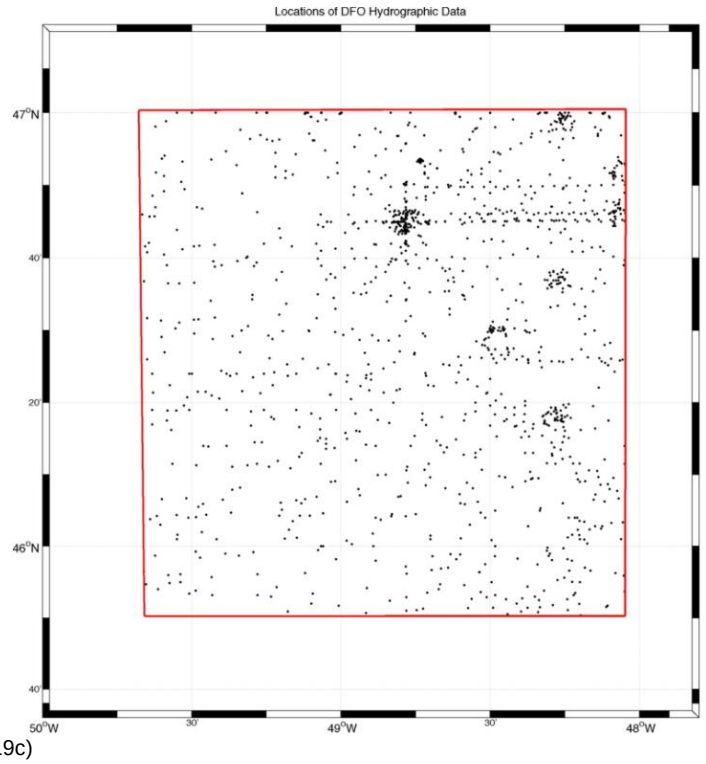

Source: based on DFO (2019c)

Figure 5-27 Location of ODI Hydrographic Observations, Project Area, 1960-2009

Depth contours of monthly mean sea temperature for the Project Area based on the ODI database (DFO 2019c) are presented in Figure 5-28. A maximum depth of 120 m is presented given the Project Area and majority of corresponding ODI observations (99%) are in this depth range. Figure 5-29 presents a companion depth contour of monthly mean salinity for the Project Area.

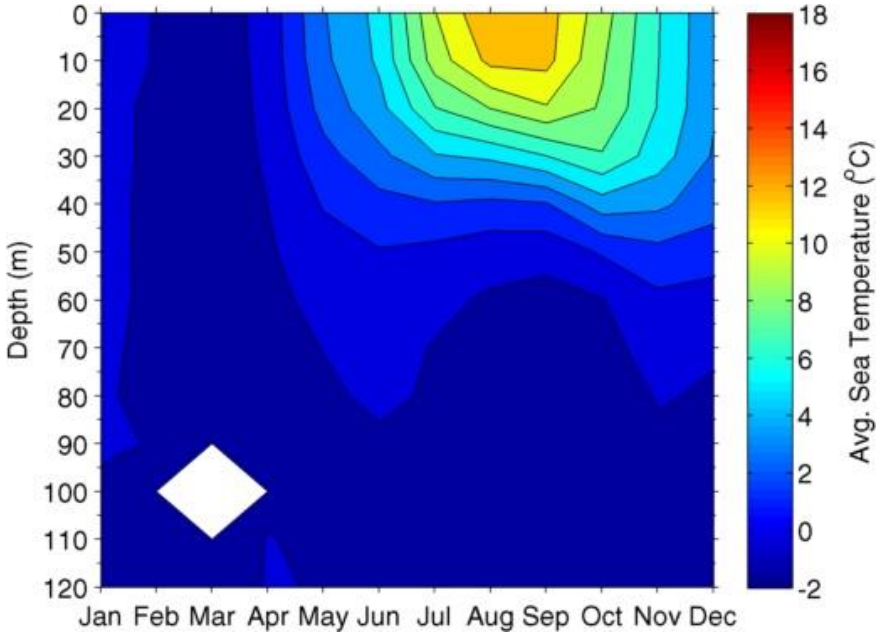

Source: based on DFO (2019c)

Figure 5-28 Monthly Average Sea Temperature

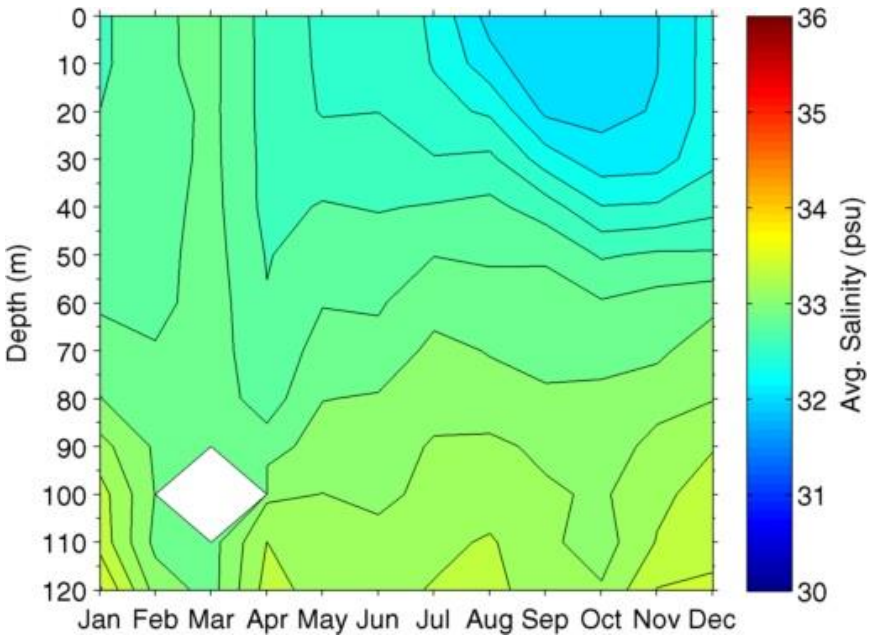

Source: based on DFO (2019c)

Figure 5-29 Monthly Average Salinity

The thermohaline structure in the water column over the Project Area can be considered as a two-layer system comprising a surface layer and a subsurface layer, separated by a thermohalocline (i.e., the portion of the water column with the greatest vertical temperature and salinity gradients). As evident in Figure 5-28, between January and March, sea temperature is vertically homogeneous. Increased solar radiation warms the surface layer in spring, and light summer winds are not able to mix the water column to as great a depth as the stronger winter winds. The result is the formation of a warm surface mixed layer with maximum monthly mean surface temperatures and a strong thermocline in August and September. Both the mixed layer and thermocline erode between October and December due to increased solar radiation and stronger storm-generated or winter winds that mix the water column to greater depths. This mixing of the warm surface layer with progressively deeper waters causes the maximum monthly mean temperatures of the subsurface water to be lagged in time by two to three months from the maximum mean temperatures of the surface layer (Seaconsult 1988).

Mean sea temperatures at the surface range from -1.2°C in March to 12.8°C in August, averaging 5.3°C annually. Minimum sea temperatures at the surface range from -1.8°C in March to 9.3°C in August, while monthly maximum temperatures range from 0.3°C in March to 18.2°C in September. At 60 m mean sea temperatures range from -1.2°C in March to 0.7°C in November. Near-bottom, below 100 m, monthly mean sea temperatures range from -1.6°C to 0.2°C and average -0.7°C (Figure 5-28).

The surface layer is warmer and less saline than the subsurface layer throughout the year (Figure 5-29). Monthly sea surface salinities range from a minimum of 31.0 PSU in August to a maximum of 34.0 PSU in April and average 32.4 PSU annually. This is consistent with the general surface pattern of warmer and fresher water in late summer and fall and colder and more saline water in winter and early spring. For the subsurface layer, lagging surface conditions by several months, the water is relatively warm and fresh in the winter and cold and saline in summer and fall.

Measurements of pH exist from the White Rose EEM from both near-field and from 28 km to the northwest and northeast of the *SeaRose FPSO* (White Rose located just east of the Project Area [Figure 5-3]). Values of pH have ranged from 6.3 to 8.1 in mid-October 2010, 7.77 and 8.04 in late August 2012, and 8.03 and 8.18 in early November 2014 (Husky Energy 2011, 2013, 2017).

Additional measurements for pH data for the region are scarce; however, two data sources are noted. One characterization comes from data collected from the World Ocean Circulation Experiment (WOCE) database for the entirety of the Atlantic Ocean (National Oceanic and Atmospheric Administration (NOAA) -National Centers for Environmental Information 2022). Figure 5-30 (left panel) shows that surface waters in the Atlantic Ocean have a pH (adjusted to 25°C temperature) range of 8.0 to 8.1, which decreases to approximately 7.7 at 1,000 m depth, then remains stable to the ocean floor. A second data source from the Global Ocean Data Analysis Project (GLODAP) dataset (Olsen et al. 2019) is a May 2001 cruise at 48.5°N, 45.0°W approximately 280 km northeast of the Project Area. The pH profile from this cruise shows surface waters with a pH around 7.9, which decreases to approximately 7.7 at 700 m depth.

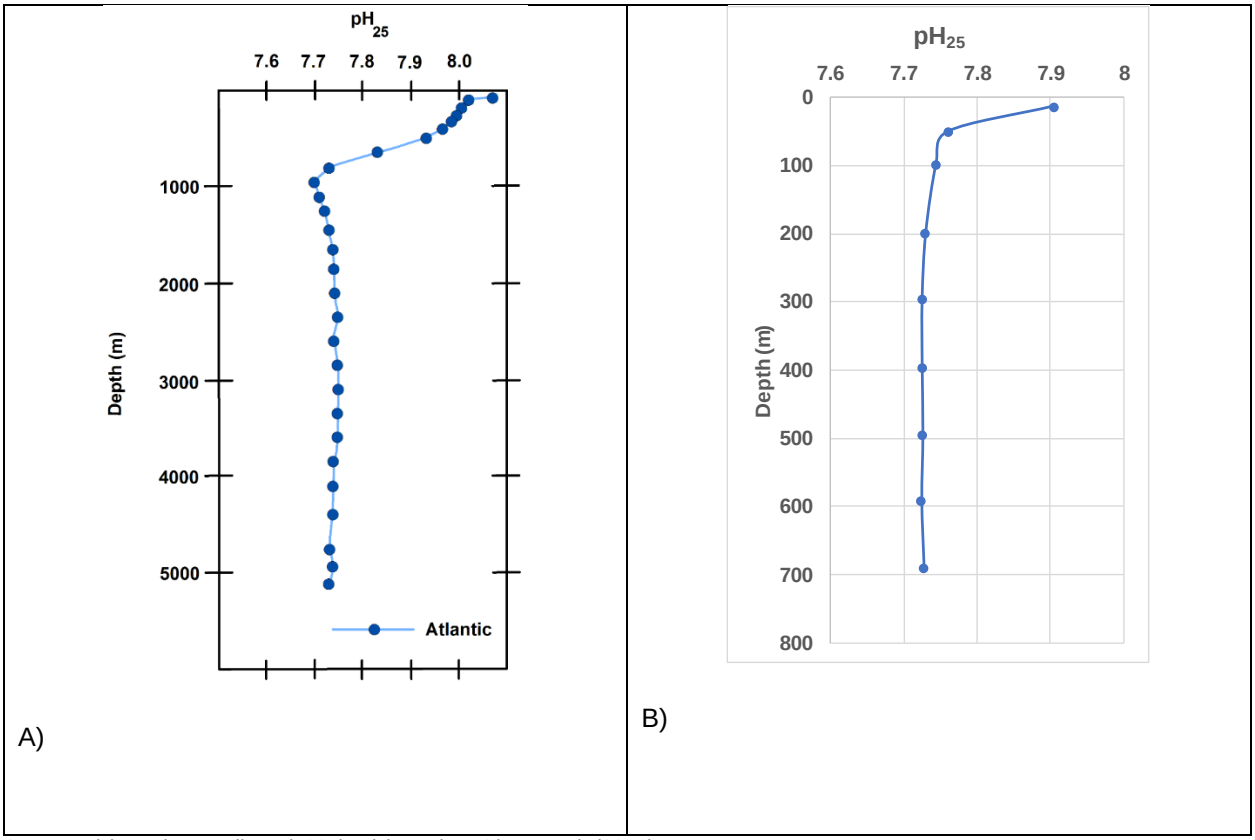

Source: A) based on Wallace (1997); B) based on Olsen et al. (2019)

Figure 5-30 pH for the Atlantic Ocean, A) from the WOCE; B) from GLODAP Cruise, May 2001

Turbidity data are similarly scarce for the Project Area. Data are available from NOAA, from a cruise in March of 2011 in an area north of Flemish Pass (Ullman et al. 2013). From this cruise, turbidity is approximately 0.2 to 0.3 nephelometric turbidity units (NTU) in near-surface waters and steadily decreases to below 0.01 at 200 m and deeper. There is some potential for seasonal variability associated with biogenic fallout.

5.4 Sea Ice and Icebergs

5.4.1 Sea ice

This section provides an overview of the sea (drift or pack) ice conditions most likely to be encountered in the Project Area. Information is drawn from the CIS Sea Ice Climatic Atlas for the East Coast 1981-2010 (CIS 2011). The atlas includes three key separate statistical analyses of conditions: i) frequency of presence of sea ice; ii) median of ice concentration when ice is present, and iii) median of predominant ice type when ice is present. Thickness can be inferred from ice type. The 1981-2010 atlas provides the most recent and comprehensive climatology description of sea ice conditions in the region[1]. A brief review of the 2011 to 2019 week ice charts is noted.

Given that the CIS Regional Ice Charts are not always prepared on the same dates each year, a seven-day period centered on historical dates is used in the ice atlas. The atlas climate data represent information from charts within three days on either side of the historical date. For example, the chart for historical date 15 January is representative for the period 12 to 18 January.

As noted in the ice atlas, variations in the extent of ice over East Coast waters, and hence the Project Area, are great due to both winds and temperatures being effective in changing the location of the ice edge. A large variability in sea ice conditions can therefore be experienced from year to year, and in a given year, on time scales of days to weeks and over comparatively small geographic scales of tens of kilometres.

To characterize overall conditions, the sea ice is described for the four corners and centre of the Project Area. Each of these five locations was overlaid on each of the weekly atlas charts. The corresponding frequency of ice presence, ice concentration and ice type was noted for all weeks for each location. The resulting tabulations are presented in Tables 5.12 to 5.14. To accompany Table 5.13 for median ice concentration, when ice is present, Figure 5-31 (derived from the MANICE publication (CIS 2005)) illustrates the scale in which ice concentration is reported, from open water (ice concentration of less than $^{1}/_{10}$) to compact/consolidated ice ($^{10}/_{10}$ concentration). To accompany Table 5.14, for median of predominant ice type, when ice is present, Table 5.15 from MANICE (CIS 2005) lists the stages of sea ice development that occur together with their associated thickness.

Values are colour-coded to show at a glance the weekly change in ice conditions for all five locations of the Project Area. It is emphasized that, for simplicity, these tables report just one value for each location whereas conditions may vary considerably across any given region. While some of the variation in conditions is discussed below, for a higher resolution study the atlas (CIS 2011) should be consulted. It is further noted that conditions reported here are from climatology and each year will be different.

For most of the Project Area the frequency of presence of sea ice during February through April is 1 to 15%, or about as frequent as every six or seven years. There is a slightly increased frequency of presence of sea ice at 16% to 33% during the first three weeks of March for the northern part of the Project Area and for the week of 2 April at the northern boundary. In general, for a given week, the sea ice is more likely of greater concentration and thickness in the northern and eastern portions and less severe in the southwest. While sea ice may on average reach the northern boundary of the Project Area by the week of 22 January,

[1] A new (30 year, 1991-2020) CIS sea ice atlas is expected in 2022; at the next opportunity that information could be included in any project assessment.

SUNCOR

the sea ice season typically lasts from the week of 5 February to the middle of April. By the end of April patches of ice may be present to the north and east of the Project Area, otherwise the region is ice free.

Table 5.12 Frequency of Presence of Sea Ice (%)

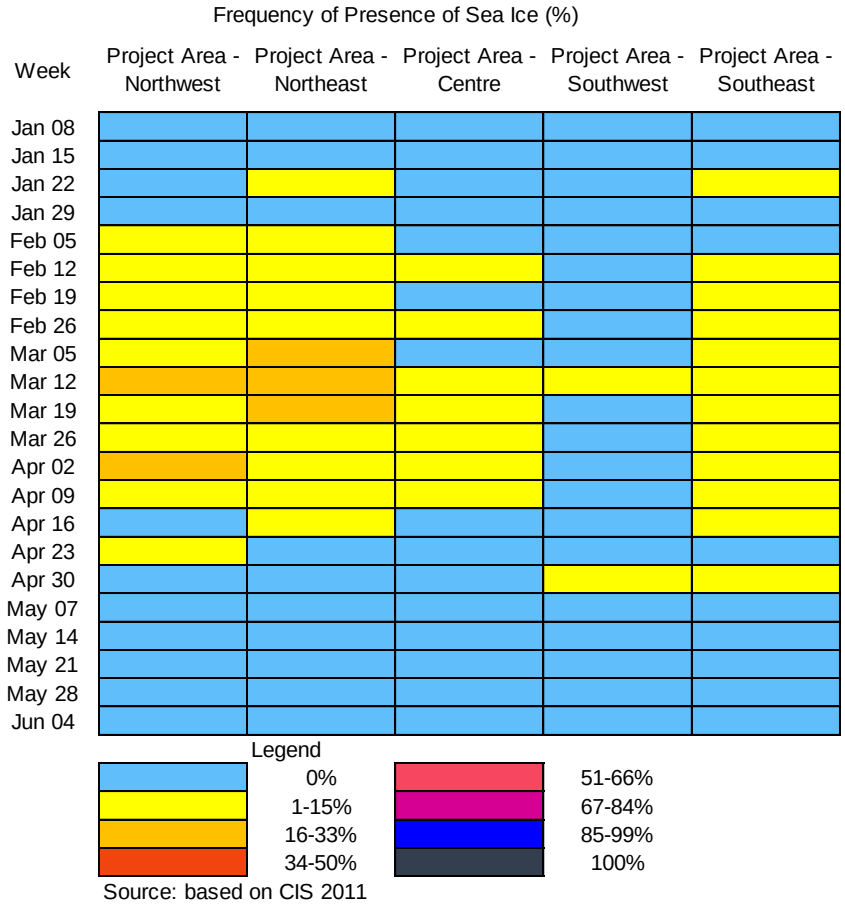

Source: based on CIS 2011

Table 5.13 Median of Ice Concentration, When Ice is Present

Median of Ice Concentration When Ice is Present

Week	Project Area - Northwest	Project Area - Northeast	Project Area - Centre	Project Area - Southwest	Project Area - Southeast
Jan 08	less than 1/10	less than 1/10	less than 1/10	less than 1/10	less than 1/10
Jan 15	less than 1/10	less than 1/10	less than 1/10	less than 1/10	less than 1/10
Jan 22	less than 1/10	7-8/10	less than 1/10	less than 1/10	1-3/10
Jan 29	less than 1/10	less than 1/10	less than 1/10	less than 1/10	less than 1/10
Feb 05	7-8/10	7-8/10	less than 1/10	less than 1/10	less than 1/10
Feb 12	7-8/10	7-8/10	1-3/10	less than 1/10	1-3/10
Feb 19	9-9+1/0	9-9+1/0	less than 1/10	less than 1/10	4-6/10
Feb 26	7-8/10	7-8/10	9-9+1/0	less than 1/10	7-8/10
Mar 05	7-8/10	7-8/10	less than 1/10	less than 1/10	7-8/10
Mar 12	7-8/10	7-8/10	4-6/10	4-6/10	7-8/10
Mar 19	7-8/10	7-8/10	7-8/10	less than 1/10	4-6/10
Mar 26	4-6/10	7-8/10	4-6/10	less than 1/10	4-6/10
Apr 02	4-6/10	7-8/10	7-8/10	less than 1/10	1-3/10
Apr 09	1-3/10	7-8/10	4-6/10	less than 1/10	7-8/10
Apr 16	less than 1/10	4-6/10	less than 1/10	less than 1/10	1-3/10
Apr 23	1-3/10	less than 1/10	less than 1/10	less than 1/10	less than 1/10
Apr 30	less than 1/10	less than 1/10	less than 1/10	1-3/10	1-3/10
May 07	less than 1/10	less than 1/10	less than 1/10	less than 1/10	less than 1/10
May 14	less than 1/10	less than 1/10	less than 1/10	less than 1/10	less than 1/10
May 21	less than 1/10	less than 1/10	less than 1/10	less than 1/10	less than 1/10
May 28	less than 1/10	less than 1/10	less than 1/10	less than 1/10	less than 1/10
Jun 04	less than 1/10	less than 1/10	less than 1/10	less than 1/10	less than 1/10

Legend

less than 1/10		7-8/10	
1-3/10		9-9+1/0	
4-6/10		10/10	

Source: based on CIS 2011

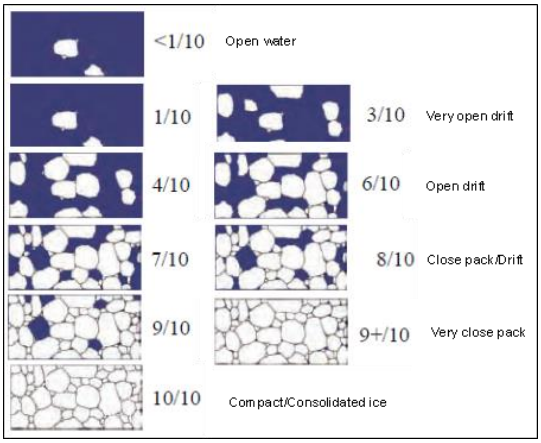

Source: CIS (2005)

Figure 5-31 Ice Concentrations from an Aerial Perspective

Table 5.14 Median of Predominant Ice Type, When Ice is Present

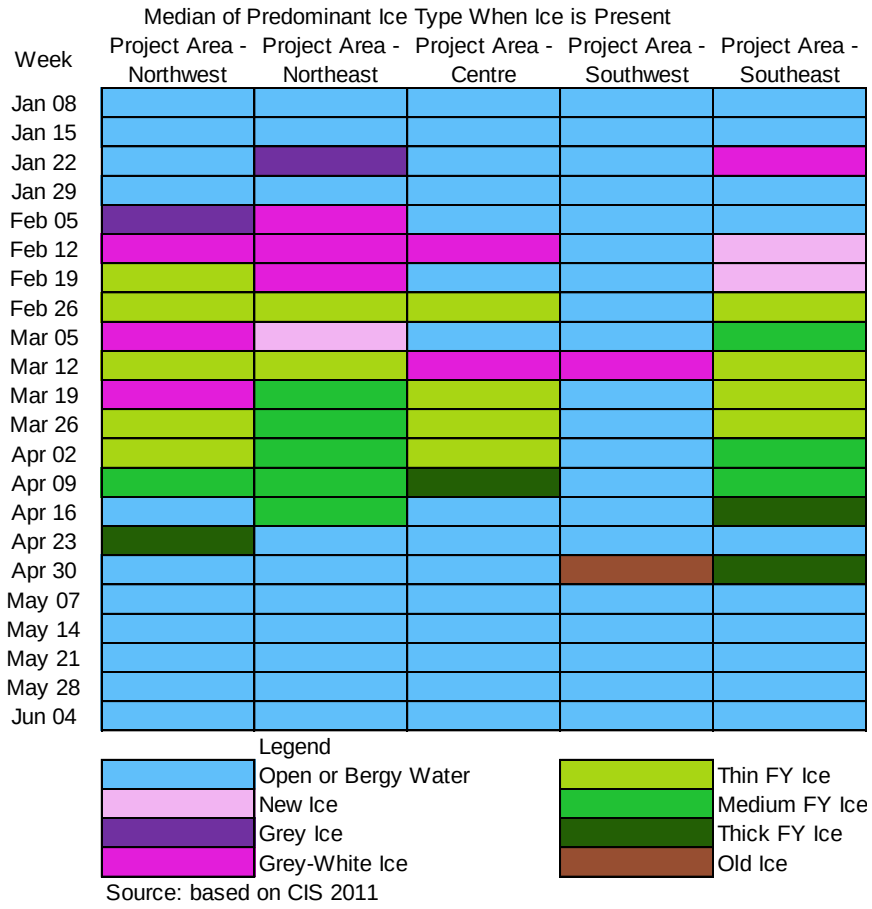

Table 5.15 Stage of Development, Sea Ice

Description	Thickness
New	<10 cm
Grey	10 to 15 cm
Grey-white	15 to 30 cm
First-year	≥30 cm
Thin first-year	30 to 70 cm
Medium first-year	70 to 120 cm
Thick first-year	>120 cm
Source: CIS (2005)	

When ice is present, the median ice concentration is generally at its largest at $7^{8}/_{10}$ between the weeks of 5 February to 9 April at the northwest and northeast with greater concentrations of $9^{9+}/_{10}$ during the weeks of 22 January for the northeast, and during mid-February for the north and central portions. For other locations in the Project Area and during other weeks, when ice is present, the median ice concentrations are generally $1^{3}/_{10}$ to $4^{6}/_{10}$. An illustration of this variability in median ice concentration is shown in Figure 5-32 for the week of 26 February, with greater concentrations in the central and northern portion of the Project Area, lesser concentrations to the southeast and no ice to the southwest.

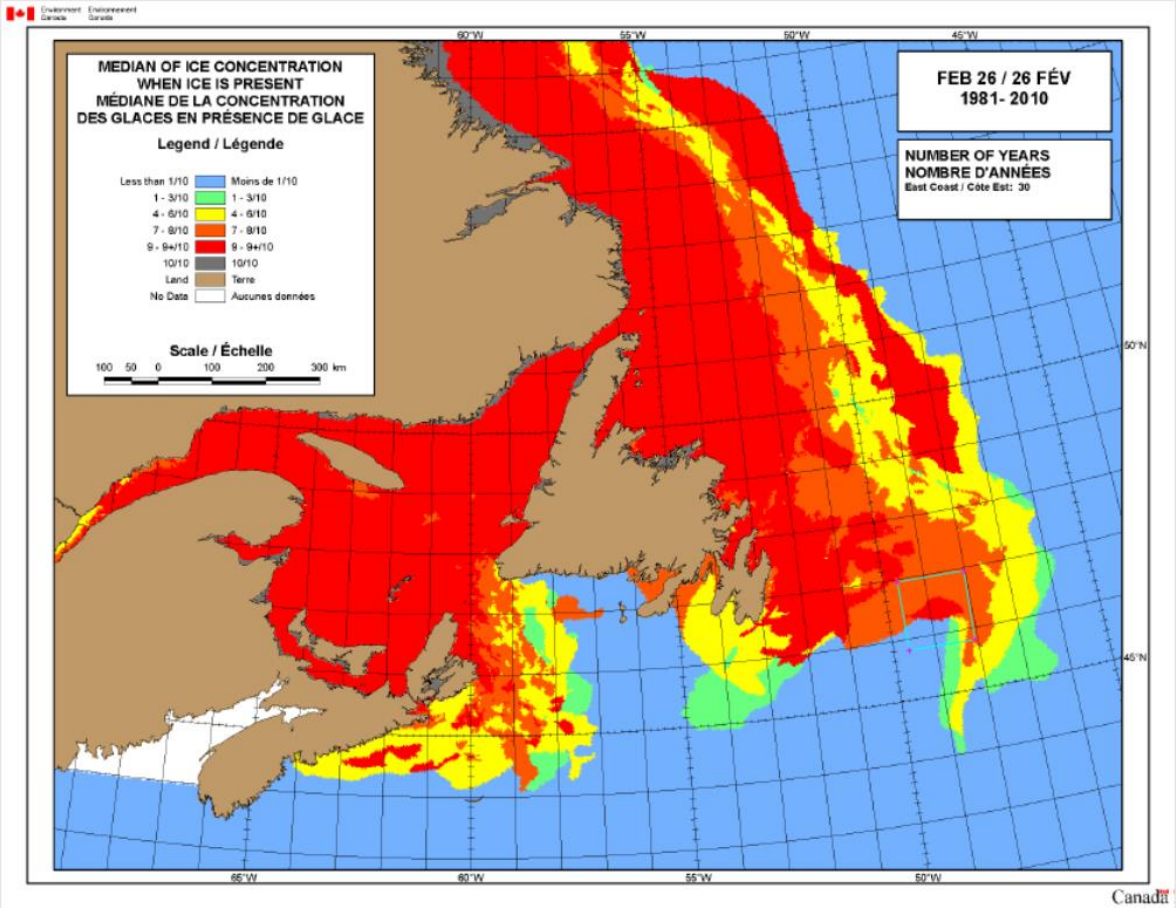

Source: CIS (2011)

Figure 5-32 Median of Ice Concentration, When Ice Is Present, Week of Feb 26

The median of the predominant ice type, when ice is present, at the north of the Project Area during the beginning of February is grey ice (10 to 15 cm) and grey-white ice (15 to 30 cm). During this period new ice (less than 10 cm) is present to the southeast.

Thin first-year (FY) ice (ice of not more than one winter's growth, 30 to 70 cm) may be present from mid-February to the first week of April, with medium FY ice (70 to 120 cm) present in the northeast and southeast. During the first two to three weeks of April thick FY ice (greater than 120 cm) maybe encountered to the north and over the centre of the Project Area. Some areas of old ice (ice that has survived at least one summer's melt; second year ice will be generally thicker than FY ice) may be encountered over the southwestern portion of the Project Area at the end of April. The week of 9 April (shown in Figure 5-33)

shows the median of predominant ice type when the ice season is at its peak in terms of the presence of thicker FY ice and progression of the sea ice season over the Project Area.

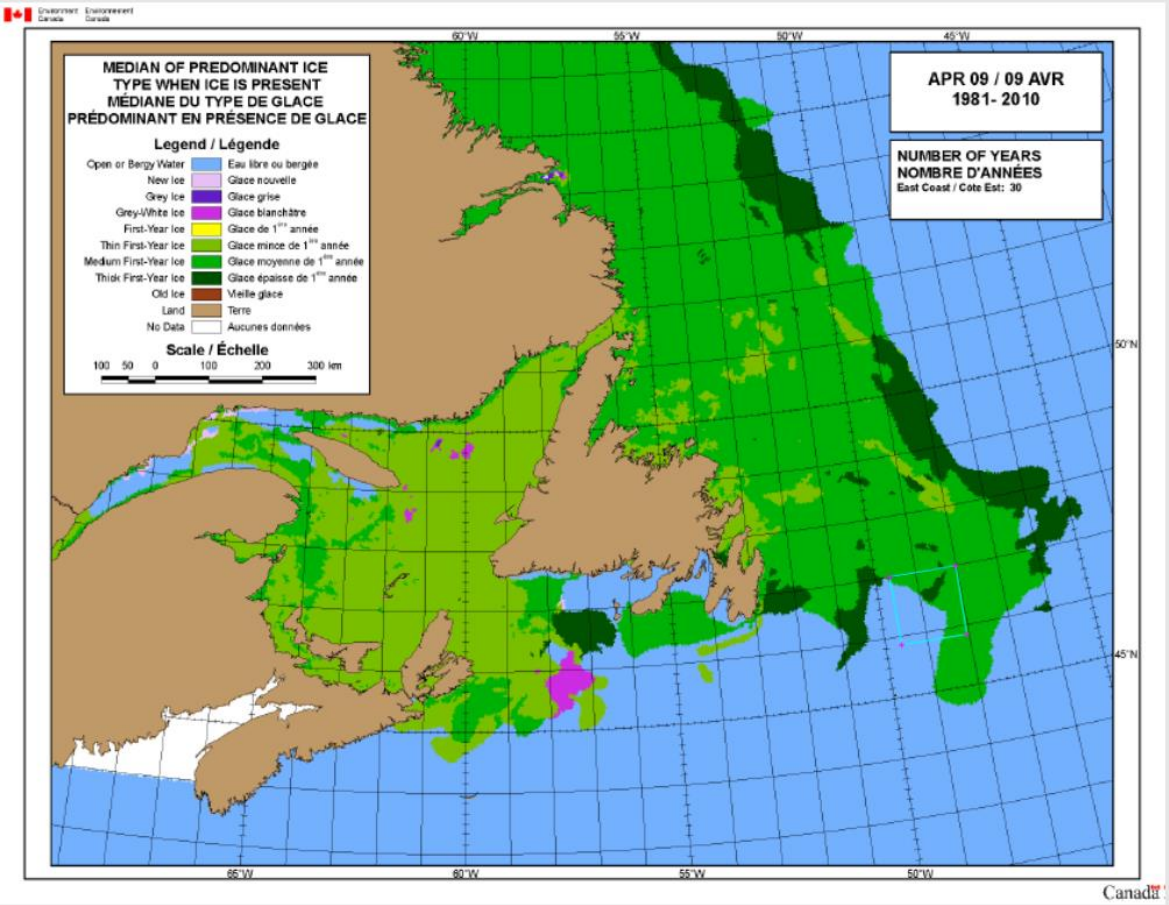

Source: CIS (2011)

Figure 5-33 Median of Predominant Ice Type When Ice Is Present, Week of Apr 9

There is potential for landfast ice nearshore. Landfast ice forms and remains fast along the coast and can extend from a few metres to several hundred kilometres offshore. Landfast ice has the potential to influence conditions within the vessel traffic routes near to St. John's. However, it is unlikely to be a factor in the Project Area itself.

A review of the CIS weekly sea ice charts for 2011 to March 2022 (i.e., the period since the ice atlas's coverage through 2010), indicates only one occurrence of sea ice in the Project Area: $^{3}/_{10}$ ice concentration of grey ice and medium FY ice in strips of concentration $^{9+}/_{10}$ for the week of 27 April 2015. There are a few weeks from 2011 to 2022 during which the sea ice reaches the edge of the Project Area, to the north and/or east, but does not enter. This sort of distribution is illustrated in Figure 5-34 for the week of 10 March 2014 (a similar occurrence for the weeks of 25 February and 11 March 2019), which shows the sea ice surrounding the Project Area to with $^{3}/_{10}$ concentration medium FY ice, with traces of old ice, to the north and $^{7}/_{10}$ concentration thin FY and grey ice in small floes to the east.

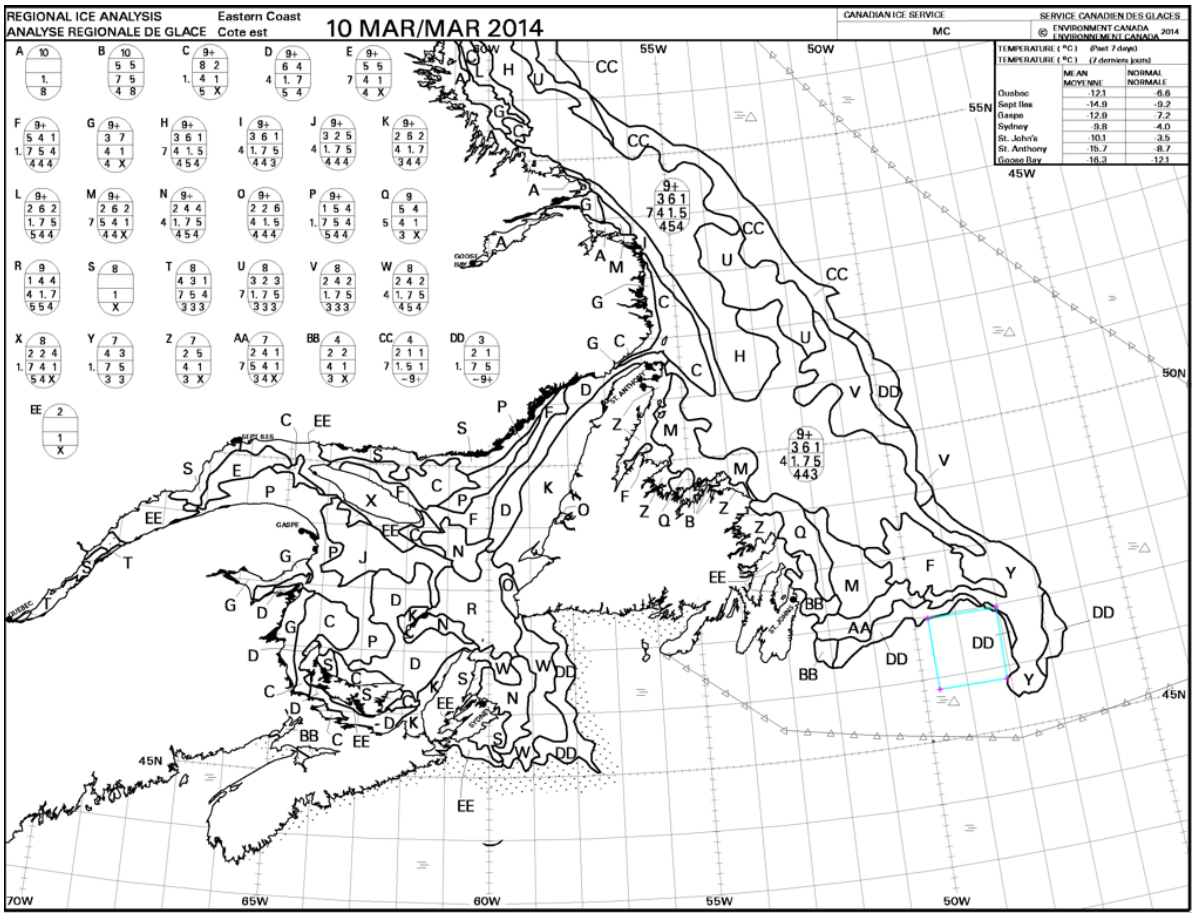

Source: CIS (2019)

Figure 5-34 Eastern Coast, Regional Ice Analysis, Eastern Coast, Week of 10 March 2014

The recent sea ice distributions rarely reach much farther south than about 48°N as illustrated for the week of 7 March 2022 with ice concentrations of $^{5}/_{10}$ including $^{4}/10$ of thin FY ice with ice concentrated in strips and patches of $^{9+}/_{10}$ concentration (Figure 5-35).

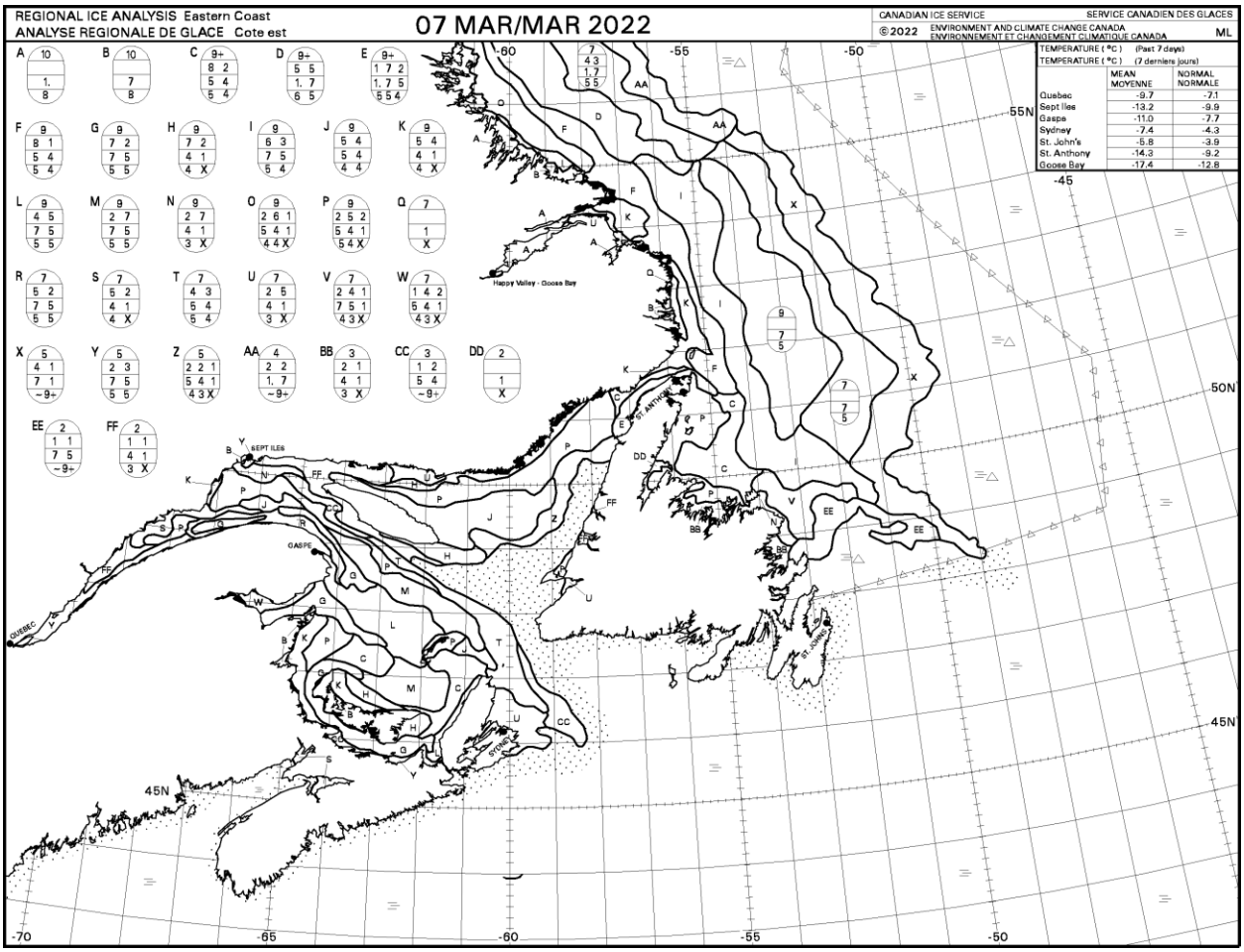

Source: CIS (2022)

Figure 5-35 Eastern Coast, Regional Ice Analysis, Eastern Coast, Week of 7 March 2022

Further information on regional ice conditions in this area is provided in the Eastern Newfoundland SEA (IAAC 2021), Section 4.1.5.

5.4.2 Icebergs

The east coast of Newfoundland and Labrador, including the Project Area on the Grand Banks, frequently experiences icebergs in their journeys south from the fjords of Greenland. Icebergs are masses of freshwater ice which calve each year from the glaciers along west Greenland. A small number of icebergs originate from east Greenland. Icebergs are moved by both the wind and ocean currents, and typically spend one to three years travelling a distance up to approximately 2,900 km (1,800 miles) to the waters of Newfoundland. The West Greenland and Labrador Currents are major ocean currents, which move the icebergs around the Davis Strait, along the coast of Labrador, to the northern bays of Newfoundland, and to the Flemish Pass and the Grand Banks.

Icebergs will deteriorate in their drift southwards due to warmer sea temperatures and wave erosion. For example, the number of days required to melt a 100 m iceberg ranges from 179 days at a sea surface temperature of -1°C to 12 days at 6°C and five days at 15°C; this assumes a wave height of approximately

2 m, wave period of 10 s and relative drift velocity of 25 cm/s (U.S. Coast Guard Navigation Center 2009). Icebergs in sea ice may be less subject to wave erosion. Smaller icebergs are more difficult to detect in sea ice.

While each year is different, icebergs will typically appear offshore by February or March. Easterly and northeasterly winds will have the effect of moving icebergs towards the Newfoundland coast. Their usual path is southward with the ocean currents. The summary of iceberg sightings for the Project Area presented here is based on two data sets. The comprehensive National Research Council-Program of Energy Research and Development (NRC-PERD) Iceberg Sighting Database (Sudom et al. 2014; NRC 2019) contains iceberg sightings from various sources including industry, aircraft and ship, and includes radar, visual and measured observations. The latest version of the database contains icebergs through 2018. Confidential observations acquired by PAL Aerospace for the east coast operators for 2014 onwards are excluded from this analysis. Observations from 2014 through 2021 are from the International Ice Patrol (IIP), 2014 to 2018 from the NRC-PERD database, and 2019 to 2021 from the IIP Iceberg Sightings Database (IIP 1995).

Statistics for observations in the Project Area for the past 30 years, 1992-2021, are reported. Iceberg re-sightings in the database are ignored; a given iceberg is counted once even though it may have multiple sightings in the Project Area. Iceberg size classes range from growlers (<1 m above water, <5 m in length and mass approximately 0.001 Mt) to very large icebergs (>75 m in height, >200 m in length, and mass over 10 Mt) (Figure 2.3, CIS 2005). Icebergs of unknown size are also reported.

The query of the NRC-PERD plus IIP databases, for the years 1992 to 2021, yields a total of 1,830 icebergs for the Project Area. Statistics for the number of icebergs by month and by year are presented in Figures 5-36 and 5-37. Table 5.16 reports iceberg counts by month and year.

Icebergs have been observed in the Project Area in all months except October and November. The greatest number of 1,561 or 85% occur from March through May (Figure 5-36), with the vast majority, 1,820 or 99%, occurring from February to July. Icebergs have been observed in April, May and June for 14 of the 30 years, in March for 13 of the 30 years and in February and July for 4 of the 30 years. The January icebergs were observed in 1993; icebergs were last observed in February in 1995; the August, September and December icebergs were from 1992.

Icebergs were present in the Project Area for 21 of the past 30 years, with the greatest numbers being 297 in 2003 and 227 in 1993 (Figure 5-37). Over the past 10 years, the greatest number of icebergs in the Project Area was 152 in 2021. The 30-year annual average is 61 icebergs. The median number of icebergs in the Project Area each year is 29. For the past 10 years the average and median are 42 and 18, respectively.

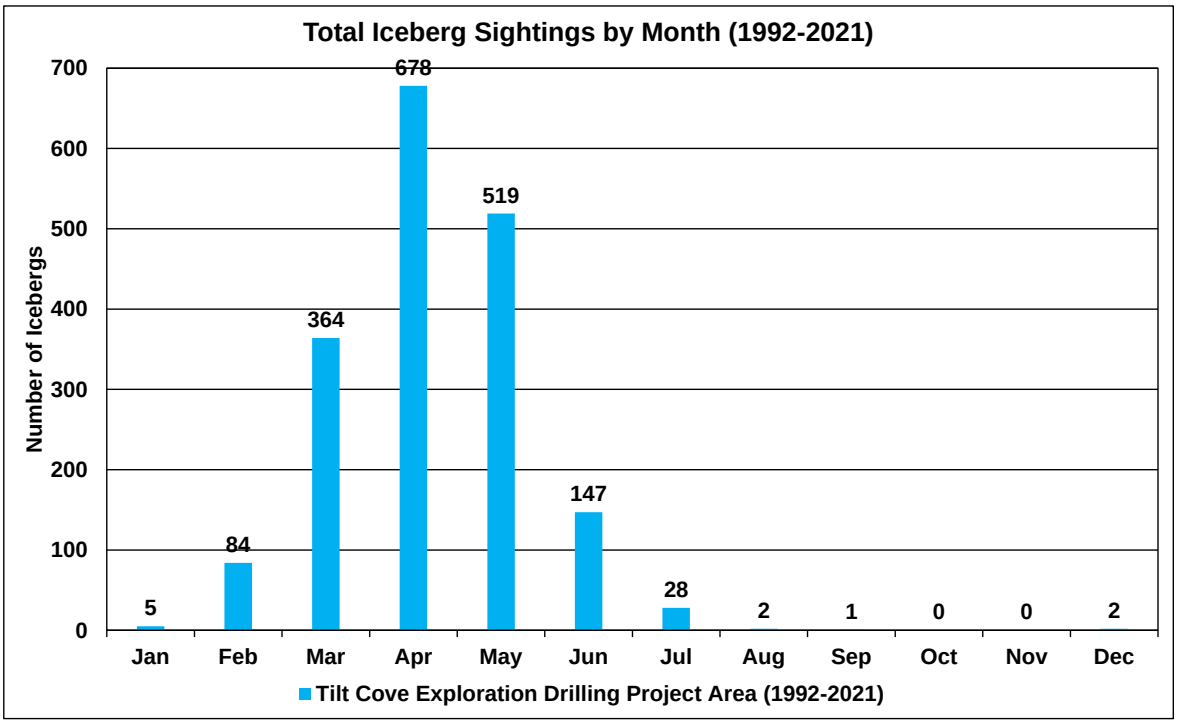

Source: based on NRC (2019), IIP (1995)

Figure 5-36 Iceberg Sightings by Month (1992-2021)

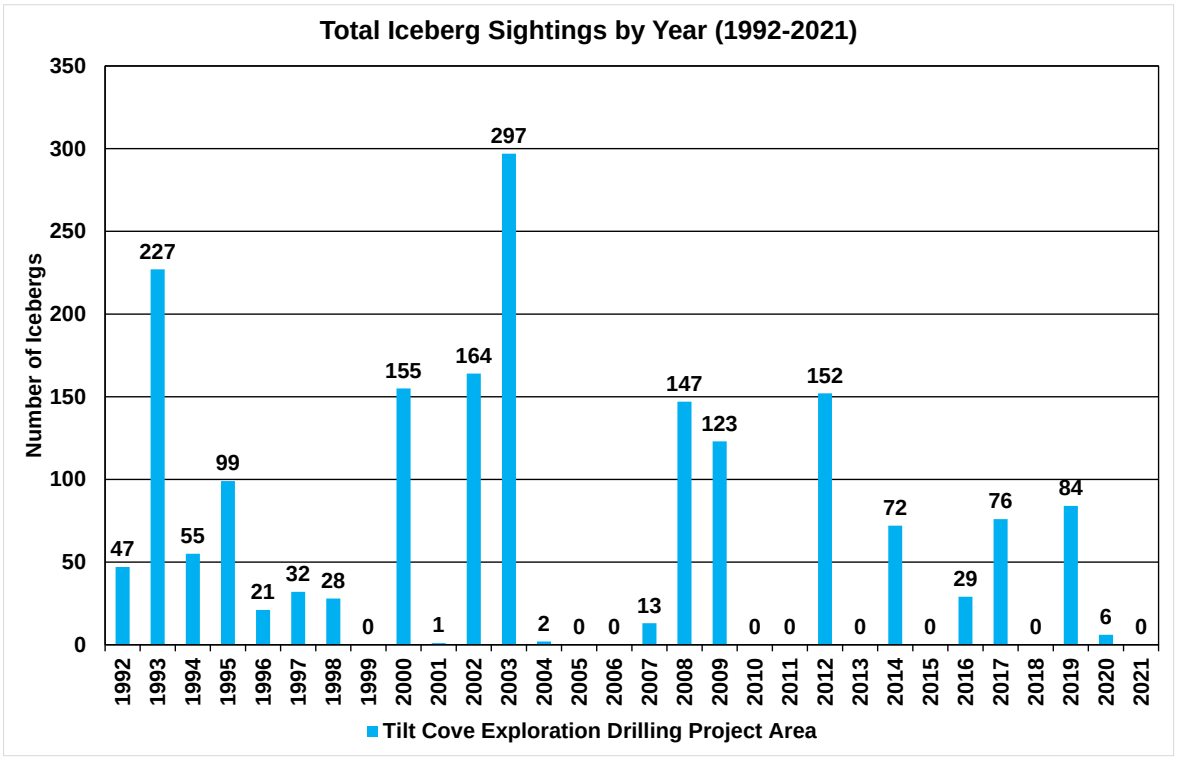

Source: based on NRC (2019), IIP (1995)

Figure 5-37 Iceberg Sightings by Year (1992-2021)

Table 5.16 Iceberg Sightings by Year and Month (1992-2021)

Year	Jan	Feb	Mar	Apr	May	Jun	Jul	Aug	Sep	Oct	Nov	Dec	Total	%
1992	0	3	1	8	24	6	0	2	1	0	0	2	47	2.6
1993	5	58	43	38	48	35	0	0	0	0	0	0	227	12.4
1994	0	19	25	5	1	3	2	0	0	0	0	0	55	3.0
1995	0	4	45	35	10	5	0	0	0	0	0	0	99	5.4
1996	0	0	0	13	1	5	2	0	0	0	0	0	21	1.1
1997	0	0	9	7	10	6	0	0	0	0	0	0	32	1.7
1998	0	0	0	1	15	12	0	0	0	0	0	0	28	1.5
1999	0	0	0	0	0	0	0	0	0	0	0	0	0	0.0
2000	0	0	44	79	10	0	22	0	0	0	0	0	155	8.5
2001	0	0	0	1	0	0	0	0	0	0	0	0	1	0.1
2002	0	0	129	21	13	1	0	0	0	0	0	0	164	9.0
2003	0	0	4	143	133	17	0	0	0	0	0	0	297	16.2
2004	0	0	0	0	1	1	0	0	0	0	0	0	2	0.1
2005	0	0	0	0	0	0	0	0	0	0	0	0	0	0.0
2006	0	0	0	0	0	0	0	0	0	0	0	0	0	0.0
2007	0	0	0	0	0	11	2	0	0	0	0	0	13	0.7
2008	0	0	0	141	4	2	0	0	0	0	0	0	147	8.0
2009	0	0	35	57	4	27	0	0	0	0	0	0	123	6.7
2010	0	0	0	0	0	0	0	0	0	0	0	0	0	0.0
2011	0	0	0	0	0	0	0	0	0	0	0	0	0	0.0
2012	0	0	0	0	149	3	0	0	0	0	0	0	152	8.3
2013	0	0	0	0	0	0	0	0	0	0	0	0	0	0.0
2014	0	0	8	44	19	1	0	0	0	0	0	0	72	3.9
2015	0	0	0	0	0	0	0	0	0	0	0	0	0	0.0
2016	0	0	0	17	4	8	0	0	0	0	0	0	29	1.6
2017	0	0	18	58	0	0	0	0	0	0	0	0	76	4.2
2018	0	0	0	0	0	0	0	0	0	0	0	0	0	0.0
2019	0	0	2	7	71	4	0	0	0	0	0	0	84	4.6
2020	0	0	1	3	2	0	0	0	0	0	0	0	6	0.3
2021	0	0	0	0	0	0	0	0	0	0	0	0	0	0.0
Min	0	0	0	0	0	0	0	0	0	0	0	0	0	
Mean	0.2	2.8	12.1	22.6	17.3	4.9	0.9	0.1	0.0	0.0	0.0	0.1	61	
Max	5	58	129	143	149	35	22	2	1	0	0	2	297	
Total	5	84	364	678	519	147	28	2	1	0	0	2	1830	
%	0.3	4.6	19.9	37.0	28.4	8.0	1.5	0.1	0.1	0.0	0.0	0.1		
Source: based on NRC (2019), IIP (1995)														

An illustration of a recent iceberg year for the Project Area is shown in Figure 5-38 for 2017, with 76 icebergs in the Project Area, compared with the 30-year historical mean of 61. All iceberg sightings (including re-sightings) are illustrated.

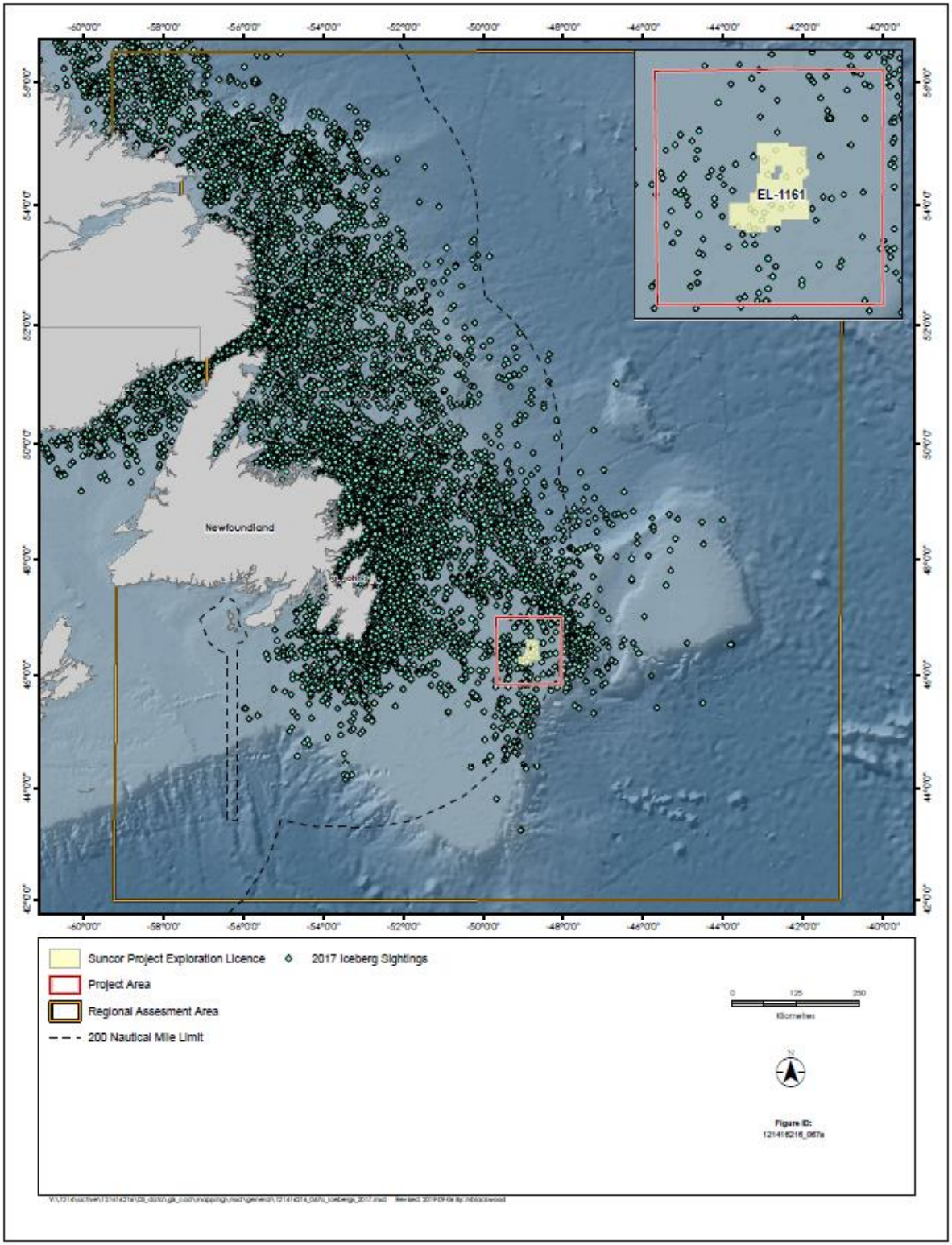

Source: based on NRC (2019)

Figure 5-38 Recorded Iceberg Sightings in 2017, Newfoundland Offshore

A total of 73%, or 1,334, of the iceberg observations have a size reported. An additional 371 icebergs have an unknown size classification. Icebergs of size 'general' have been grouped with those of unknown size. In instances where there are multiple sightings of the same iceberg and different sizes are reported, the largest size is used (e.g., for an iceberg with size values of small and medium, the medium size class is selected). The iceberg size distribution is shown in Figure 5-39. Of the 1,705 icebergs in the Project Area, from the 1992 to 2021 queries, where size is known, 17.8% are growlers or bergy bits, 66.7% are small or medium, 14.2% are large, and 1.4% (18 icebergs) are very large.

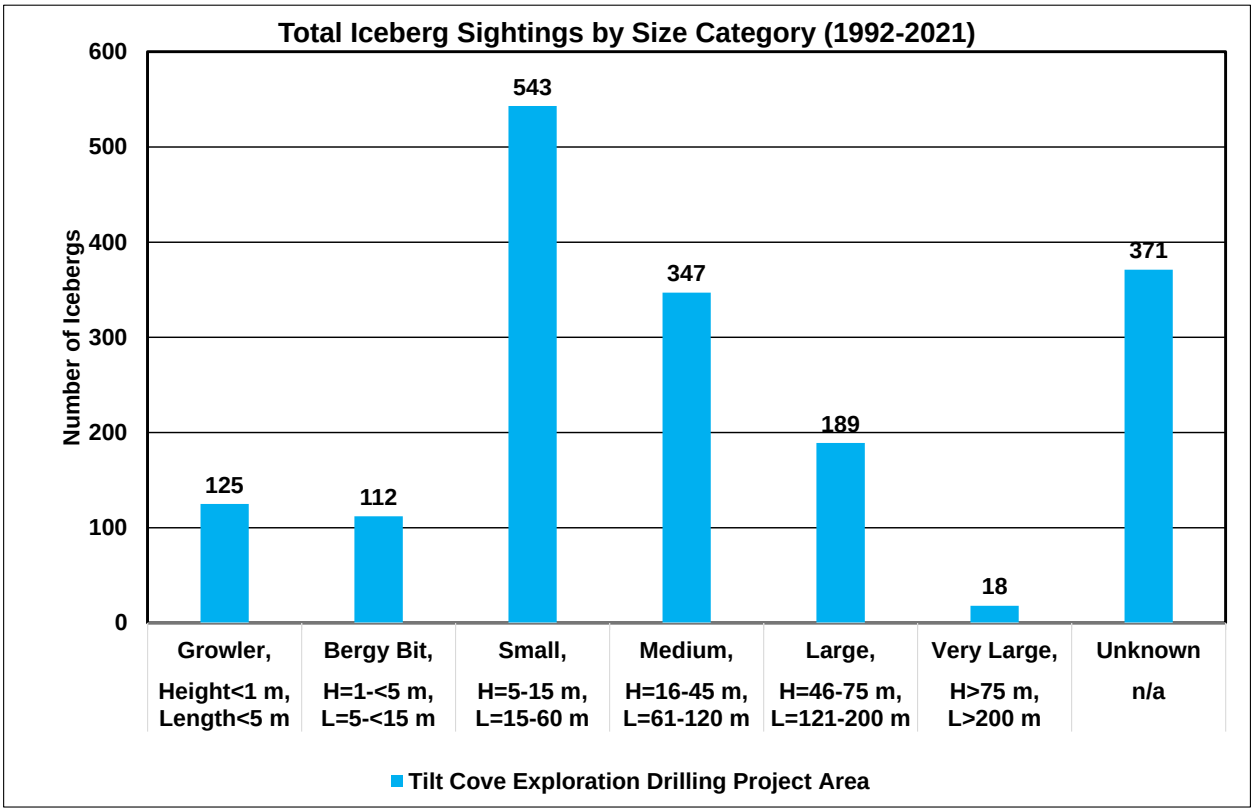

Source: based on NRC (2019), IIP (1995)

Figure 5-39 Iceberg Sightings by Size Category (1992-2021)

5.5 Air Quality

There are no site-specific ambient air quality data for the Project Area. The existing atmospheric environment within the Project Area can be generally categorized as good, with occasional point source human exposure to exhaust contaminants from existing offshore oil production facilities (i.e., Hebron, Hibernia, Terra Nova, and *SeaRose*), supply ships, and other vessels in the area. Devices on the installations that continuously monitor air quality indicate it is below exposure limits. Vessel emissions are regulated by the International Marine Organization (IMO) through the International Convention for the Prevention of Pollution from Ships (MARPOL). This region also receives long-range air contaminants from the industrial mid-west and northeastern seaboard of the United States.

5.6 Acoustic Environment

Sound from a point source emanates in a spherical pattern until it reaches the sea surface or seabed, at which point the spreading becomes cylindrical. Seabed conditions and bathymetry of the Project Area are discussed in Sections 5.1 and 5.3.1, respectively. Underwater sound modelling conducted for this Project (Alavizadeh and Deveau 2020) is provided in Appendix D.

The ambient ocean soundscape is a combination of natural and anthropogenic sources (refer to Figure 5-40). Sea ice (main contributor), precipitation (a common contributor; typically concentrated at frequencies above 500 Hz), and wind are the primary physical environment sources of sound, with low frequencies (<100 Hz) generated by earthquakes and other geological events. Vessel traffic, activities associated with oil and gas exploration and extraction (including air traffic / helicopters), and fishing activities other than fishing vessel movement are the main sources of anthropogenic sound) (Delarue et al. 2018).

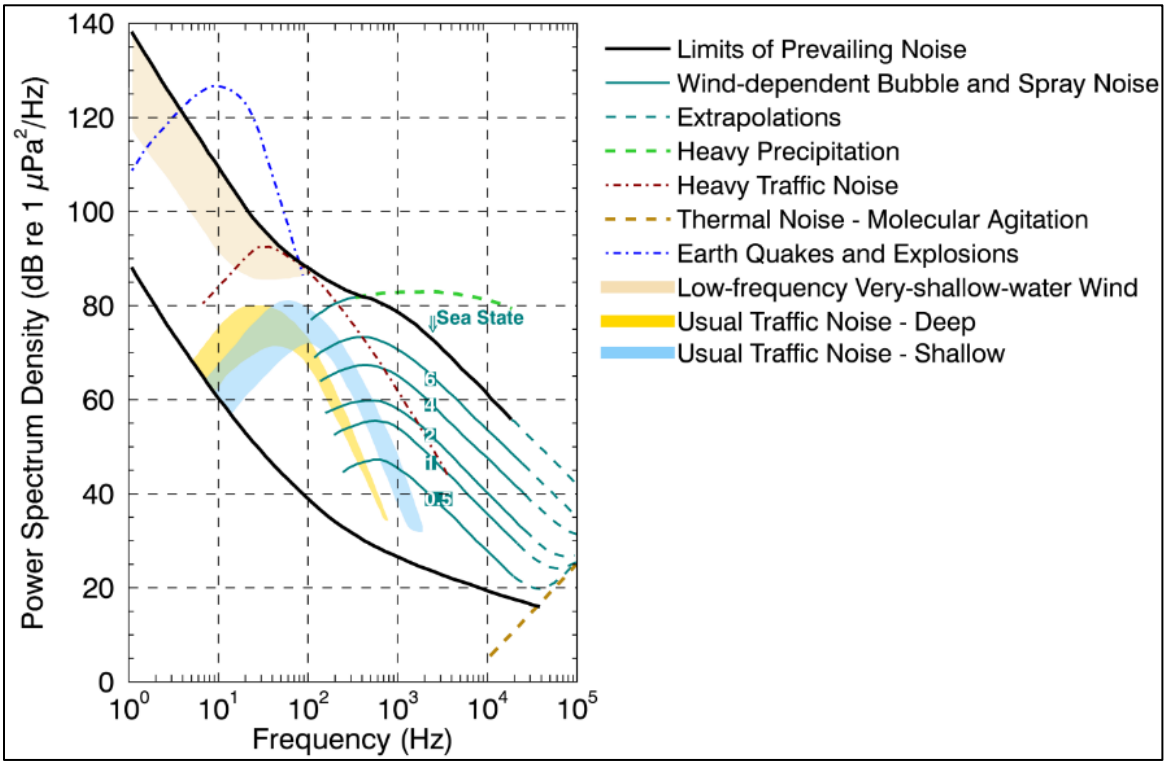

Source: adapted from Wenz (1962), in Delarue et al. 2018

Figure 5-40 Wenz Curves Describing Pressure Spectral Density Levels of Marine Ambient Noise from Weather, Wind, Geologic Activity, and Commercial Shipping

The Environmental Studies Research Fund (ESRF) conducted a recording program in shallow and deep water over a two-year (2015 to 2017) period to characterize the east coast of Canada's underwater soundscape and the occurrence of marine mammals (Delarue et al. 2018). The study involved the deployment of 20 acoustic recorders from Dawson Canyon off Halifax, NS, to Nain Bank on the Labrador shelf (Figure 5-41). Station 18, located approximately 300 km east of St. John's, NL, at a depth of 110 m, is closest to the Project Area. The Hibernia oil platform is located 17 km from Station 18. The maximum

and minimum broadband SPL measured in 2015-16 were 142.8 and 104.7 dB re 1 µPa, respectively, and 144.4 and 104.1 dB re 1 µPa in 2016–17 (Delarue et al. 2018).

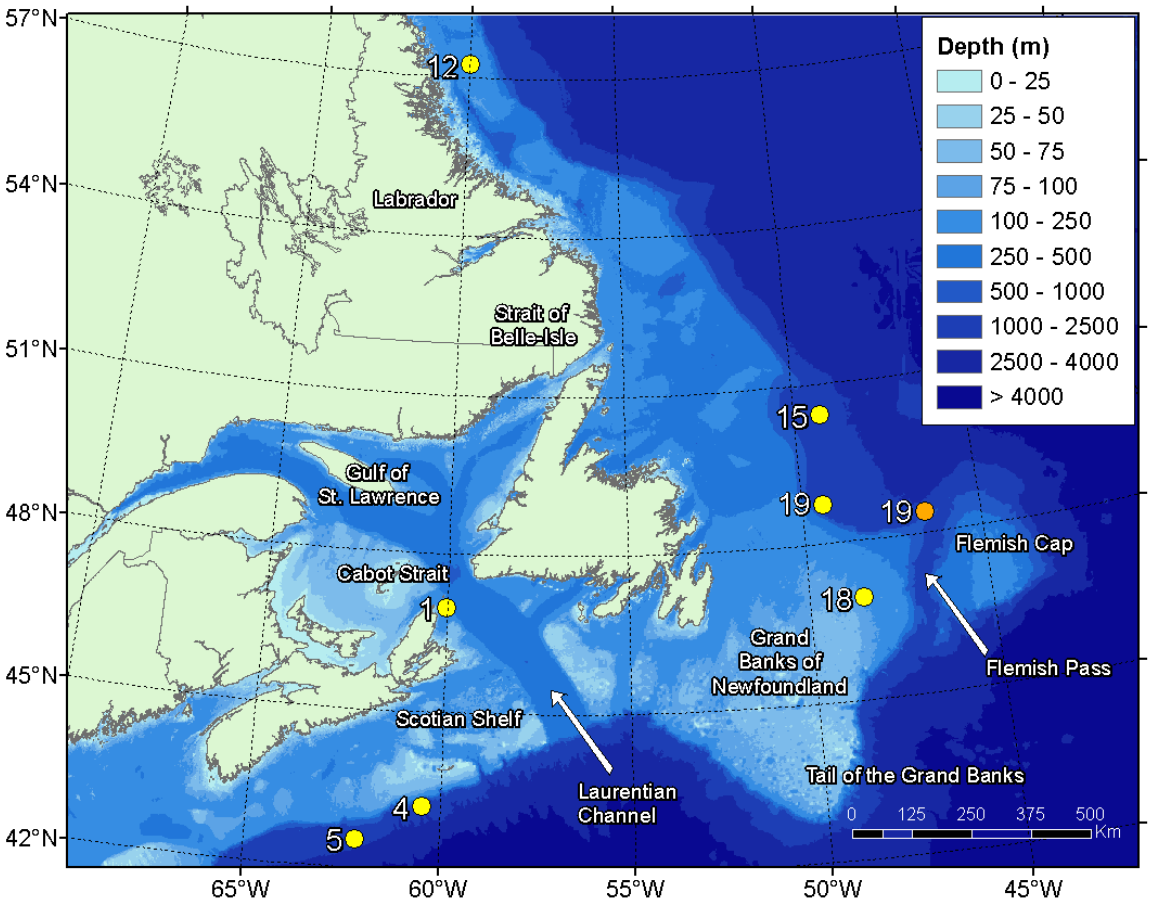

Source: Delarue et al. 2018
Note: The orange dot represents the location of Station 19 in 2016-2017

Figure 5-41 Key ESRF Study Station Locations for Ambient Marine Noise

The main soundscape features were fin whale vocalizations (20 Hz), vessel traffic (offshore supply vessels servicing the Hibernia platform) (30 to 300 Hz), and continuous sound from the machinery on the Hibernia platform (200 Hz) (Delarue et al. 2018). In the first year's deployment, distant seismic noise was also detected in October 2015 and in June and July 2016. In the second year, seismic survey sounds were detected from the end of July to November 2016 and again in June and July 2017.

Fin whale notes were detected from September to mid-March in both years. Fin whales sing from October to March on the Grand Banks, increasing the total sound level across the Grand Banks 5 to 10 dB (in the 10 to 45 Hz band) by their notes. Distant seismic noise was also detected at Station 18 (Delarue et al. 2018).

5.7 Climate Change

Climate change refers to any long-term change in the magnitude, variability and timing of the various elements of Earth's climate system, including the atmosphere, ocean and cryosphere. As reported in the scientific assessments of global climate change regularly developed by the International Panel on Climate Change (IPCC), there is a considerable evidence that the atmosphere and ocean have warmed, snow and ice amounts have been diminished, sea level has risen and the concentration of GHGs have increased since the late 19th century (IPCC 2013a, 2021a). Changes have also been observed in the intensity and frequency of damaging extreme weather and climate events worldwide since the 1950s (IPCC 2013a, 2021a; World Meteorological Organization 2019). Given these findings, climate change can be considered one of the defining challenges of the 21st century (Bush and Lemmen 2019).

This section discusses general climate change considerations relevant to offshore Newfoundland and is organized according to atmospheric variables (wind, temperature, precipitation and storms), oceanographic variables (ocean-water temperatures, waves, currents and sea level), and cryospheric variables (sea ice and icebergs). Given the temporal scope of the project extends to 2029, it is unlikely that the physical environment in the Project Area will experience substantial climate change impacts beyond what is presently found in recent trends and interannual variability. Climate change is therefore unlikely to have a direct and significant adverse environmental effect on the Project beyond the overall design and planning measures being undertaken to address the physical environmental parameters discussed above.

Global climate models (GCMs) are a class of computer-driven models that provide projections of climate change based on a range of future scenarios that incorporate anthropogenic GHG emissions and land use changes. All models used to project climate change have some amount of inherent uncertainty and climate scientists use ensembles of models to analyze and compare a range of simulations and projections (i.e., too much weight is not put on one single prediction) (Bush and Lemmen 2019). The Coordinated Modelling Intercomparison Project (CMIP) was established by the World Climate Research Programme to ensure historical simulations and future climate projections are performed using the same GHG forcing scenarios. The sixth phase of this project (CMIP6) provided the climate model results assessed in the IPCC Sixth Assessment Report (IPCC 2021a). Future climate projections in CMIP6 used five Shared Socio-economic Pathways (SSPs) to describe alternative trajectories for GHG emissions and the resulting atmospheric GHG concentrations from the year 2015 to 2100.

Some specific atmospheric, ocean, and cryosphere changes for selected variables are included in the following sections, drawing on the IPCC Working Group I Interactive Atlas (IPCC 2021c) and employing the CMIP6 model projections dataset. Generally, it is the median estimate values presented below for the short-term period (2021-2040), for a high emissions scenario, SSP5-8.5, and relative to 1995-2014. The estimates are estimated based on visual inspection of results presented in the Atlas.

5.7.1 Atmospheric Climate Changes

5.7.1.1 Wind

Research on the mechanisms and causes of observed and projected changes in mean and extreme wind speeds are limited (Bush and Lemmen 2019). As such, confidence over global estimates of changes to surface wind speed is low in comparison to other climate variables (e.g., temperature and precipitation).

SUNCOR

The IPCC 6th assessment indicates a potential decrease in wind speeds (1% in the short term) in the Project Area (IPCC 2021c).

5.7.1.2 Temperature

Savard et al. (2016) reported a statistically significant increase in mean annual air temperatures in coastal meteorological stations in Eastern Canada from 1900 to 2010. Stations along the Atlantic Ocean warmed by 0.75 ±0.34°C and this trend is expected to continue and intensify over the coming decades (Savard et al. 2016).

As reported in Finnis and Daraio (2018), daily mean, minimum and maximum temperatures are projected to increase throughout the province of Newfoundland and Labrador, with the largest changes expected to occur in winter. The largest changes in air temperature are projected to occur at high latitude (e.g., northern Labrador) and away from coastlines. Regions located near large water bodies (e.g., the Avalon Peninsula) are expected to experience less of a temperature change as open water changes temperature slowly, which tends to reduce the immediate impact of a warming planet (Finnis and Daraio 2018). The IPCC 6th assessment indicates a potential increase in air temperature (1°C in the short term) in the Project Area (IPCC 2021c).

5.7.1.3 Precipitation

There is medium confidence that average annual mean precipitation in Canada has increased as a result of climate change (Bush and Lemmen 2019). Modest increases in mean precipitation are projected over the island of Newfoundland in winter and spring, and throughout most of Labrador year-round (Finnis and Daraio 2018). In Eastern Newfoundland, where offshore temperatures are close to 0°C between September and May, the projected increase in temperature (1.5°C to 2.5°C) implies precipitation will fall more often as rain than as snow (Finnis and Daraio 2018).

The impact of climate change on precipitation in Newfoundland and Labrador is most apparent when considering intense or multi-day events. On the island of Newfoundland, increases in maximum precipitation are projected to be strongest in winter when precipitation is driven by the passage of low-pressure systems and associated fronts. In Labrador, the biggest changes in precipitation are projected to occur in summer as a result of increased diurnal heating (Finnis and Daraio 2018). Most models examined in Finnis and Daraio (2018) predict an increase in extreme precipitation (i.e., increased amounts of precipitation during defined return-period events). The IPCC 6th assessment indicates a potential increase in total precipitation (1% in the short term) in the Project Area (IPCC 2021c).

5.7.1.4 Storms

There is evidence that storm tracks over the North Atlantic have shifted 180 km northward (60º west to 10º east) for the 1982-2001 period relative to the 1958-1977 period (Wang et al. 2006). This northward shift in winter storm tracks is predominantly caused by a warming arctic and a weakening polar-equatorial temperature gradient (Loder et al. 2013). A weaker polar-equatorial temperature gradient results in more persistent weather patterns (e.g., prolonged droughts, floods, cold spells and heat waves) in mid-latitudes (Francis and Varrus 2012). Given the relatively limited amount of published literature focused on winds in

the marine regions off Canada, there is generally low confidence associated with storm trends (Bush and Lemmen 2019).

An Atlantic hurricane (or tropical storm) is a tropical cyclone that forms in the Atlantic Ocean usually in the summer or fall. There is medium confidence of an increase of tropical storms and, along the Atlantic Coast, storms will be more intense with higher wind, precipitation, and storm surge totals when they do occur (IPCC 2021a).

5.7.2 Oceanographic Changes

5.7.2.1 Ocean-Water Temperatures

It is virtually certain that ocean depths from 0 to 700 m warmed since the 1970s (IPCC 2021a).

Ocean-water bodies in Canada's East Coast region are made of three distinct layers: the surface layer, a cold intermediate layer and a deeper layer (Galbraith and Larouche 2013). Surface waters in the region increased by 0.32°C from 1945-2010 in response to rising air temperatures (Han et al. 2013a). During the 1982-2006 period, increases of 1.04°C and 0.89°C in surface-water temperature were observed for the Labrador Sea and the Scotian Shelf, respectively (Sherman et al. 2009). The Project Area has experienced warming in mean monthly water temperatures at a depth of approximately 5 m from 1976-1995 to 1996-2015 (Figure 5-42).

Future warming in the North Atlantic south of Greenland is expected to be limited as the expected reduction in the strength of the Atlantic Meridional Overturning will bring less heat northward (Drijfhout et al. 2012; Caesar et al. 2018). Global models have difficulty resolving ice-ocean variability in the Labrador Sea (i.e., many climate models often simulate excessive mixing, which would result in an under-prediction of the impact of climate change on ice sheets and sea level) and it is unclear whether the projected ocean-temperature anomaly that exists in the North Atlantic south of Greenland will extend westward into coastal waters off Newfoundland and Labrador (de Jong et al. 2009; Hansen et al. 2016). The IPCC 6th assessment indicates a potential increase in sea surface temperature (1°C to 1.5°C in the short term) in the Project Area (IPCC 2021c).

5.7.2.2 Waves

In a business-as-usual climate scenario, where warming continues in-line with current trends, there will likely be significant changes in wave conditions along 50% of the world's coasts (Morim et al. 2019). While robust changes in projected mean wave heights are likely in some areas of the world (e.g., the North Pacific Ocean), decreases in the North Atlantic are likely, which is consistent with the relatively uniform decrease in projected surface wind speeds in the northern hemisphere extra-tropical storm belt (Morim et al. 2019). However, it is also possible that there are increases in wave heights during some periods due to the reduction in sea ice (Bush et al. 2022). Given the inherent limitations of historical observational data, there is a relatively low level of confidence on wave projections (Bush and Lemmen 2019).

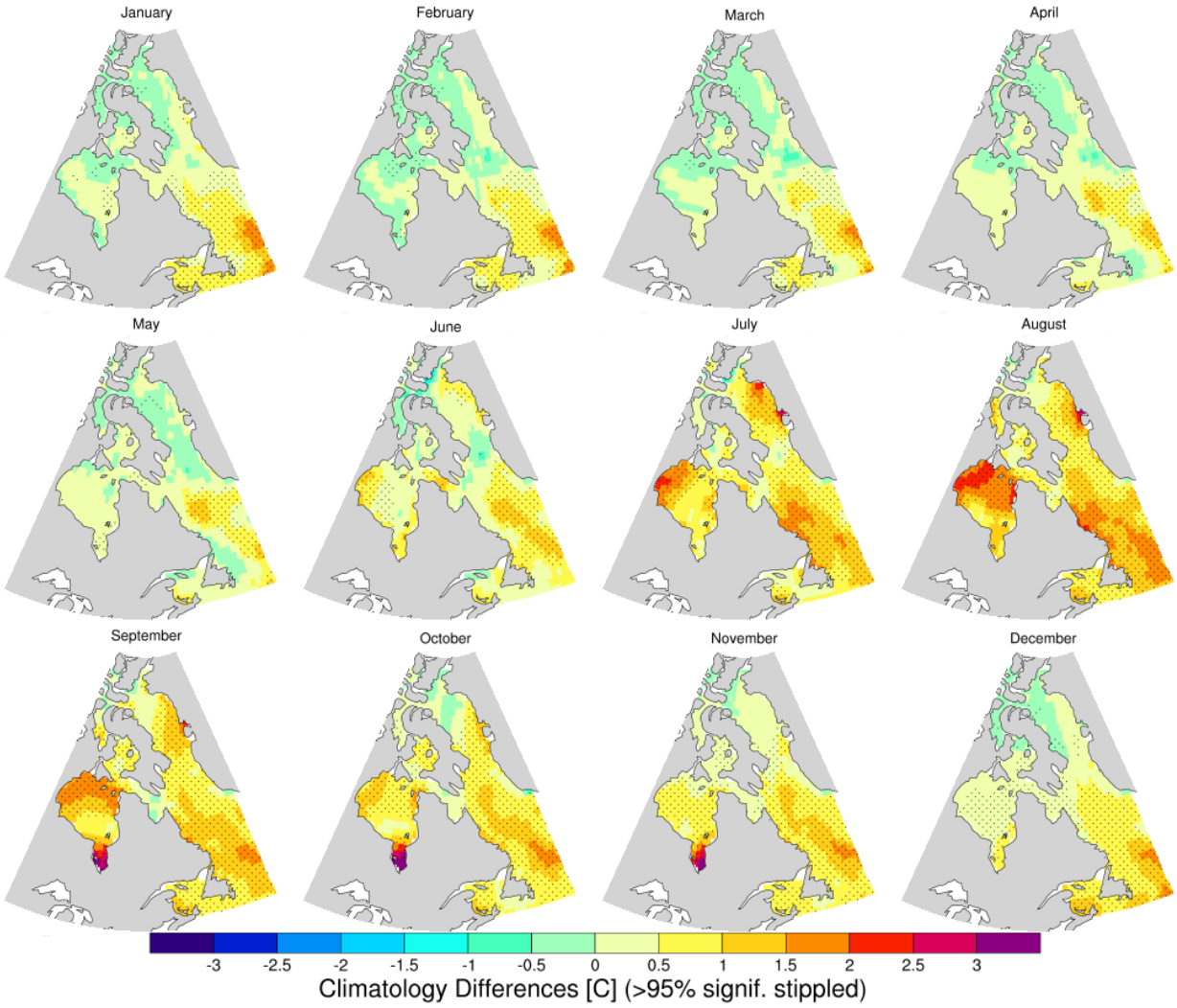

Source: Amec Foster Wheeler (2017b)

Figure 5-42 Changes in Mean Monthly Water Temperature From 1976-1995 to 1996-2015 at a Depth of Approximately 5 m Based on European Center for Medium-Range Weather Forecasting Reanalysis Data

5.7.2.3 Currents

The Newfoundland Shelf (extending from the Strait of Belle Isle southward and then westward to Cabot Strait) and the Labrador Shelf (extending from the Hudson Strait to the Strait of Belle Isle) are subject to the direct influence of water and ice outflows from the Arctic through the Canadian Arctic Archipelago and the North Atlantic subpolar surface gyre (Han et al. 2019). The North Atlantic subpolar surface gyre, in which the Project Area resides, has been declining for the past two decades (Han and Tang 2001; Han et al. 2010, 2013b). This decline is likely associated with multi-decadal variability, rather than a long-term trend (Wang et al. 2015).

The Labrador Current, a component of the North Atlantic subpolar surface gyre, is positively correlated with the winter North Atlantic Oscillation (NAO) in regions north of the Grand Banks, and negatively correlated in regions further south (Han et al. 2013b). With the general weakening of the NAO from 1992-2011, the Labrador Current also became weaker in strength but extended farther towards the equator, well beyond the tail of the Grand Banks. A potential mechanism for this is the southward shift of the Gulf Stream which correspondingly allowed this southward extension of the Labrador Current. A regional ice-ocean climate model developed in Han et al. (2019) projects freshwater transport of the Labrador current will double due to freshening from 2011 to 2069 under a medium-level emission scenario. There is less certainty in a projected small increase in the volume transport of the Labrador Current in Han et al. (2019) and in general, there is a great deal of uncertainty surrounding these climate projections, due in part to the limited capability of current climate models to simulate important processes in the complex atmosphere-ice-ocean system (Sgubin et al. 2017). It therefore remains unclear if significant changes to major currents will occur in the Project Area over the next several decades.

5.7.2.4 Sea Level

A rise in global sea level at a rate of 3.2 ± 0.4 mm/year from 1993-2009 is considered to be the result of thermal expansion of the ocean caused by warming, increased water amounts from melting ice sheets and glaciers, glacial isostatic adjustments (rising or falling land), and changes in the strength of the Gulf Stream (Church and White 2011; Yin 2012).

The rate of annual sea level rise may increase beyond present day trends as the largest single uncertainty in projected sea level rise remains the potential collapse of the Antarctic ice sheet (Robel et al. 2019). Multi-meter sea level rise by the end of the century driven by accelerated melting of ice sheets in Greenland and Antarctica associated with rising temperatures was postulated by Hansen et al. (2016). Bamber et al. (2019) suggest global mean sea level rise in excess of 2 m by the end of the century is plausible under a business-as-usual emission scenario. Local changes in sea level can be significantly different from the global mean (Cazenave and Nerem 2004), and sea levels around eastern Newfoundland and Labrador are projected to rise by approximately 0.25 m by 2040 (IPCC 2021c).

5.7.3 Ice Conditions

The Arctic has undergone substantial warming since the mid-20th century and the reduction in glaciers and ice caps in the Canadian Arctic has accelerated over the last decade (IAAC 2021; Bush and Lemmen 2019).

5.7.3.1 Sea Ice

Based on observations over the past three decades, annual mean Arctic sea ice extent has decreased (approximately 40% in September and approximately 10% in March) (IPCC 2021a). Between 2011 and 2020, annual average Arctic sea ice area reached its lowest level since at least 1850 (IPCC 2021a). The rate of decline in winter season sea ice area between 1969-2016 for eastern Newfoundland waters is 10.6% per decade and it is very likely that increased temperatures will result in the continued reduction of sea ice extent (Bush and Lemmen 2019).

Based on historical trends and projections for the shrinking Arctic sea ice cover, it is likely that the extent and thickness of sea ice will be reduced for the Project Area. The timing of freeze-up, timing of melting, and the variability of the sea ice season are all expected to change (Finnis and Daraio 2018). The IPCC 6th assessment indicates a potential decrease in sea ice (0.5% in the short term) in the Project Area (IPCC 2021c).

In addition to sea ice that develops in the Project Area (which is expected to decline), there is also risk of Arctic sea ice breaking off and transporting to the Project Area. Although the Arctic ice pack declined in aerial extent and thickness, it has become increasingly mobile. Greater (more severe) than normal ice concentrations and pieces of thicker multi-year sea ice within the ice cover presented unusually hazardous conditions for marine traffic along Canada's East Coast region during the spring of 2017 (Barber et al. 2018). An increasingly mobile Arctic ice pack caused by a changing climate may increase ice hazards off Newfoundland's coast in areas where multiyear ice from the high Arctic has not typically been encountered (Barber et al. 2018).

5.7.3.2 Icebergs

Icebergs that appear in the North Atlantic are remnants of terrestrial ice calved primarily off West Greenland glaciers, and to a lesser extent the ice caps on Ellesmere, Devon and the Baffin Islands (Marko et al. 1994). The regional iceberg climate is determined by the rate at which icebergs calve and their size distribution. Both factors are affected by local oceanic and atmospheric circulation patterns, water temperature, the frequency and the duration of open water conditions (Marko et al. 2014). In general, an observed downward trend in iceberg severity since the 1990s is consistent with changes in regional climate (Marko et al. 2014). Specifically, warmer air temperatures, increased sea surface temperature, and increased wave action on the icebergs due to reduced sea ice cover may increase iceberg melt and deterioration rates.

A study of sea ice area and extent and iceberg season length and iceberg fluxes indicate a significant negative trend for iceberg season length south of 48°N during the period 1980 to 2011 (Figure 5-43). The annual iceberg flux also shows decadal-scale variations which, unlike the length of the iceberg season, are not particularly high in the 1910s and 1920s but are highest after 1980. It is also noted there is likely to be high uncertainty in long-term trends of iceberg fluxes because of changes in iceberg detection technology, search effort, and reporting (Peterson et al. 2015).

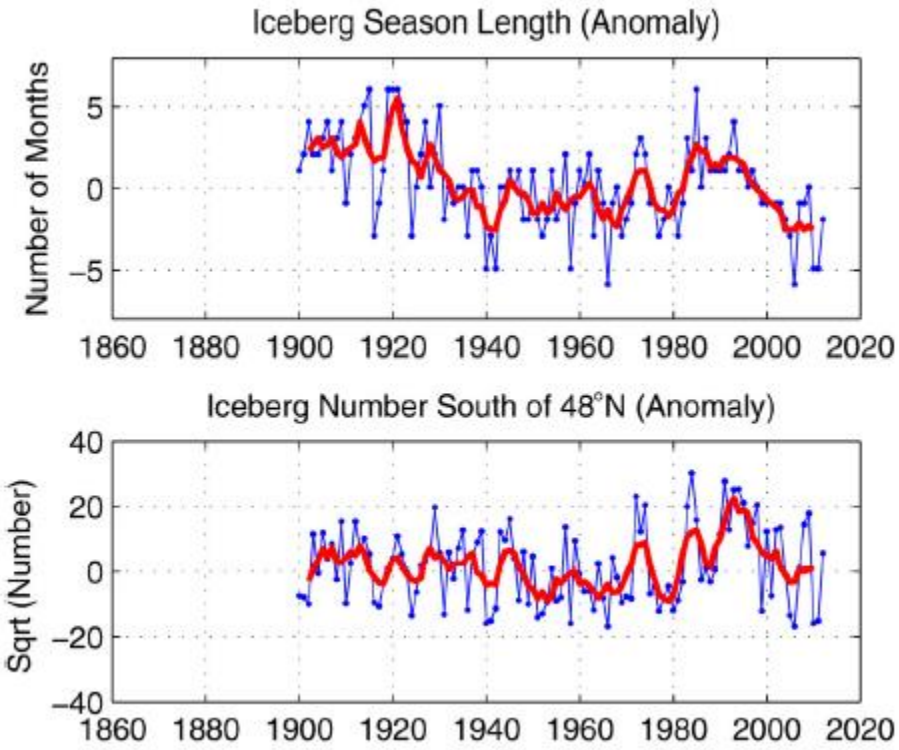

Source: Peterson et al (2015)

Figure 5-43 Iceberg Season Length and Numbers South of 48°N Anomalies

5.8 References

Alavizadeh, Z, and T.J. Deveau. 2020. Underwater Sound Associated with the Tilt Cove Exploration Drilling Project: Jeanne d'Arc Basin, Offshore Eastern Newfoundland. Document 01845, Version 1.0. Technical report by JASCO Applied Sciences for Stantec Consulting Ltd. v + 55 pp.

Amec Foster Wheeler. 2017a. ARP Pilot Area 4 Climatological Report: Port Hawkesbury and the Strait of Canso. Prepared for Environment and Climate Change Canada. Available from: http://climate-scenarios.canada.ca.

Amec Foster Wheeler. 2017b. Climate Change Impacts on Fish Growth Potential in Baffin Bay and the Labrador Sea (Draft report). Prepared for Department of Fisheries and Oceans.

Atkinson, D.E., Forbes, D.L., and T. James. 2016. Dynamic coasts in a changing climate. In: D.S. Lemmen, F.J. Warren, T.S. James and C.S.L. Mercer Clarke (eds.), Canada's Marine Coasts in a Changing Climate. Government of Canada, Ottawa, ON.

Bamber, J., M. Oppenheimer, R. Kop, W. Aspinall and R. Cooke. 2019. Ice sheet contributions to future sea-level rise from structure expert judgement. Proceedings of the National Academy of Sciences of the United States of America, 116(23): 11195-11200.

Banke, E. 1989. Recent Groundings and Scours on the Grand Banks of Newfoundland. (No. Open File #2528). Atlantic Geosciences Centre.

Barber, D.G., D.G. Babb, J.K. Ehn, W. Chan, L. Matthes, L.A. Dalman, Y. Campbell, M.L. Harasyn, N. Firoozy, N. Theriault, J.V. Lukovich, T. Zagon, T. Papakyriakou, D.W. Capelle, A. Forest and A. Gariepy. 2018. Increasing mobility of high Arctic Sea ice increases marine hazards off the east coast of Newfoundland. Geophysical Research Letters, 45: 2370-2379.

Barnes, E. 2013. Revisiting the evidence linking Arctic amplification to extreme weather in midlatitudes. Geophysical Research Letters, 40: 1-6.

Bernier, N.B. and K.R. Thompson. 2006. Predicting the frequency of storm surges and extreme sea levels in the northwest Atlantic, J. Geophys. Res., 111, C10009. http://dx.doi.org/10.1029/2005JC003168.

Bowyer, P. (Editor). 1995. Where the Wind Blows. A Guide to Marine Weather in Atlantic Canada. Environment Canada: xiii + 178 pp.

Bush, E. and D. Lemmen. (Editors). 2019. Canada's Changing Climate Report. Government of Canada, Ottawa, ON. 444 pp.

Bush, E., Bonsal, B., Derksen, C., Flato, G., Fyfe, J., Gillett, N., Greenan, B.J.W., James, T.S., Kirchmeier-Young, M., Mudryk, L., Zhang, X. 2022 Canada's Changing Climate Report in Light of the Latest Global Science Assessment. Government of Canada, Ottawa, ON. 37p.

Caesar, L., S. Rahmstorf, A. Robinson, G. Feulner and V. Saba. 2018. Observed fingerprint of a weakening Atlantic Ocean overturning circulation. Nature, 556: 191-196.

Caires, A., A. Sterl, A. Bidlot, N. Graham and V.R. Swail. 2004. Intercomparison of different wind-wave re-analyses. Journal of Climate, 17(10):1893-1913.

Cameron, G.D.M. and M.A. Best. 1985. Surface Features of the Continental Margin of Eastern Canada. Map compilation for the Atlantic. Geoscience Centre, Bedford Institute of Oceanography, Bedford, NS.

Capotondi, A., M.A. Alexander, N.A. Bond, E.N. Curchitser and J.D. Scott. 2012. Enhanced upper ocean stratification with climate change in the CMIP3 models. Journal of Geophysical Research, 117: C04031.

Cazenave, A. and R.S. Nerem. 2004. Present-day sea level change: observations and causes. Rev. Geophys., 42 (RG3001).

Chavas, D.R., N. Lin N, W. Dong, and Y. Lin. 2016. Observed Tropical Cyclone Size Revisited. American Meteorological Society, 29: 2923-2939. https://journals.ametsoc.org/doi/full/10.1175/JCLI-D-15-0731.1

Church, J.A. and N.J. White. 2011. Sea-level rise from the late 19th to the early 21st century. Surveys in Geophysics, 32(3-4): 585-602.

CIS (Canadian Ice Service). 2005. MANICE, Manual of Standard Procedures for Observing and Reporting Ice Conditions, Revised Ninth Edition. Prepared for Labrador Hydro Project, St. John's, NL. Available at: http://www.ec.gc.ca/Glaces-Ice/default.asp?lang=En&n=2CE448E2-1. November 2016.

CIS (Canadian Ice Service). 2011. Sea Ice Climatic Atlas, East Coast, 1981-2010. Available at: http://www.ec.gc.ca/GLACES-ICE/DEFAULT.ASP?lang=En&n=AE4A459A-1. Accessed October 2016.

CIS (Canadian Ice Service). 2019. Ice Archive. Available at: http://iceweb1.cis.ec.gc.ca/Archive/page1.xhtml. Accessed June 2019.

CIS (Canadian Ice Service). 2022. Ice Archive. Available at: http://iceweb1.cis.ec.gc.ca/Archive/page1.xhtml. Accessed April 2022.

C-NLOPB (Canada-Newfoundland and Labrador Offshore Petroleum Board). 2019. Schedule of Wells. Available at: https://www.cnlopb.ca/wells/. Accessed May 2019.

Cohen, J., J. Screen, J. Furtado, M. Barlow, D. Whittleston, D. Coumou, J. Francis, K. Dethloff, D. Entekhabi, J. Overland and J. Jones. 2014. Recent Arctic Amplification and Extreme Mid-latitude Weather. Nature Geoscience, 7: 627-637.

de Jong, M.F., S.S. Drijfhout, W. Hazeleger, H.M. van Aken and C. Severijns. 2009. Simulations of hydrographic properties in the northwestern North Atlantic Ocean in coupled climate models. Journal of Climate, 22: 1767-1786.

Delarue, J., K.A. Kowarski, E.E. Maxner, J.T. MacDonnell and S.B. Martin. 2018. Acoustic Monitoring Along Canada's East Coast: August 2015 to July 2017. Document Number 01279, Environmental Studies Research Fund Report Number 215, Version 1.0. Technical report by JASCO Applied Sciences for Environmental Studies Research Fund, Dartmouth, NS. 120 pp + Appendices.

DFO (Fisheries and Oceans Canada). 2015a. WebDrogue Drift Prediction Model v0.7. Department of Fisheries and Oceans, Canada. http://www.bio.gc.ca/science/research-recherche/ocean/webdrogue/index-en.php.

DFO (Fisheries and Oceans Canada). 2015b. WebTide Tidal Prediction Model v0.7.1. Department of Fisheries and Oceans, Canada. http://www.bio.gc.ca/science/research-recherche/ocean/webtide/index-en.php.

DFO (Fisheries and Oceans Canada). 2019a. Marine Environmental Data Section. Download Wave Data for WEL447 http://isdm.gc.ca/isdm-gdsi/waves-vagues/data-donnees/data-donnees-eng.asp?medsid=WEL447. Accessed June 2019.

DFO (Fisheries and Oceans Canada). 2019b. ODI: database inventory of moored current meters, thermographs and tide gauges from the East Coast of Canada, 1960 to present. Department of Fisheries and Oceans, Canada. Available at: http://www.bio.gc.ca/science/data-donnees/base/data-donnees/odi-en.php. Ocean Data Inventory Database accessed July 2019.

DFO (Fisheries and Oceans Canada). 2019c. ODI: database inventory of moored current meters, thermographs and tide gauges from the East Coast of Canada, 1960 to present. Department of Fisheries and Oceans, Canada. Available at: http://www.bio.gc.ca/science/data-donnees/base/data-donnees/odi-en.php. Hydrographic Database accessed July 2019.

DFO (Fisheries and Oceans Canada). 2022. MSC50 Wind and Wave Climate Hindcast. Marine Environmental Data Section Archive, https://meds-sdmm.dfo-mpo.gc.ca/ Ecosystem and Oceans Science, Department of Fisheries and Oceans Canada. Data obtained March 2022.

Dupont, F., C.G. Hannah, D.A. Greenberg, J.Y. Cherniawsky and C.E. Naimie. 2002. Modelling System for Tides. Canadian Technical Report of Hydrography and Ocean Sciences 221: vii + 72 pp.

Drijfhout, S., G.J. van Oldenborgh and A. Cimatoribus. 2012. Is a Decline of AMOC Causing the Warming Hole above the North Atlantic in Observed and Modeled Warming Patterns? Journal of Climate, 25(24): 8373-8379.

ECCC (Environment and Climate Change Canada). 2016. Lightning Maps and Statistics (1999-2013) Environment and Climate Change Canada.

ECCC (Environment and Climate Change Canada. 2022. National Pollutant Release Inventory. Facility Report using data search tool. Accessed August 24, 2022.

Fader, G.B.J. and L.H. King. 1981. A reconnaissance survey of teh surficial geology of the Grand Banks of Newfoundland. Geological Survey of Canada No. Paper 81-1A: 45-56.

Finnis, J. and J. Daraio. 2018. Projected Impacts of Climate Change for the Province of Newfoundland & Labrador: 2018 Update. Prepared for Government of Newfoundland and Labrador. Available at: https://www.exec.gov.nl.ca/exec/occ/publications/Final_Report_2018.pdf

Francis, J. and S. Vavrus. 2012. Evidence linking Arctic amplification to extreme weather in mid-latitudes. Geophysical Research Letters, 39(6): L06801.

Freeman, E., S.D. Woodruff, S.J. Worley, S.J. Lubker, E.C. Kent, W.E. Angel, D.I. Berry, P. Brohan, R. Eastman, L. Gates, W. Gloeden, Z. Ji, J. Lawrimore, N.A. Rayner, G. Rosenhagen and S.R. Smith. 2017. ICOADS Release 3.0: A major update to the historical marine climate record. Int. J. Climatol., 37” 2211-2232. https://doi.org/10.1002/joc.4775

Galbraith, P.S. and Larouche, P. 2013. Trends and variability in eastern Canada sea-surface temperatures; in Aspects of climate change in the Northwest Atlantic off Canada, Canadian Technical Report of Fisheries and Aquatic Sciences, 3045: 1-18.

Government of Canada. 2018. CMIP5 Graphics and Tables. Available at: http://climate-scenarios.canada.ca/index.php?page=download-cmip5.

Government of Canada. 2019. Canadian Tropical Cyclone Season Summaries: 2010 to 2016. Available at: https://www.canada.ca/en/environment-climate-change/services/hurricane-forecasts-facts/tropical-cyclone-season-summaries-2010-2016.html

Grant, A.C. and K.D. McAlpine. 1990. The continental margin around Newfoundland: Chapter 6 in Geology of the Continental Margin of Eastern Canada. Pp. 239-292. In: M.J. Keen and G.L. Williams (eds.). Geology of Canada: Vol. 2. Geology of the Continental Margin of Eastern Canada, Geological Survey of Canada.

Gregory, D.N. 2004. Ocean Data Inventory (ODI): A Database of Ocean Current, Temperature and Salinity Time Series for the Northwest Atlantic. DFO Canadian Science Advisory Secretariat Research Document 2004/097.

Han, G., N. Chen and Z. Ma. 2013b. Interannual-to-decadal variations of the Labrador current. In: J.W. Loder, G. Han, P.S. Galbraith, J. Chassé and A. van der Baaren (eds.), Aspects of climate change in the Northwest Atlantic off Canada. Canadian Technical Report of Fisheries and Aquatic Sciences 3045, Catalogue no. Fs97-6/3045E. DFO, Dartmouth, NS.

Han, G., Z. Ma and H. Bao. 2013a. Trends of temperature, salinity, stratification and mixed-layer depth in the Northwest Atlantic. In J.W. Loder, G. Han, P.S. Galbraith, J. Chassé, and A. van der Baaren (eds.), Aspects of climate change in the Northwest Atlantic off Canada. Canadian Technical Report of Fisheries and Aquatic Sciences 3045, Catalogue no. Fs97-6/3045E. DFO, Dartmouth, NS.

Han, G., Z. Ma, Z. Long, W. Perrie and J. Chasse. 2019. Climate Change on Newfoundland and Labrador Shelves: Results from a Regional Downscaled Ocean and Sea-Ice Model Under an A1B Forcing Scenario 2011-2069. Atmosphere-Ocean 57(1): 3-17.

Han, G., K. Ohashi, N. Chen, P. Myers, N. Nunes and J. Fischer. 2010. Decline and partial rebound of the Labrador Current 1993-2004: Monitoring ocean currents from altimetric and conductivity-temperature-depth data. Journal of Geophysical Research, 115: C12012.

Han, G. and C. Tang. 2001. Interannual variations of volume transport in the western Labrador Sea based on TOPEX/Poseidon and WOCE data. Journal of Physical Oceanography, 31: 199-211.

Hansen, J., M. Sato, P. Hearty, R. Ruedy, M. Kelley, V. Masson-Delmotte, G. Russell, G. Tselioudis, J. Cao, E. Rignot, I. Velicogn, B. Tormey, B. Donovan, E. Kandiano, K. von Schuckmann, P. Kharecha, A. Legrande, M. Bauer and K.-W. Lo. 2016. Ice melt, sea level rise and superstorms: evidence from paleoclimate data, climate modeling, and modern observations that 2 °C global warming could be dangerous. Atmospheric Chemistry and Physics, 16: 3761-3812.

Holland, G.J. 1993. "Ready Reckoner" - Chapter 9, Global Guide to Tropical Cyclone Forecasting, WMO/TC-No. 560, Report No. TCP-31, World Meteorological Organization; Geneva, Switzerland.

Huppertz, T.J. and D.J.W. Piper. 2009. The influence of shelf-crossing glaciation on continental slope sedimentation, Flemish Pass, Eastern Canadian continental margin. Marine Geology, 265.

Husky Energy. 2011. White Rose Environmental Effects Monitoring Program 2010. Prepared by Stantec Consulting Ltd. for Husky Energy, St. John's, NL.

Husky Energy. 2012. Husky Energy White Rose Extension Project Environmental Assessment. Prepared by Stantec Consulting Ltd. For Husky Energy. St John's, NL.

Husky Energy. 2013. White Rose Environmental Effects Monitoring Program 2012. Prepared by Stantec Consulting Ltd. for Husky Energy, St. John's, NL.

Husky Energy. 2017. White Rose Environmental Effects Monitoring Program 2014. Prepared by Stantec Consulting Ltd. for Husky Energy, St. John's, NL.

Husky Energy. 2018. Husky Energy Exploration Drilling Project 2018-2025 Environmental Assessment.

IAAC (Impact Assessment Agency of Canada). 2021. Regional Assessment of Offshore Oil and Gas Exploratory Drilling East of Newfoundland and Labrador - GIS Decision Support Tool. Available at: https://nloffshorestudy.iciinnovations.com/mapviewer

IIP (International Ice Patrol). 1995, updated 2020. International Ice Patrol (IIP) Iceberg Sightings Database, Version 1. [Data Set ID:G00807]. Boulder, Colorado USA. NSIDC: National Snow and Ice Data Center. https://doi.org/10.7265/N56Q1V5R. [17 Mar 2022].

International Standards Organization. 2015. ISO/DIS 19901-1:2005, Petroleum and natural gas industries – Specific requirements for offshore structures – Part 1: Metocean design and operating conditions. Available at: https://www.iso.org/standard/34586.html

IPCC (Intergovernmental Panel on Climate Change). 2013a. Climate Change 2013: The Physical Science Basis (Contribution of Working Group I to the Fifth Assessment Report of the Intergovernmental Panel on Climate Change). Stocker, T., Qin, D., Plattner, G.-K., Tignor, M., Allen, S., Boschung, J., Nauels, A., Xia, Y., Bex, V. and P. Midgley (Eds.) Cambridge University Press, Cambridge, United Kingdom and New York, NY, USA. 1535 pp.

IPCC (Intergovernmental Panel on Climate Change). 2013b. Summary for policymakers. In: T.F. Stocker, D. Qin, G.-K. Plattner, M. Tignor, S.K. Allen, J. Boschung, A. Nauels, Y. Xia, V. Bex, and P.M. Midgley (eds.), Climate Change 2013: The Physical Science Basis. Contribution of Working Group I to the Fifth Assessment Report of the Intergovernmental Panel on Climate Change. Cambridge University Press, Cambridge, UK and New York, NY.

IPCC (Intergovernmental Panel on Climate Change). 2014. Climate Change 2014: Synthesis Report. Contribution of Working Groups I, II and III to the Fifth Assessment Report of the Intergovernmental Panel on Climate Change [Core Writing Team, R.K. Pachauri and L.A. Meyer (eds.)]. IPCC, Geneva, Switzerland. 151 pp.

IPCC (Intergovernmental Panel on Climate Change). 2021a. Climate Change 2021: The Physical Science Basis (Contribution of Working Group I to the Sixth Assessment Report of the Intergovernmental Panel on Climate Change). Masson-Delmotte, V., P. Zhai, A. Pirani, S.L. Connors, C. Péan, S. Berger, N. Caud, Y. Chen, L. Goldfarb, M.I. Gomis, M. Huang, K. Leitzell, E. Lonnoy, J.B.R. Matthews, T.K. Maycock, T. Waterfield, O. Yelekçi, R. Yu, and B. Zhou (Eds.) Cambridge University Press. In Press. 3949 p.

IPCC (Intergovernmental Panel on Climate Change). 2021b. Summary for policymakers. In Masson-Delmotte, V., P. Zhai, A. Pirani, S. L. Connors, C. Péan, S. Berger, N. Caud, Y. Chen, L. Goldfarb, M. I. Gomis, M. Huang, K. Leitzell, E. Lonnoy, J.B.R. Matthews, T. K. Maycock, T. Waterfield, O. Yelekçi, R. Yu and B. Zhou (Eds.), Climate Change 2021: The Physical Science Basis. Contribution of Working Group I to the Sixth Assessment Report of the Intergovernmental Panel on Climate Change. Cambridge University Press. In Press.

IPCC (International Panel on Climate Change). 2021c. IPCC WGI Interactive Atlas: Regional Information Available at: https://interactive-atlas.ipcc.ch/. Accessed March 2022.

James, T.S., J.A. Henton, L.J. Leonard, A. Darlington, D.L. Forbes and M. Craymer. 2014. Relative sea-level projections in Canada and the adjacent mainland United States (Open file 7737). Natural Resources Canada, Geological Survey of Canada, Ottawa, ON.

Keen, M.J. and D.J.W. Piper. 1990. Geological and historical perspective, Chapter1. Pp. 5-30. In: M.J. Keen and G.L. Williams (eds.). Geology of Canada - Vol. 2: Geology of the Continental Margin of Eastern Canada, Geological Survey of Canada.

King, E.L.H. 2010. Quaternary geology of Laurentian Channel and Grand Banks of Newfoundland. Geological Survey of Canada.

King, E.L.H. 2014. Quaternary unconsolidated sediment thickness on the Grand Banks of Newfoundland and Northeast Newfoundland Shelf: A GIS database (No. Open File 7513). Geological Survey of Canada.

King, EL.H. and B. MacLean. 1970. Pockmarks on the Scotian Shelf. GSA Bulletin, 81(10): 3141-3148. https://doi.org/10.1130/0016-7606(1970)81[3141:POTSS]2.0.CO;2

Lazier, J.R.N., and D.G. Wright. 1993. Annual velocity variations in the Labrador Current. Journal of Physical Oceanography, 23: 659-678.

Lemmen, D.S., F.J. Warren, T.S. James, and C.S.L. Mercer Clark. (Editors). 2016. Canada's Marine Coasts in a Changing Climate. Government of Canada, Ottawa, ON. 274 pp.

Loder, J.W., G. Han, P.S. Galbraith, J. Chassé and A. van der Baaren (Editors). 2013. Aspects of climate change in the Northwest Atlantic off Canada. Canadian Technical Report of Fisheries and Aquatic Sciences 3045. (Catalogue no. Fs97-6/3045E). DFO, Dartmouth, NS.

Louden, K.E., B.E. Tucholke and G.N. Oakey. 2004. Regional anomalies of sediment thickness, basement depth and isostatic crustal thickness in the North Atlantic Ocean. Earth and Planetary Science Letters, 224(1): 193-211. https://doi.org/10.1016/j.epsl.2004.05.002

Marko, J.R., D. Fissel, M. de Saavedra Alvarez, E. Ross and R. Kerr. 2014. Iceberg Severity off the East Coast of North America in Relation to Upstream Sea Ice Variability: An Update. Conference Proceedings from Oceans. St. John's, NL.

Marko, J.R., D. Fissel, P. Wadhams, P. Kelly and R. Brown. 1994. Iceberg Severity off Eastern North America: Its Relationship to Sea Ice Variability and Climate Change. Journal of Climate, 7: 1335-1351.

Meehl, G.A., T.F. Stocker, W.D. Collins, P. Friedlingstein, A.T. Gaye, J.M., Gregory, A. Kitoh, R. Knutti, J.M. Murphy, A. Noda, S.C.B. Raper, I.G. Watterson, A.J. Weaver and Z. Zhao. 2007. Global climate projections. Pp. 747-845. In: S. Solomon, D. Qin, M. Manning, Z. Chen, M. Marquis, K.B. Averyt, M. Tignor and H.L. Miller (eds.). Climate Change 2007: The Physical Science Basis (Contribution of Working Group I to the Fourth Assessment Report of the Intergovernmental Panel on Climate Change), Cambridge University Press, Cambridge, UK and New York, NY.

Morim, J., M. Hemer, X.L. Wang, N. Cartwright, C. Trenham, A. Semedo, I. Young, L. Bricheno, P. Camus, M. Casas-Prat, L. Erikson, L. Mentaschi, N. Mori, T. Shimura, B. Timmermans, O. Aarnes, Ø. Breivik, A. Behrens, M. Dobrynin, M. Menendez, J. Staneva, M. Wehner, J. Wolf, B. Kamranzad, A. Webb, J. Stopa and F. Andutta. 2019. Robustness and Uncertainties in Global Multivariate Wind-wave Climate Projections. Nature Climate Change, 9: 711-718.

NHC (National Hurricane Center). 2022a. NHC Data Archive: best Track Data (HURDAT2). Available at: https://www.nhc.noaa.gov/data/#hurdat Accessed April 2022.

NHC (National Hurricane Center). 2022b. Tropical Cyclone GIS Data Format. Available at: https://www.coast.noaa.gov/hurricanes/#map=4/32/-80 . Accessed April 2022.

NOAA (National Oceanic and Atmospheric Administration) – National Centers for Environmental Information. 2022. World Ocean Circulation Experiment (WOCE) Global Data Resource. Available at: https://www.ncei.noaa.gov/access/metadata/landing-page/bin/iso?id=gov.noaa.nodc:NODC-WOCE-GDR#:~:text=WOCE%20was%20a%20part%20of,understood%20but%20important%20physical%20processes.

NRC (National Research Council). 2019. NRC-PERD Iceberg Sighting Database, Update 2018, March 2019.

Olsen, A., N. Lange, R.M. Key, T. Tanhua, M. Álvarez, S. Becker, H.C. Bittig, B.R. Carter, L. Cotrim da Cunha, R.A. Feely, S.M.A.C. van Heuven, M. Hoppema, M. Ishii, E. Jeansson, S.D. Jones, S. Jutterström, M.K. Karlsen, A. Kozyr, S.K. Lauvset, C. Lo Monaco, A. Murata, F.F. Pérez, B. Pfeil, C. Schirnick, R. Steinfeldt, T. Suzuki, M. Telszewski, B. Tilbrook, A. Velo and R. Wanninkhof. 2019. Global Ocean Data Analysis Project version 2.2019 (GLODAPv2.2019) (NCEI Accession 0186803). version 2.2019. NOAA National Centers for Environmental Information. Dataset. https://doi.org/10.25921/xnme-wr20. Accessed July 2019.

Overland, J.E. 1990. Prediction of vessel icing for near-freezing temperatures. Weather Forecasting, 5: 62-77.

Peterson, I.K., R. Pettipas and A. Rosing-Asvid. 2015. Trends and Variability in Sea Ice and Icebergs off the Canadian East Coast, Atmosphere-Ocean, 53:5, 582-594, DOI:10.1080/07055900.2015.1057684

Piper, D.J.W. 1991. Seabed geology of the Canadian eastern continental shelf. Continental Shelf Research, 11(8): 1013-1035. https://doi.org/10.1016/0278-4343(91)90089-O

Piper, D.J.W. 2005. Late Cenozoic Evolution of the Continental Margin of Eastern Canada. Norwegian Journal of Geology, 85: 231-244.

Piper, D.J.W. and D.C. Campbell. 2005. Quaternary geology of Flemish Pass and its application to geohazard evaluation for hydrocarbon development. Geological Association of Canada Special Paper, 43: 29-43.

Research Data Archive / Computational and Information Systems Laboratory / National Center for Atmospheric Research / University Corporation for Atmospheric Research, Physical Sciences Division/Earth System Research Laboratory / OAR / NOAA / U.S. Department of Commerce, Cooperative Institute for Research in Environmental Sciences / University of Colorado, National Oceanography Centre / University of Southampton, Met Office / Ministry of Defence / United Kingdom, Deutscher Wetterdienst (German Meteorological Service) / Germany, Department of Atmospheric Science / University of Washington, Center for Ocean-Atmospheric Prediction Studies / Florida State University, and National Centers for Environmental Information / NESDIS / NOAA / U.S. Department of Commerce. 2016, updated monthly. International Comprehensive Ocean-Atmosphere Data Set (ICOADS) Release 3, Individual Observations. Research Data Archive at the National Center for Atmospheric Research, Computational and Information Systems Laboratory. https://doi.org/10.5065/D6ZS2TR3. Accessed 06 Apr 2022.

Robel, A.A., H. Seroussi and G.H. Roe. 2019. Marine ice sheet instability amplifies and skews uncertainty in projections of future sea-level rise. PNAS July 8, 2019.

Savard, J.-P., D. van Proosdij and S. O'Carroll. 2016. Perspectives on Canada's East Coast Region. In D.S. Lemmen, F.J. Warren, T.S. James and C.S.L. Mercer Clarke (eds.), Canada's Marine Coasts in a Changing Climate. Government of Canada, Ottawa, ON.

Seaconsult Ltd. 1988. Physical Environmental Data for Production Systems at Terra Nova. Report prepared for Petro-Canada Inc.

Sgubin, G., D. Swingdeouw, S. Drijfhout, Y. Mary and A. Bennabi. 2017. Abrupt cooling over the North Atlantic in modern climate models. Nature Communications, 8: 1-12.

Shaw, J. 2006. Paleogeography of Atlantic Canadian continental shelves from the last glacial maximum to the present, with an emphasis on Flemish Cap. Journal of Northwest Atlantic Fisheries Science, 37: 119-126.

Shaw, J., D.J.W. Piper, G.B.J. Fader, E.L. King, B.J. Todd, T. Bell, M.J. Batterson and D.G.E. Liverman. 2006. A conceptual model of the deglaciation of Atlantic Canada. Quaternary Science Reviews, 25(17): 2059-2081. https://doi.org/10.1016/j.quascirev.2006.03.002

Sherman, K., I. Belkin, K.D. Friedland, J. O'Reilly and K. Hyde. 2009. Accelerated warming and emergent trends in fisheries biomass yields of the world's large marine ecosystems. AMBIO: A Journal of the Human Environment, 38(4): 215-224.

Sonnichsen, G.V. and E.L. King. 2005. Grand Bank seabed and shallow subsurface geology in relation to subsea engineering design. In In: R.N. Hiscott and A.J. Pulham (eds.). Petroleum Resources and Reservoirs of the Grand Banks, Eastern Canadian Margin. Geological Association of Canada Special Paper, 43: 11-27.

Sonnichsen, G.V., T. King, I. Jordaan and C. Li. 2005. Probabilistic Analysis of Iceberg Scouring Frequency Based on Repetitive Seabed Mapping Offshore Newfoundland and Labrador. Presented at the Port and Ocean Engineering under Arctic Conditions Conference (POAC '05), Potsdam, NY.

Sonnichsen, G.V., K. Moran, C.F.M. Lewis and G.B.J. Fader. 1994. Regional Seabed Geology and Engineering Considerations for Hibernia and Surrounding Areas. Energy Exploration and Exploitation, 12(4): 325-345.

Stoffyn-Egli, P., G.V. Sonnichsen and A. Zawadski. 1992. Clay-size minerals and near-surface stratigraphy on the Northeastern Grand Banks, Newfoundland. Geological Survey of Canada, No. 92-1EL: 323-331.

Sudom, D., G.W. Timco and A. Tivy. 2014. Iceberg sightings, shapes and management techniques for offshore Newfoundland and Labrador: Historical data and future applications. OCEANS 2014, September 14-19, 2014, St. John's, NL.

Swail, V.R. and A.T. Cox. 2000. On the use of NCEP/NCAR reanalysis surface marine wind fields for a long term North Atlantic wave hindcast. Journal of Atmospheric and Ocean Technology, 17: 532-545.

Swail, V.R., V.J. Cardone, M. Ferguson, D.J. Gummer, E.L. Harris, E.A. Orelup and A.T. Cox. 2006. The MSC50 Wind and Wave Reanalysis. Presented at the 9th International Wind and Wave Workshop, Victoria, BC.

Ullman, D. and University of Rhode Island Graduate School of Oceanography. 2013. Physical and chemical profile data collected from CTD in the R/V Knorr cruise KN200-2 during March 2011 in the North Atlantic Ocean (NODC Accession 0100287). Version 1.1. National Oceanographic Data Center, NOAA.

U.S. Coast Guard Navigation Center 2009. How does IIP Determined the Deterioration and Drift of Icebergs. Available at: https://www.navcen.uscg.gov/?pageName=iipHowDoesIIPDetermineTheDeteriorationAndDriftOfIcebergs. Accessed October 2018.

Wallace, D. 1997. Total CO2 and total alkalinity data obtained during the R/V Meteor cruise in the North Atlantic Ocean during WOCE Section A02b (11 June - 03 July, 1997). Carbon Dioxide Information Analysis Center, Oak Ridge National Laboratory, US Department of Energy, Oak Ridge, Tennessee. http://dx.doi.org/10.2172/10191502

Wang, X.L., V.R. Swail and F.W. Zwiers. 2006. Climatology and changes of extra-tropical cyclone activity: Comparison of ERA-40 with NCEP/NCAR Reanalysis for 1958–2001. Journal of Climate, 19: 3145-3166.

Wang, Z., Y. Lue, F. Dupont, J. Loder, C. Hannah and D. Wright. 2015. Variability of sea surface height and circulation in the North Atlantic: forcing mechanisms and linkages. Progress in Oceanography, 132: 273-286.

Woolf, D.K., P.G. Challenor and P.D. Cotton. 2002. Variability and predictability of North Atlantic wave climate. Journal of Geophysical Research, 107: 3145-3158.

World Meteorological Organization. 2019. Atlas of mortality and economic losses from weather, climate and water extremes (1970-2019). World Meteorological Organization. No. 1267.

Wu, Y., C. Tang and C. Hannah. 2012. The circulation of eastern Canadian seas. Progress in Oceanography, 106: 28-48. ISSN 0079-6611, https://doi.org/10.1016/j.pocean.2012.06.005.

Yin, J. 2012. Century to multi-century sea level rise projections from CMIP5 models. Geophysical Research Letters, 39(17).